Summer 8-15-2012

Calcium cycling disturbances and arrhythmogenesis

Namit Gaur
Washington University in St. Louis

WASHINGTON UNIVERSITY IN ST. LOUIS

School of Engineering and Applied Sciences

Department of Biomedical Engineering

Dissertation Examination Committee:

Yoram Rudy, Chair
Igor R. Efimov
Vitaly Klaychko
Daniel Moran
Jeanne M. Nerbonne
Kathryn A. Yamada

Calcium Cycling Disturbances and Arrhythmogenesis

By

Namit Gaur

A dissertation presented to the
Graduate School of Arts and Sciences
of Washington University in
partial fulfillment of the
requirements for the degree
of Doctor of Philosophy

August 2012

Saint Louis, Missouri

Abstract

In this work, a detailed multiscale computational model of Ca cycling and action potential in a ventricular myocyte is developed and used to study mechanisms of arrhythmias associated with mutations in the ryanodine receptor (RyR). The multiscale ventricular myocyte model reproduces experimentally observed Ca dynamics both at the local dyadic scale and at the global whole-cell scale, while also simulating the action potential (AP) shaped by membrane ionic currents. The model represents stochastic activation of L-type Ca channels (LCCs) and RyRs in the dyads and simulates random generation of Ca sparks both during excitation-contraction coupling (ECC) and during diastole. The kinetic model of RyR includes regulation of its openings by calsequestrin (CSQN). The model reproduces graded release and variable gain at the cellular level, *i.e* total sarcoplasmic reticulum (SR) release is a graded function of the amplitude of L-type calcium current (I_{CaL}) and of voltage. The model was used to simulate whole-cell (macroscopic) consequences of changes in local (microscopic) dyadic properties associated with pathologies such as heart failure or impairment of CSQN function.

In addition, the model is used to study mechanisms of cellular arrhythmogenic behaviors associated with Ca handling abnormalities. Specifically, we study Catecholaminergic Polymorphic Ventricular Tachycardia (CPVT) associated with mutations in RyR. Results indicate that increased cytosolic Ca sensitivity of RyRs as a result of mutations, in combination with β-adrenergic stimulation (βAS), results in increased propensity for formation of spontaneous SR Ca release and Ca waves. The spontaneous release activates the electrogenic Na-Ca exchange current (I_{NaCa}) which can

prolong the AP to cause reactivation of I_{CaL} to form early afterdepolarizations (EADs) when it occurs during the phase-2 of AP. During diastole, the spontaneous Ca waves can activate I_{NaCa} generating delayed afterdepolarizations (DADs) which can then reach the threshold for activation of I_{CaL} to form triggered activity (TA). The mechanistic basis for prevention of triggered arrhythmias in CPVT by the pharmacological agent flecainide was found to be due to its effect on mean open time of RyR rather than due to its effect on blocking the fast Na current (I_{Na}). However, such preventive action was not associated with abolition of Ca waves.

EADs and TA also occurred in a simulated hypoxic ventricular myocyte in the presence of βAS. These arrhythmogenic events were due to increased sensitivity of I_{CaL} to βAS during hypoxic conditions.

Acknowledgments

My thanks to Dr. Yoram Rudy for helpful and insightful suggestions for this work. Also my thanks to Dr. Livia Hool for comments and suggestions and gratitude to thesis committee members for their guidance. My thanks to all labmates of Rudy lab past and present for suggestions and comments.

Table of contents

List of Figures

Chapter 1. Background and Introduction

Calcium(Ca) is the element that couples electrical activity at the surface membrane of the ventricular myocyte with mechanical myofibril contraction through a process called excitation-contraction coupling (ECC) (Bers, 2002). During ECC, a small amount of Ca entry via voltage activated L-type Ca channels (LCCs) during an action potential (AP) initiates roughly a ten-fold greater release of Ca through ryanodine receptors (RyRs) located on the terminal cisternae of the sarcoplasmic reticulum (SR) membrane through a process called calcium-induced-calcium release (CICR) (Fabiato, 1985). The release occurs in confined dyadic spaces along periodic invaginations in the surface membrane called t-tubules, situated along the so called Z-planes. A typical ventricular myocyte has about 10000 of such units, where Ca release occurs stochastically via random openings of LCCs and RyRs. After the SR release is terminated and Ca unbinds from the contractile machinery of the cell, a portion of the Ca is extruded via the Na-Ca exchanger (NCX) and the remainder is uptaken back into SR via the sarcoplasmic endoplasmic reticulum Ca ATPAse pump (SERCA), completing the Ca cycle and thus allowing muscle relaxation.

Normally, calcium release from sarcoplasmic reticulum (SR) is initiated by an action potential. However, spontaneous SR Ca release can occur in the absence of action potential excitation (Lakatta et al., 1992). Spontaneous Ca release can occur in localized regions of the cell. When local Ca releases become sufficiently synchronized in space and time they can form Ca waves which can then travel along the length of the cell. The Ca waves can activate sarcolemmal Na/Ca exchange current and generate delayed afterdepolarizations (DAD). If the DAD is of sufficient magnitude, it can form a triggered action potential and arrhythmia.

The mechanisms of initiation and propagation of spontaneous Ca release as well as mechanisms related to Ca-induced Ca release during normal excitation-contraction coupling remains poorly understood. Because of the inherent nonlinear nature of calcium regulation, intuitive approaches are unreliable. Mathematical modeling thus is important in understanding these phenomena, and in investigating phenomena that are not accessible by experiments.

Most of the mathematical models of CICR are common pool models. In a common pool model, the Ca carried by LCC enters a common space (or pool) in which SR Ca is released. The rapid increase of Ca in this space causes rapid regenerative all-or-none Ca release. However, as shown experimentally (Wier et al., 1994), the Ca release flux is a smooth, continuous function of trigger influx, a behavior known as graded release (Fabiato, 1985). Such behavior of CICR can only be reproduced by mathematical models which describe the stochastic Ca release processes at the level of local dyadic SR Ca release. Experimental results indicate that once the SR reaches a certain threshold of Ca concentration, SR Ca release occurs spontaneously(Eisner et al., 2009). In many common pool models, the process of spontaneous SR Ca release is programmed as a threshold phenomenon. The stochastic nature of local dyadic Ca release events, which can then propagate across the dyads to form spontaneous Ca waves, is not taken into account in common pool models.

One of the major goals of this work was to develop a computational model of ventricular myocyte Ca cycling that can describe local stochastic dyadic Ca release arising out of stochastic LCC and RyR openings in the dyad and at the same time be able to describe whole-cell Ca transients, graded release and spontaneous SR Ca release.

Another goal was to connect the Ca cycling component of the model to the whole-cell electrophysiological component with the goal of studying mechanisms of arrhythmogenic cellular behavior arising out of disturbances of Ca cycling in a ventricular myocyte.

Abnormalities of Ca handling have been implicated in various pathophysiological conditions such as heart failure and genetic mutations of proteins associated with SR Ca release: RyR and calsequestrin (CSQN). Several factors such as changes in structure of the cell(Song et al.), alterations in the SR Ca release process via modifications of RyR and CSQN function(Priori and Chen, 2011), increased cell Ca extrusion via NCX upregulation, or reduced Ca uptake via SERCA downregulation have been indicated. A better understanding of how abnormalities of Ca handling can lead to formation of arrhythmogenic spontaneous SR Ca release and/or systolic dysfunction may ultimately lead to better treatment and prevention of arrhythmias.

Catecholaminergic polymorphic ventricular tachycardia (CPVT) is a malignant clinical disease that causes syncope and sudden death in children. It occurs in the absence of structural heart disease. The electrocardiogram (ECG) pattern in CPVT during exercise indicates bidirectional ventricular tachycardia (VT) characterized by an alternating beat-to-beat ECG QRS axis. Bidirectional VT is similar to Ca-overload induced triggered arrhythmias occurring by digitalis intoxication(Sipido, 2006). Studies in cells isolated from knock-in mouse carriers of RyR2 mutations indicated presence of delayed afterdepolarizations (DADs) and/or triggered activity (Cerrone et al., 2005; Liu et al., 2006). Functional characteristics of these mutants compared to wild-type hypothesizes enhanced sensitivity of RyR activation by Ca(Fernandez-Velasco et al., 2009; Jiang et al., 2004) leading to spontaneous SR Ca release, yet the precise underlying mechanisms by

which such enhanced sensitivity of RyR activation to Ca can trigger cellular arrhythmogenic behavior in a ventricular myocyte remains unknown.

In this work, we developed a multiscale model of a ventricular myocyte that scales processes from single channel LCC and RyR stochastic openings in dyadic spaces to whole-cell electrophysiology and Ca cycling. The model was able to reproduce properties of local Ca dynamics in the junctional SR (JSR) and the cytosol at the level of Ca sparks, while predicting whole-cell Ca transients and electrophysiological responses of the myocyte. The model was further used to investigate whole-cell consequences of pathological changes in dyadic properties, such as structural changes in heart failure, which can lead to changes in volume and/or composition of the dyad. The effect of CSQN impairment on the calcium release process was investigated and it was found that CSQN can play an important role in both restitution and termination of SR Ca release.

We also used the model to study the initiation of fatal arrhythmias associated with Ca handling disturbances in a ventricular myocyte, such as occur in CPVT. Specifically, how mutations in the gene encoding the SR Ca release channel, RyR can lead to conditions promoting cellular triggers for arrhythmia: early afterdepolarizations (EADs), delayed afterdepolarizations (DADs) and triggered activity (TA). Preventive measures in this setting were studied by targeted block of ionic currents that define the membrane potential, or of intracellular Ca cycling fluxes via RyR or SERCA.

In a related project, arrhythmogenic effects of acute cellular hypoxia were studied. Acute effects occur on the time scale of seconds or minutes and are unlikely to affect metabolic or transcriptional state of the cell. Acute hypoxia alters the function of several ion channels that determine the plateau-phase of an action potential, but the net

effect on AP morphology is not known. We used the Luo-Rudy computer model of the guinea-pig ventricular myocyte(Luo and Rudy, 1994) to determine the effects of hypoxia on AP configuration with and without β-adrenergic stimulation (βAS). Results demonstrated the major role of augmentation of L-type Ca channels during hypoxia. βAS in this setting resulted in cellular arrhythmogenic behaviors in the form of EADs and TA. These simulation results and model predictions were confirmed experimentally.

Chapter 2. Contributions of ion-channel currents to ventricular action potential changes and induction of early afterdepolarizations during acute hypoxia

2.1 Abstract

Variability in delivery of oxygen can lead to electrical instability in the myocardium and the generation of arrhythmias. In addition ischemic heart disease and angina are associated with an increase in circulating catecholamines that further increases the risk of developing ventricular tachyarrhythmias. The net effects of acute hypoxia and catecholamines on the cardiac action potential (AP) are unknown. We incorporated all published data on the effects of hypoxia on the late Na^+ current (I_{NaL}), the fast Na^+ current (I_{Na}), the L-type Ca^{2+} channel current (I_{CaL}) and the slow (I_{Ks}) and rapid components of the delayed rectifier K^+ current (I_{Kr}) in the absence and presence of β-adrenergic receptor stimulation (βAS) into the Luo-Rudy model of the ventricular myocyte AP. Hypoxia alone had little effect on the AP configuration or AP duration. However in the presence of βAS, hypoxia caused a prolongation of the AP and early afterdepolarizations (EADs) and spontaneous tachycardia were induced. EADs occurs predominantly due to the increased sensitivity of I_{CaL} to βAS during hypoxia. βAS is necessary to induce EADs as EADs are never observed during hypoxia in the absence of βAS.

2.2 Introduction

Ventricular tachycardia and ventricular fibrillation are a major cause of death in patients with myocardial infarction and a reduced left ventricular ejection fraction (Zipes and Wellens, 1998). Typically arrhythmias occur as a result of re-entrant excitation or increased automaticity. Early afterdepolarizations (EADs) are depolarizations of the membrane potential that occur predominantly during phase 2 or 3 of the cardiac action potential (AP) and can degenerate to polymorphic ventricular tachycardia (El-Sherif, 2001; Sims et al., 2008). EADs and triggered activity can induce reentrant arrhythmias. Generation of EADs requires an inward current that is large enough to depolarize the membrane potential (January and Riddle, 1989; Marban et al., 1986).

Variability in delivery of oxygen can lead to electrical instability in the myocardium and the generation of arrhythmias (Keating and Sanguinetti, 2001). The cellular consequences of temporary acute hypoxia (seconds to minutes) differ significantly from chronic hypoxia (hours to days) or anoxia. A rapid decrease in oxygen supply to cardiac myocytes from 150mm Hg to 15mm Hg is not energy limiting and does not deplete ATP (Casey et al., 2002) but can alter the function of a number of cardiac ion channels (Fearon et al., 1997; Hool, 2000, 2001, 2004; Hool, 2005; Hool and Arthur, 2002; Ju et al., 1994, 1996; Smani et al., 2002; Wang et al., 2007). Under these conditions, hypoxia increases late Na^+ current (I_{NaL}) while decreasing fast Na^+ current (I_{Na}) in rat ventricular myocytes (Ju et al., 1994, 1996; Wang et al., 2007). It has been proposed that the increase in I_{NaL} may be arrhythmogenic (Saint, 2008). In addition acute hypoxia decreases the current through L-type Ca^{2+} channels (I_{CaL}) (Fearon et al., 1997; Fearon et al., 1999; Fearon et al., 2000; Hool, 2000, 2001; Hool and Arthur, 2002; Smani

et al., 2002) and the slow component of the delayed rectifier K^+ channel (I_{Ks}) without affecting the rapid component (I_{Kr}) (Hool, 2004). However the net effects of acute hypoxia on action potential (AP) configuration in cardiac myocytes are not known.

Ischemic heart disease and angina are also associated with an increase in circulating and tissue catecholamines that increases the risk of developing ventricular tachyarrhythmias and sudden cardiac death (Dorian, 2005). Hypoxia decreases the half-constant ($K_{0.5}$) for activation of I_{CaL} by the β-adrenergic receptor (βAR) agonist isoproterenol (ISO) (Hool, 2000). However hypoxia also increases the sensitivity of I_{Ks} to βAR stimulation (βAS) without altering I_{Kr} and this could counteract the effects of hypoxia on I_{CaL} (Hool, 2004). In this study we used the Luo-Rudy model of a ventricular myocyte (LRd model) (Luo and Rudy, 1994) to determine the effects of acute hypoxia on the AP in the absence and presence of βAS. Incorporating all published data on the effects of acute hypoxia (PO_2 of 15-20mmHg) on Na^+, Ca^{2+} and K^+ currents we find that in the absence of βAS hypoxia has little effect on the AP configuration and duration. However in the presence of βAS, hypoxia causes a prolongation of the AP and triggers EADs and triggered activities (TA). We produce experimental data in guinea pig ventricular myocytes that support these theoretical findings and determine that EADs are generated predominantly due to hypoxia-induced increased sensitivity of I_{CaL} to βAS activation.

2.3 Methods

2.3.1 Modeling

2.3.1.1 Cell Model

The theoretical dynamic model of a mammalian ventricular AP, the LRd model, provides the basis for the simulations (Faber and Rudy, 2000). The model is predominantly based on guinea pig experimental data. The membrane ionic channel currents are formulated mathematically using Hodgkin-Huxley formalism. Ionic pumps and exchangers are also included in the model. The model accounts for processes that regulate intracellular ionic concentration changes of Na^+, K^+ and Ca^{2+}. Intracellular processes represented in the model include Ca^{2+} uptake and Ca^{2+} release by the sarcoplasmic reticulum (SR) and the buffering of Ca^{2+} by calmodulin and troponin (in the myoplasm) and calsequestrin (in the SR). Experimental data on voltage dependence of conductance and open time duration (Ju et al., 1994, 1996) were used to formulate and include a model of I_{NaL} in the model. βAS effects were included in the model by using the $K_{0.5}$ for enhancement of I_{CaL} and I_{Ks} due to ISO as observed experimentally (Hool, 2000, 2004), and by upregulation of SR Ca^{2+} uptake. ISO effect on inward rectifying potassium current (I_{K1}) (Koumi et al., 1995) was also considered in simulations of the progressive effect of hypoxia on APs.

2.3.1.2 Effects of hypoxia on ion channels

Hypoxia decreases I_{Na} and increases I_{NaL} in ventricular myocytes (Ju et al., 1994, 1996; Wang et al., 2007). The effect of hypoxia on the sodium current was modeled by reducing conductance of I_{Na} by 10% and increasing the conductance of I_{NaL} so that current was in the range of 0.1-0.5% of I_{Na} as seen experimentally (Wang et al., 2007). Hypoxia decreases I_{CaL} and I_{Ks} in the absence of βAS (Hool, 2000, 2004). Hypoxia also

decreases $K_{0.5}$ for activation of I_{CaL} and I_{Ks} by ISO (Hool, 2000, 2004). Both of these effects were included in the model. These responses are reversible with an increase in oxygen tension to normoxia (room oxygen).

2.3.1.3 Protocol

During pacing, a stimulus of -80 μA/μF is applied for a duration of 0.5ms. The model is paced with a conservative current stimulus carried by K^+ (Hund et al., 2001). A variable adaptive time step algorithm was used to simulate action potentials (Luo and Rudy, 1994). Steady state was reached after 88 simulated beats. The ventricular action potential cell model was coded in C++ and run on Linux cluster nodes.

Definition of variables, parameters and model equations used in this study are provided in Appendix A.

2.3.2 Experiments

2.3.2.1 Isolation of ventricular myocytes and patch-clamp studies

Guinea-pig ventricular myocytes were isolated as described previously (Hool, 2000). The current-clamp configuration of the patch-clamp technique was used to record action potentials in the myocytes. External solution contained (in mmol/L): 140 NaCl, 5.4 KCl, 2.5 $CaCl_2$, 0.5 $MgCl_2$, 5.5 Hepes, 11.0 glucose, pH 7.4 at 37°C. Upon achieving whole-cell patch configuration, action potentials were elicited by applying a 0.4 ms pulse of 60-100nA using a basic cycle length of 1000 ms. Microelectrodes were made from borosilicate glass (Sigma) using a microelectrode puller (PC-10, Narishige, Tokyo, Japan) and back-filled with solution containing (in mmol/L): 120 potassium-L-glutamate, 20 KCl, 10 NaCl, 2 $MgCl_2$, 5 Hepes, 0.1 EGTA, 5.0 MgATP, pH 7.05 at 37°C. A total of 30 μmol/L $CaCl_2$ was added giving a free Ca^{2+} concentration of 115 nmol/L as calculated

using the MAXchelator program (http://www.standford.edu/~cpatton/webmaxc/webmaxclite115.htm). Membrane responses were filtered at 5 kHz, digitized at 20 kHz and analysed using an Axopatch 200B amplifier in conjunction with pCLAMP 10.2 acquisition and analysis software (Molecular Devices). Solutions were made hypoxic by bubbling the reservoir leading to the bath with 100% nitrogen and using a combination of stainless steel (Alltech) and silastic tubing (Cole-Parmer) for the delivery of solutions. Within 1-2 min, a consistent PO_2 of 17 mmHg was achieved assessed using an oxygen sensitive probe (Precision Measurement Engineering) as described previously (Hool, 2000). When cells were placed in the chamber, a fast-flow system was used to rapidly (< 1 sec) change the extracellular solutions bathing the myocyte from which action potentials were being recorded, and minimize contamination of the cell from extracellular solutions containing a higher PO_2. All hypoxia experiments were performed at a PO_2 of 17 mmHg consistent with previously published experimental data we incorporated into the model. To minimize the possibility of oxidative degradation, ascorbic acid is commonly added to solutions containing the βAR agonist isoproterenol (ISO). However, to prevent any direct effect of the antioxidant on channel function, ascorbic acid was omitted from all solutions and solutions containing ISO were prepared fresh and changed every 60 min.

2.4 Results

2.4.1 Effect of hypoxia on I_{Na}, I_{CaL}, I_{Kr}, I_{Ks} and the AP in the absence of βAS

We incorporated in the model the experimentally measured effects of hypoxia on I_{Na}, I_{CaL}, I_{Kr} and I_{Ks} in the absence of βAS. In experiments, exposure to hypoxia reversibly reduces peak I_{CaL} by approximately 25% at 0 mV (Fearon et al., 1997; Fearon et al.,

1999; Fearon et al., 2000; Hool, 2000, 2001; Hool and Arthur, 2002; Smani et al., 2002) without shifting the I-V relationship (Figure 2-1A). Figure 2-1B shows the simulated I-V relationship for I_{CaL} during control (normoxic) conditions and during hypoxia in the absence of ISO. There is a reduction in current amplitude but no shift in the I-V relationship, in good agreement with the experimental data. Acute hypoxia also causes a 21.9 ± 1.8 % reversible decrease in steady state I_{Ks} current during a voltage-step to +50 mV (Hool, 2004) (Figure 2-1C).

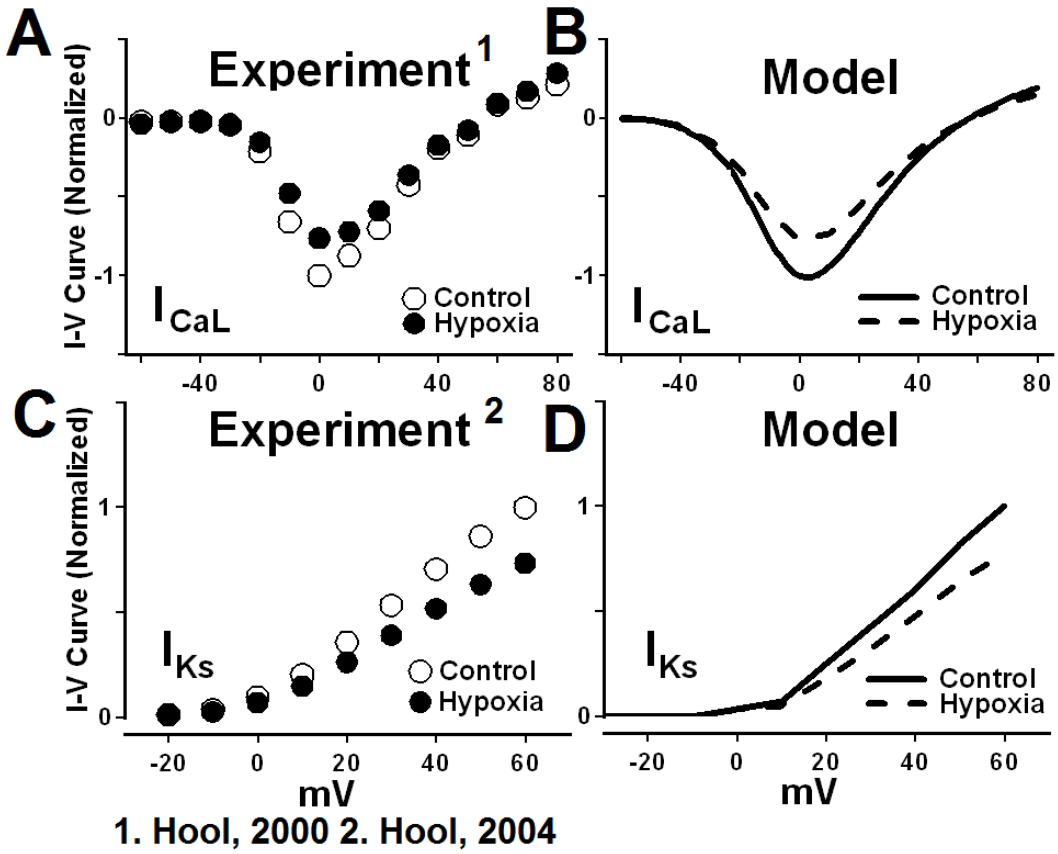

Figure 2-1 Hypoxia inhibits basal (no βAS) I_{CaL} and basal I_{Ks}. (A) Experimental data and (B) Simulated data show inhibition of basal I_{CaL} by hypoxia. (C) Experimental data and (D) Modeled data show inhibition of basal I_{Ks} by hypoxia.

Simulations demonstrate that hypoxia is associated with a 26.5% decrease in current at +50 mV, in good agreement with experimental data (Figure 2-1D).

We modeled the effects of hypoxia in the absence of βAS on the AP at two pacing cycle lengths (CL) of 300ms and 1000ms (Figure 2-2). The APD_{90} for CL of 300ms is 160ms and the APD_{90} for CL of 1000ms is 225ms. When the effects of hypoxia on I_{NaL} alone were incorporated in the model, the APD_{90} for CL of 300ms is 162ms and for CL of 1000ms is 233ms, with no change in resting membrane potential (RMP) or action potential peak (APP). Incorporating the effects of hypoxia on I_{NaL} and I_{Na} in the model did not alter APD_{90} at CL of 300ms (162ms) or CL of 1000ms (232ms) and there was no change in RMP or APP. We conclude that neither I_{NaL} nor I_{Na} alter the AP parameters during hypoxia. The effects of hypoxia on I_{NaL} and I_{Na} were included in all the hypoxia simulations reported below.

2.4.2 Combined effect of hypoxic I_{CaL} and I_{Ks} on AP.

When the effects of hypoxia on I_{CaL}, I_{Na} and I_{NaL}, but not on I_{Ks} are incorporated in the model, the APD_{90} at CL of 300ms is reduced by 4% to 153ms and at CL of 1000ms by 9% to 205ms (Figure 2-2B). In some studies, a slight leftward shift in the voltage-dependence of I_{CaL} during hypoxia has been reported (Fearon et al., 1997; Smani et al., 2002). This shift was incorporated in the model but did not significantly alter the AP morphology although there was a slight decrease in APD (APD_{90}=151ms at CL of 300ms and APD_{90}=200ms at CL of 1000ms).

Next we modeled the effect of hypoxia on I_{Na}, I_{NaL} and I_{Ks} but not on I_{CaL} (Figure 2-2C). Under these conditions, hypoxia causes a prolongation of APD_{90} by 8% to 173ms at CL=300ms and by 14% to 256 ms at CL=1000ms. Finally we modeled all the known

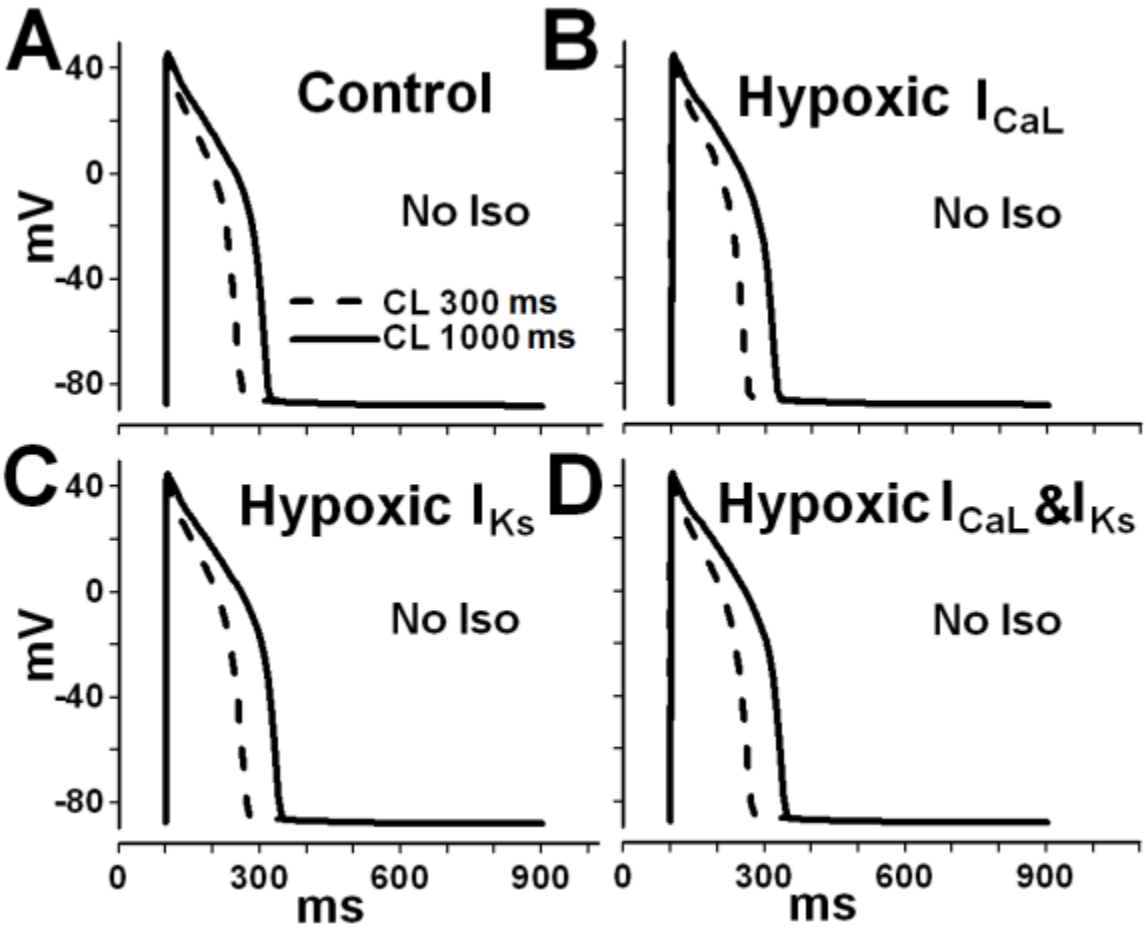

Figure 2-2 The effect of hypoxia on the AP. (A) Simulation data showing an AP in a normoxic cell paced at 300ms and 1000ms cycle length (CL). (B) Effect of hypoxic I_{CaL}, (C) Effect of hypoxic I_{Ks} and (D) Effect of both hypoxic I_{CaL} and I_{Ks}.

effects of hypoxia on all depolarizing and repolarizing currents (I_{Na}, I_{NaL}, I_{CaL}, I_{Ks} and I_{Kr}) (Figure 2-2D). There was very little effect on APD compared to normoxic controls (Figure 2-2A). To further examine a possible arrhythmogenic role for I_{NaL} we modeled the effect of hypoxia on I_{NaL} at twice the value reported in published studies (Ju et al., 1994, 1996). There was no significant effect on APD or AP morphology (at CL of 1000ms APD_{90}=234ms, RMP = -88 mV and APP = 45 mV). We conclude that hypoxia alone does not significantly alter the AP.

2.4.3 Modeling βAS in the absence and presence of hypoxia

The effects of βAS on I_{CaL} are well documented (McDonald et al., 1994). Binding of the βAR leads to activation of cAMP and protein kinase A (PKA) dependent phosphorylation of the channel protein that then increases current magnitude. βAS also leads to an increase in the magnitude of I_{Ks} as a result of direct phosphorylation of the channel (Walsh and Kass, 1991). Neither the function of I_{NaL} nor I_{Na} is regulated by PKA or βAS at low concentrations of ISO (Palygin et al., 2008).

We modeled the concentration-dependence of I_{CaL} and I_{Ks} on ISO. In the absence of hypoxia, ISO increases I_{CaL} with a concentration that produces half-maximal activation ($K_{0.5}$) at 5.3 ± 0.7nmol/L (Hool, 2000). When cells were exposed to hypoxia, the $K_{0.5}$ for I_{CaL} was significantly decreased to 1.6 ± 0.1nmol/L and the current was maximally stimulated with 10nmol/L ISO (Hool, 2000). In the model, we used a $K_{0.5}$ value of 5.3nmol/L under normoxic conditions and 1.6nmol/L ISO during hypoxia for enhancement of I_{CaL}. Figure 2-3A shows that the model prediction of I_{CaL} enhancement by ISO is in good agreement with experimental data. In the absence of hypoxia, exposure of myocytes to 1nmol/L ISO produces a subthreshold response for I_{Ks} and the current is maximally stimulated in the presence of 1μmol/L ISO (Hool, 2004). The $K_{0.5}$ for enhancement of the current in the absence of hypoxia is 18.3 ± 3.9nmol/L. In the presence of hypoxia, 0.1nmol/L ISO produced a threshold response and I_{Ks} was near-maximally activated at 10nmol/L ISO. The $K_{0.5}$ for enhancement of the current was significantly decreased to 1.88 ± 0.43nmol/L under hypoxic conditions. Hypoxia did not alter the response to 1μmol/L ISO, a maximally stimulating concentration of the agonist. In the model we used the $K_{0.5}$ value of 15nmol/L during normoxia (control) and a value

of 1.5nmol/L during hypoxia. These values are within the range of observed experimental values (Figure 2-3B).

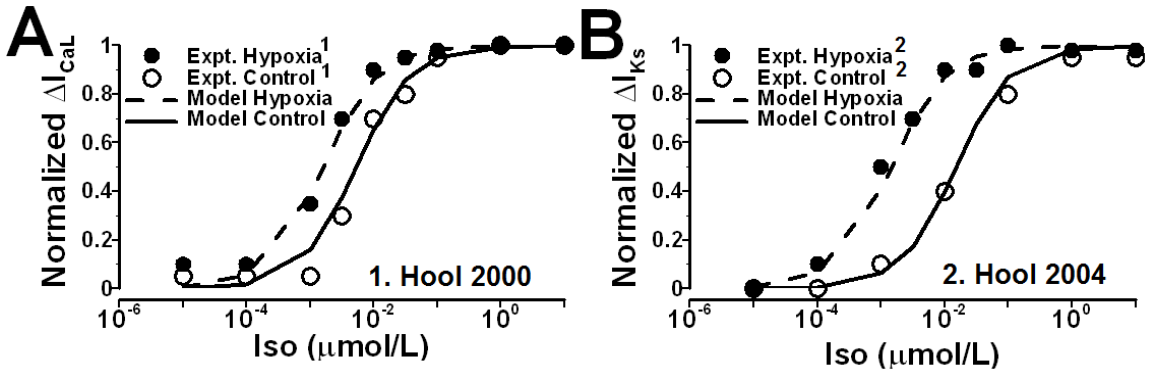

Figure 2-3 Dependence of change in peak I_{CaL} and peak I_{Ks} on ISO concentration in the absence and presence of hypoxia. (A) Simulated (Model), experimental (Expt.) data are shown for hypoxia and control (normoxia) for effect of ISO on I_{CaL}. (B) Simulated (Model), experimental (Expt.) data showing effect of ISO on I_{Ks}.

In the absence of hypoxia, 10nmol/L ISO increases I_{CaL} to 72.1% of the current produced by a maximally stimulating concentration of ISO (1 μmol/L) in the same cell (Hool, 2000) (Figure 2-4A). The peak current is increased 2.8-fold. Corresponding simulations in Figure 2-4B are in good agreement with the experimental data in Figure 2-4A. Exposure to 10nmol/L ISO in the presence of hypoxia (Figure 2-4C) increases the magnitude of the peak current an additional 22.2% (compared to the case of a control cell). Corresponding simulations in Figure 2-4D are in good agreement with the experimental data in Figure 2-4C.

In the presence of a saturating concentration of ISO (1 μmol/L) there is approximately 3-fold increase in steady state I_{Ks} (Hool, 2004) (Figure 2-4E). In the absence of hypoxia 10nmol/L ISO increases I_{Ks} to approximately 45.5% of the current

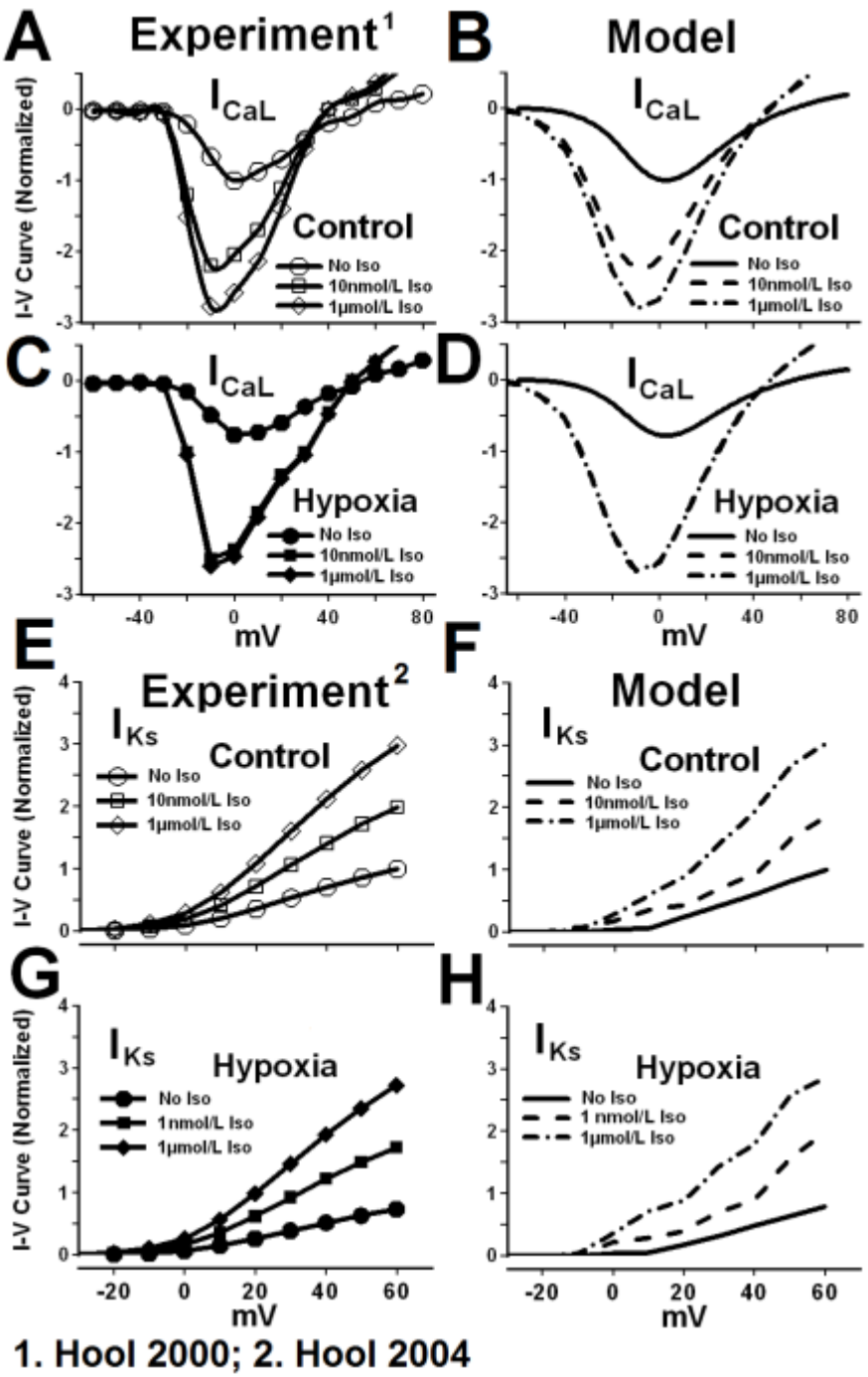

Figure 2-4 The effect of ISO in the absence and presence of hypoxia on voltage dependence of I_{CaL} and I_{Ks}. (A) Experimental (B) Simulated data showing effect of ISO on I_{CaL} in a normoxic (control) cell. (C) Experimental (D) Model data for the effect of ISO on I_{CaL} in hypoxic cell. (E) Measured (F) Simulated data showing effect of ISO on I_{Ks} in a control (normoxic) cell. (G) Measured (H) Model prediction for effect of ISO on I_{Ks} in a hypoxic cell.

produced by 1μmol/L ISO within the same cell (Figure 2-4E), while in the presence of hypoxia 1nmol/L Iso increases I_{Ks} approximately 56.5% of the current produced by 1μmol/L Iso in the same cell(Hool, 2004) (Figure 2-4G). The magnitude of current density produced by 1nmol/L Iso during hypoxia was comparable to the current density produced by 10nmol/L ISO in room oxygen over the entire voltage range. Figure 2-4F demonstrates the effect of 10nmol/L Iso on I_{Ks} during normoxia predicted by the model. Figure 2-4H demonstrates simulations for the effect of 1nmol/L ISO on I_{Ks} in the presence of hypoxia.

2.4.4 Effects of hypoxia on I_{CaL} and the AP in the presence of βAS

The modeling results in Figures 2-1, 2-3 and 2-4 serve as validation that the model reproduces the experimental effects on individual membrane currents. In this section, we explore the effects of hypoxia and βAS on the whole cell AP. Since hypoxia affects both the plateau-forming depolarizing current I_{CaL} and repolarizing current I_{Ks}, in addition to affecting their sensitivity to ISO, it is unclear which of these currents plays a dominant role in shaping the AP morphology during hypoxia. Therefore, we first investigated the role of each channel in isolation and then combined their effects.

We investigated the effect of hypoxia on the AP while varying the amount of ISO to determine if and at what ISO concentration arrhythmic disturbances occur. At low concentrations of ISO, we observed the generation of EADs. The threshold for EAD generation in the I_{CaL} hypoxic cell was 0.6nmol/L at 1000ms CL (Figure 2-5B). In the absence of ISO or at the same level of ISO (0.6nmol/L) there was no evidence of rhythm disturbance in a control normoxic cell (Figure 2-5A, 2-5D). The APD_{90} in a control cell, with the addition of 0.6nmol/L ISO, increased 8% to 244ms at CL of 1000ms and by 4%

to 166ms at CL of 300ms with no changes in RMP or APP. When I_{CaL} was made hypoxic, the APD_{90} at CL 1000ms was prolonged extensively by 82%and EADs were observed (Figure 2-5B). At CL of 300ms APD_{90} was increased by 13% (relative to control) to 180ms but EADs were not generated.

At 1000ms CL, prolongation of the AP led to the generation of an EAD. This is in contrast to the reduction of APD_{90} measured during hypoxia in the absence of ISO (Figure 2-2B). The concentration of Iso that induced EADs in the model (0.6nmol/L) is close to $K_{0.5}$ for activation of I_{CaL} by ISO during hypoxia (1.6nmol/L) and to the threshold for activation of I_{Ks} under normoxic conditions (Figure 2-3). The prolongation of APD was not sufficient to generate EADs at 300ms at any concentration of ISO.

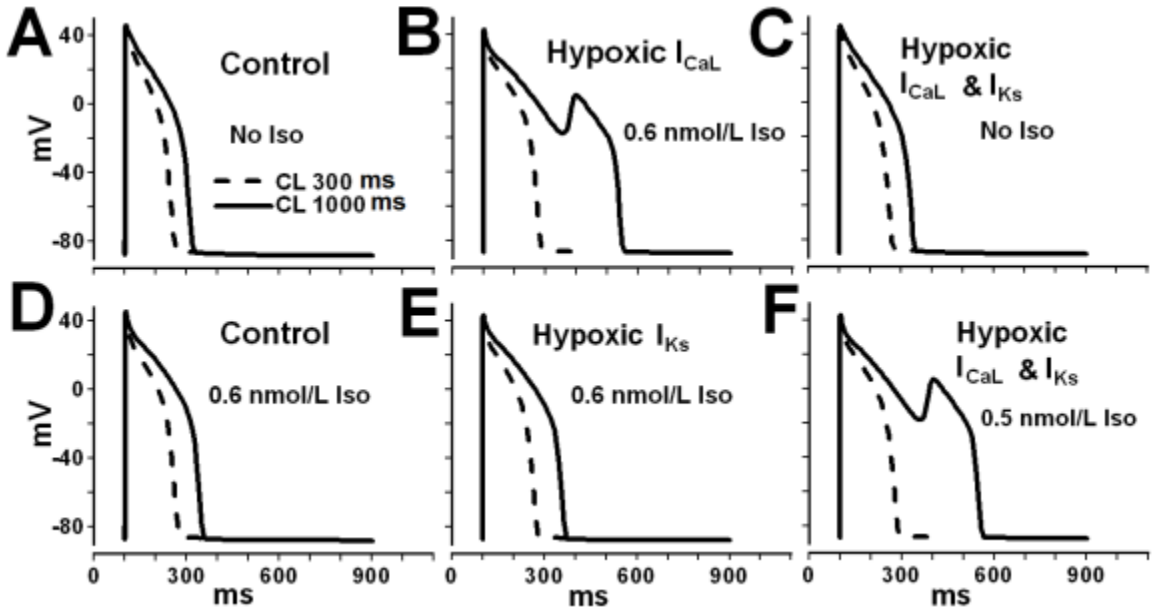

Figure 2-5 The effect of hypoxia and ISO on the AP and induction of EADs. (A) Simulation data showing an AP paced at 300ms and 1000ms cycle length (CL) in a normoxic cell (B) the effect of hypoxic I_{CaL} and ISO (C) the effect of hypoxic I_{CaL} and I_{Ks} and no ISO (D) the effect of ISO in a normoxic cell (E) the effect of hypoxic I_{Ks} and ISO and (F) the combined effect of hypoxic I_{CaL}, I_{Ks} and ISO.

2.4.5 Effects of hypoxia on I_{Ks} and the AP in the presence of βAS

Next we investigated the effect of hypoxic I_{Ks} on the AP while varying the amount of ISO. We kept the values of other ion channels and transporters at normoxic levels in the model, except I_{NaL} and I_{Na} which were set at hypoxic values. We examined the effect of 0.6nmol/L ISO in the presence of hypoxic I_{Ks} at CL of 1000ms. From Figure 2-5E it is seen that EADs were not observed for either CL of 1000ms or 300ms. The APD_{90} for CL of 1000ms was increased by 26% compared to control (from 225ms to 284ms) and for CL of 300ms 11% (from 160ms to 177ms). EADs were not generated over a wide range of Iso concentrations when only I_{Ks} channels were made hypoxic. This is due to the early enhancement of I_{Ks} as a result of increased sensitivity to ISO during hypoxia ($K_{0.5}$ = 1.9nmol/L).

2.4.6 Combined effects of hypoxia on I_{Ks} and I_{CaL} in the presence of βAS

Next we modeled the combined effects of hypoxic I_{CaL} and I_{Ks} in the presence of βAS. We progressively increased the concentration of ISO in the cell until EADs were observed at CL of 1000ms. The level of ISO at which EADs first occurred was 0.5nmol/L. The APD_{90} at CL of 300ms was increased by 14% to 182ms and for CL 1000ms by 103% to 457ms (Figure 2-5F). The concentration of ISO that induces EADs is lower than $K_{0.5}$ for activation of I_{Ks} during hypoxia (1.9nmol/L) implying that I_{Ks} current magnitude remains close to the basal hypoxic level and is not sufficient to counter the pro-arrhythmogenic effects of I_{CaL}.

In summary, the simulations predict that during periodic pacing in the presence of βAS, the primary reason for EAD generation during hypoxia is increased I_{CaL}. This effect may be augmented by the reduced outward current produced by I_{Ks} during hypoxia.

However, the effect of hypoxia on I_{Ks} alone is insufficient to generate EADs. In addition, βAS is necessary to induce EADs, as EADs are never observed under hypoxic conditions in the absence of βAS.

2.4.7 Effects of hypoxia on post-pause APs

During periodic pacing, the simulations did not generate EADs in a cell paced at CL of 300ms. However, a case of clinical importance is periodic excitation followed by a pause (Viskin et al., 2000). We examined the effect of a 1000ms pause on a cell paced at a regular rate at 300ms CL. In the absence of βAS EADs were not induced when the effects of hypoxia on I_{CaL} (Figure 2-6B), on I_{Ks} (Figure 2-6C), or the combined effects of hypoxia on I_{CaL} & I_{Ks} were included (Figure 2-6D).

The concentration of ISO that produced a threshold for EAD generation for hypoxic I_{CaL} was 0.6nmol/L ISO (Figure 2-6B). At this concentration, EADs were not generated in a control or hypoxic I_{Ks} cell (Figures 2-6A and 2-6C). The combined effect of hypoxic I_{CaL} and I_{Ks} on a post-pause AP is shown in Figure 2-6D. The threshold concentration of ISO for induction of EADs decreases from 0.6 to 0.4nmol/L. We conclude that in a post-pause AP, the primary cause for EAD formation is the effect of hypoxia on I_{CaL} in the presence of βAS. Reduced I_{Ks} plays a secondary role and does not by itself induce EADs at ISO concentrations that generate EADs as a result of increased I_{CaL}.

2.4.8 Sustained triggered activity

In the model, when we only include the effect of ISO on inward rectifier K^+ current (I_{K1}) (Koumi et al., 1995), in the absence of hypoxia, there is no evidence of rhythm disturbance (result not shown). APs follow the periodic pacing and when pacing

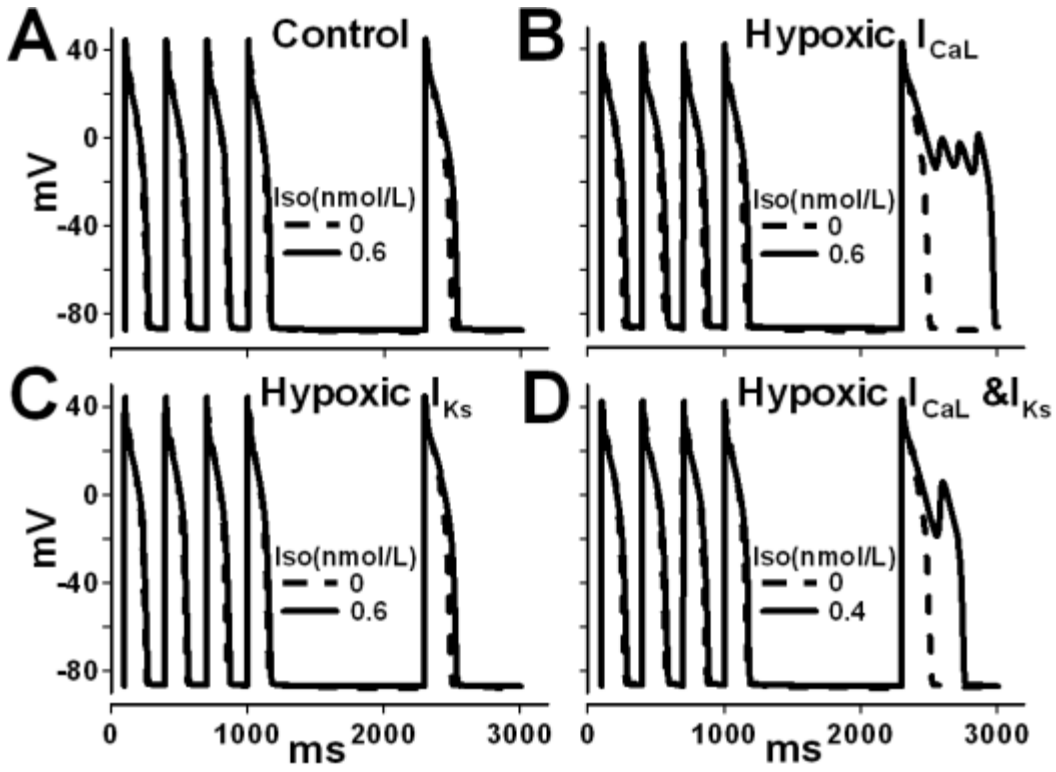

Figure 2-6 The effect of pause during hypoxia in the absence and presence of ISO. (A) Simulated AP pre- and post-pause in a control cell (normoxia) (B) cell with hypoxic I_{CaL} alone (C) cell with hypoxic I_{Ks} alone and (D) cell with combined hypoxic I_{CaL} and I_{Ks}.

is stopped after 50 seconds, the cell becomes quiescent. Similar results were obtained for a hypoxic cell. However in the presence of 1nmol/L ISO with its time-dependent effect on I_{CaL} and I_{Ks} and instantaneous effect on I_{K1}, the hypoxic cell generates EADs. Shortly thereafter, the cell generates triggered non-paced beats (Figure 2-7). The pattern of EADs and triggered beats continues until pacing is stopped after the 50^{th} beat. After cessation of pacing, the cell continues to beat periodically with a CL of 464ms. There is no evidence of spontaneous activity in a control (non-hypoxic) cell in the presence of 1nmol/L Iso (result not shown).

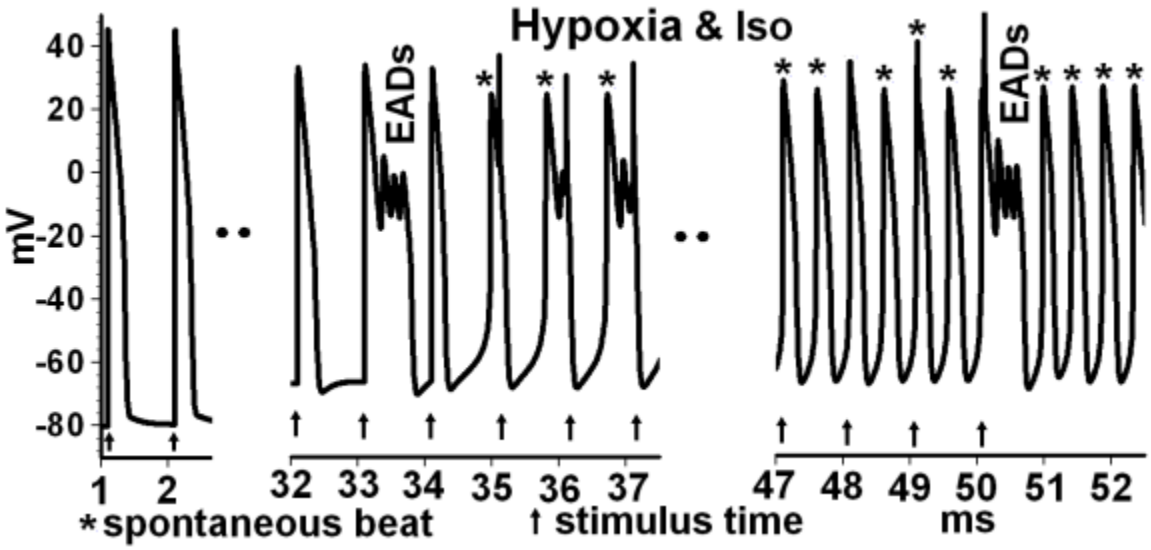

Figure 2-7 The effect of hypoxia and ISO on the generation of sustained triggered activity. Vertical arrows indicate application of pacing stimulus. Asterisks indicate spontaneous (triggered) APs.

2.4.9 Experimental effects of hypoxia on the AP in the absence and presence of βAS

We investigated experimentally in guinea-pig ventricular myocytes the model predictions of the effects of hypoxia in the absence and presence of βAS. Reducing PO_2 from normoxic (PO_2 of 150mmHg) to hypoxic conditions (PO_2 of 17mmHg) for 60s did not significantly alter RMP, APP or APD (Figure 2-8A). We then exposed the myocyte to hypoxia in the presence of 1nmol/L ISO, a concentration of the βAS agonist that is sub-threshold for activation of I_{CaL} and I_{Ks} at normoxia (see Figure 2-3). The addition of ISO did not alter RMP (-81±3mV vs -81±3mV) or APP (45±2mV vs 44±2mV), but significantly increased APD by 10% (182±20ms vs 201±25ms, $P<0.05$, n=5). Increasing the concentration to 3nmol/L ISO significantly increased APD by 32% without altering RMP or APP (Figure 2-8B). Three of seven cells exposed to hypoxia + 3nmol/L ISO generated EADs and then started to beat spontaneously at CL of about 500ms, close to the CL of 464ms predicted by the model (Figure 2-8C & D). The upstroke velocity $(dV/dt)_{max}$ of a paced beat was 138 mV/ms and of a spontaneous beat 73.5 mV/ms. This

confirms the model prediction (not shown) that the upstroke in a paced beat is generated by I_{Na} and in a spontaneous beat by I_{CaL}. Importantly, 3nmol/L ISO did not alter AP parameters under normoxic conditions (RMP = -78±3mV vs. -79±4mV, APP = 41±5mV vs. 38±6m, APD= 238±55ms vs 233±58ms, all P>0.5, n=3), indicating that it is the combination of acute hypoxia and βAS that is responsible for AP prolongation and EAD formation.

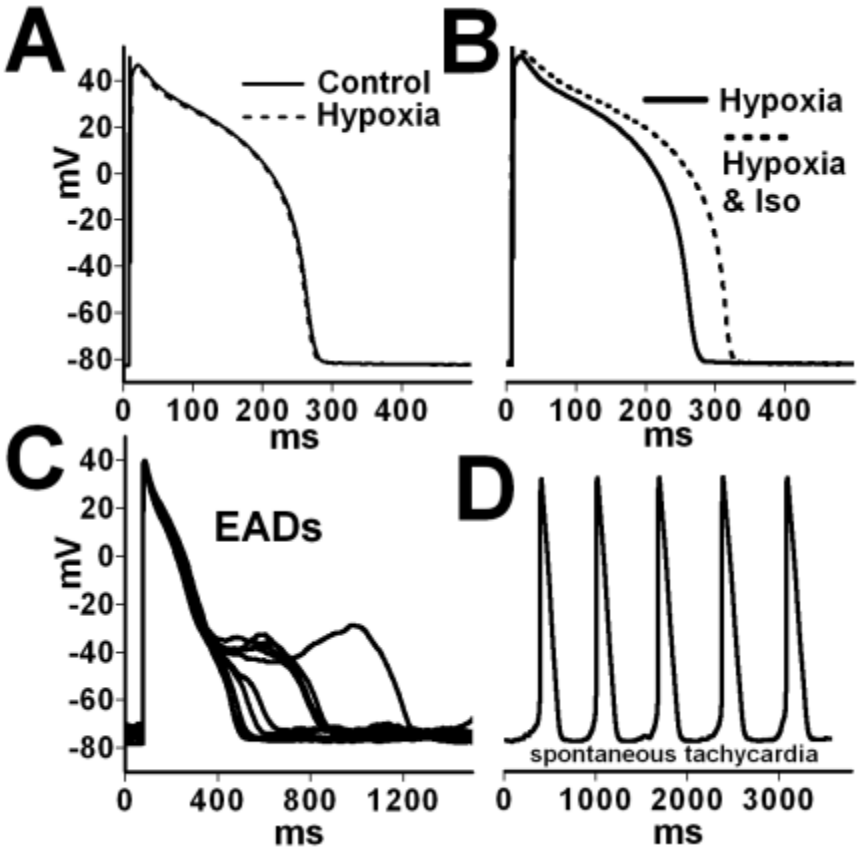

Figure 2-8 Experiments showing the effects of hypoxia and Iso on APs. (A) Effect of reducing PO_2 from 150mm Hg (normoxia) to 17mm Hg (hypoxia) on the AP (B) Effect of hypoxia + 3nmol/L ISO on the AP (C) Progression to EAD formation in the same cell (D) Progression to sustained triggered activity in the same cell. In panel 2-8D, the myocyte was not stimulated and APs were spontaneous

2.5 Discussion

Although it is well recognized that arrhythmias are a significant cause of death in ischemic heart disease, the role of acute hypoxia in induction of arrhythmia is not well understood. We incorporated all published data reporting the effects of acute hypoxia on I_{Na}, I_{CaL}, I_{Ks} and I_{Kr} into the LRd model of a cardiac ventricular AP and determined the effect on AP morphology and APD. In the absence of βAS, hypoxia has little effect on the AP (Figures 2-2, 2-5, 2-6) even when we modeled the effects of hypoxia on I_{NaL} and I_{Na} at twice the rates reported in published studies (Ju et al., 1994, 1996; Wang et al., 2007). In the presence of βAS in a paced cell, EADs are generated only at CL of 1000ms when the effects of hypoxia on I_{CaL} are modeled alone or together with hypoxic I_{Ks} (Figure 2-5). Experimental results confirm the modeling results (Figure 2-8). Similar results were obtained for pause-induced EADs at a shorter CL of 300ms (Figure 2-6). EADs quickly degenerate into spontaneous tachycardia only in a hypoxic cell in the presence of 1nmol/L ISO when we also include the effect of ISO on I_{K1} (Figure 2-7).

Oxygen is the substrate for the production of reactive oxygen species. A rapid decrease in oxygen tension that is not energy limiting (and not ATP depleting; thus ATP dependent potassium current (I_{KATP}) is not activated) is associated with a decrease in cellular reactive oxygen species and a more reduced cellular redox state (Hool, 2000; Hool and Arthur, 2002; Hool et al., 2005; Michelakis et al., 2002; Weir and Archer, 1995; Weir et al., 2002). Electrophysiological effects of acute myocardial ischemia where there is complete cessation of perfusion and I_{KATP} plays an important role has been investigated elsewhere.(Shaw and Rudy, 1997) The increase in sensitivity of I_{CaL} to ISO during hypoxia occurs as a result of modification of thiol groups on the channel or a

regulatory protein such as PKA because exposing myocytes to dithiothreitol and intracellular perfusion with catalase mimic the effect of hypoxia.(Hool, 2000; Hool and Arthur, 2002) Our results suggest that a reduced redox state is protective with respect to cellular excitability because we could not induce EADs in a native cell during hypoxia or when modeling hypoxia alone. However in the presence of βAS an increase in calcium influx through I_{CaL} prolongs APD and triggers EADs. The frequency of EADs is influenced by the modal gating of I_{CaL}. Increased ratios of channels gating in mode 2 (that occurs with βAS) are associated with increased frequency of EADs (Tanskanen et al., 2005).

Sympathetic stimulation increases the risk of arrhythmia. β-blockers are the only class of antiarrhythmics that have been demonstrated to decrease mortality (Dorian, 2005). The results of this study are consistent with previously published data indicating that decreasing calcium influx through the channel or decreasing adrenergic stimulation can reduce the incidence of EADs. CaMKII inhibitory peptide can eliminate EADs and ventricular tachycardia (Wu et al., 2002) as can PKA inhibitors and βAS (Dorian, 2005; Gallacher et al., 2007; Mazur et al., 1999; Thomas et al., 2008). We conclude that I_{CaL} is the primary initiator of EADs and spontaneous tachycardia occur during hypoxia as a result of increased sensitivity of the channel to βAS.

Chapter 3. Multiscale modeling of calcium cycling in cardiac ventricular myocyte: Macroscopic consequences of microscopic dyadic function

3.1 Abstract

In cardiac ventricular myocytes, calcium (Ca) release occurs at distinct structures (dyads) along t-tubules, where L-type Ca channels (LCCs) appose sarcoplasmic reticulum (SR) Ca release channels (RyR2s). We developed a model of the cardiac ventricular myocyte that simulates local stochastic Ca release processes. At the local Ca release level, the model reproduces Ca spark properties. At the whole-cell level, the model reproduces the action potential, Ca currents and Ca transients. Changes in microscopic dyadic properties (e.g., during detubulation in heart failure) affect whole-cell behavior in complex ways, which we investigate by simulating: 1) changes in dyadic volume and number of LCCs/RyR2s in the dyad, 2) effects of calsequestrin (CSQN) as Ca buffer (CSQN buffer) or as luminal Ca sensor (CSQN regulator). Results: 1) Increased dyadic volume and reduced LCCs/RyR2s decrease Excitation-Contraction coupling gain and cause asynchrony of SR Ca release, while inter-dyad coupling partially compensates for the reduced synchrony. 2) Impaired CSQN buffer depresses Ca transients without affecting synchrony of SR Ca release. 3) When CSQN regulator function is impaired, inter-dyad coupling augments diastolic Ca release activity to form Ca waves and long-lasting Ca release events.

3.2 Introduction

Ca release in a ventricular myocyte occurs in local domains along t-tubules called dyadic spaces. In this space about 50-200 Ryanodine Receptors (RyR2s) in the terminal cisternae of the sarcoplasmic reticulum (SR), called junctional SR (JSR), closely appose 5-15 L-type Ca channels (LCCs) situated along the t-tubules (Franzini-Armstrong et al., 1999). Ca release from RyR2s can occur in two ways: During Excitation-Contraction coupling (ECC), LCCs open in response to membrane potential and cause influx of Ca into the dyadic space from the extracellular space. This Ca influx triggers a much larger Ca release from the RyR2s through a process called calcium-induced-calcium release (CICR) (Fabiato, 1985). Ca release can also occur spontaneously without influx of Ca from LCCs in the dyad (Cheng et al., 1993). A typical ventricular myocyte has about 10,000-50,000 dyads (Bers, 2002). Global macroscopic Ca release in the whole-cell is then the cumulative sum of microscopic local Ca releases from the dyads. To understand how modifications of Ca release processes at the dyadic level translate into changes in whole-cell Ca behavior, it is necessary to model Ca release processes at the local dyadic level and extend this modeling framework to include sarcolemmal ionic currents, pumps and exchangers to form an integrated model of the cell. This is a major objective of the current work, motivated by the fact that various disease processes alter dyadic structure/function to cause abnormal cellular phenotypes.

In a normal ventricular myocyte, t-tubules form a regular network of invaginations mainly in the transverse direction (Soeller and Cannell, 1999). The cell-wide regular network of t-tubules ensures that Ca release occurs nearly synchronously during excitation due to membrane depolarization (Cheng et al., 1994). There is evidence

that in the failing heart, remodeling processes lead to disarray of t-tubules (Song et al., 2006b). A family of proteins known as junctophilin-2 (JPH2) plays a role in co-localization of t-tubules and SR, thereby ensuring proper coupling between LCCs and RyR2s in the dyad (Takeshima et al., 2000). JPH-2 deficiency has been reported during heart failure and can lead to depressed contractility as well as hyperactive RyR2s (van Oort et al., 2011). Such deficiencies may result in changes of structural dyadic properties. ECC in a ventricular myocyte can be quite sensitive to structural changes in the dyad that affect the coupling between LCCs and RyR2s in tight restricted spaces. It is important to understand how such changes on the molecular scale alter the whole-cell ECC gain and other cellular properties.

Calsequestrin (CSQN), a native SR protein can play an important role in the CICR process by functioning both as a Ca buffer in the SR (MacLennan and Wong, 1971) and as a luminal Ca sensor by regulating RyR2 openings via interaction with anchoring proteins Triadin (Tn) and Junctin (Jn) (Gyorke et al., 2004). Recently, mutations in CSQN that cause changes in its Ca buffering capacity or its ability to interact with RyR2 (Dirksen et al., 2007; Rizzi et al., 2008) have been implicated in hereditary cardiac arrhythmias. The mutation-induced disturbances occur at the level of the dyad, but have important global consequences at the level of the whole cell. Understanding relationships between dyadic processes and whole-cell function requires a multiscale model of Ca cycling.

Motivated by the examples above, the major goals of this work are: (i) To develop a gating model of RyR2 in which RyR2 opening is a function of cytosolic Ca and CSQN. (ii) To create a model of the dyad that takes into account the stochastic nature of LCC

and RyR2 openings. (iii) To build a multiscale model of ventricular myocyte Ca cycling and electrophysiology and (iv) To investigate how changes in microscopic properties of the dyad affect whole-cell behavior. We examine the following changes in dyad properties: (a) Impaired buffering capacity of CSQN. (b) Impaired luminal Ca sensor function (RyR2 gating regulation by CSQN). (c) Changes in the number of LCCs/RyR2s in the dyad and (d) changes in dyadic volume.

3.3 Methods

Summary of important model properties is presented. Detailed methods, descriptions, definition of variables and abbreviations, and model equations are provided in Appendix B. Formulation of sarcolemmal ionic currents, pumps and exchangers are adapted from the existing guinea-pig ventricular myocyte model (Faber et al., 2007). The following subscripts are used in abbreviations: **SR** - sarcoplasmic reticulum, **NSR** - network SR, **JSR** - junctional SR, **ss** –subsarcolemmal space (submembrane), **d** – dyadic space, **i** – myoplasm. Superscripts **cell** and **dyad** denote whole-cell and dyadic values, respectively.

3.3.1 Dyad Model

Each dyad (diagram in Figure 3-1) comprises the following Ca distribution compartments: myoplasm, NSR, JSR, dyadic space and submembrane space. In the control myocyte model, it is assumed that 15 LCCs and 100 RyR2s are present in a dyad.

3.3.2 Multiscale Ventricular Myocyte Model

Figure 3-1 shows schematic diagram of the multiscale ventricular myocyte model and its components. The model consists of 10,000 dyads in which Ca release occurs stochastically. Each dyad communicates with its neighboring dyads via Ca diffusion in

the NSR and the dyadic space. Membrane ionic currents, pumps and exchangers sense local Ca concentrations in their compartment. Dyadic concentrations are averaged to represent whole-cell macroscopic values. Dyadic currents are added to represent whole-cell values.

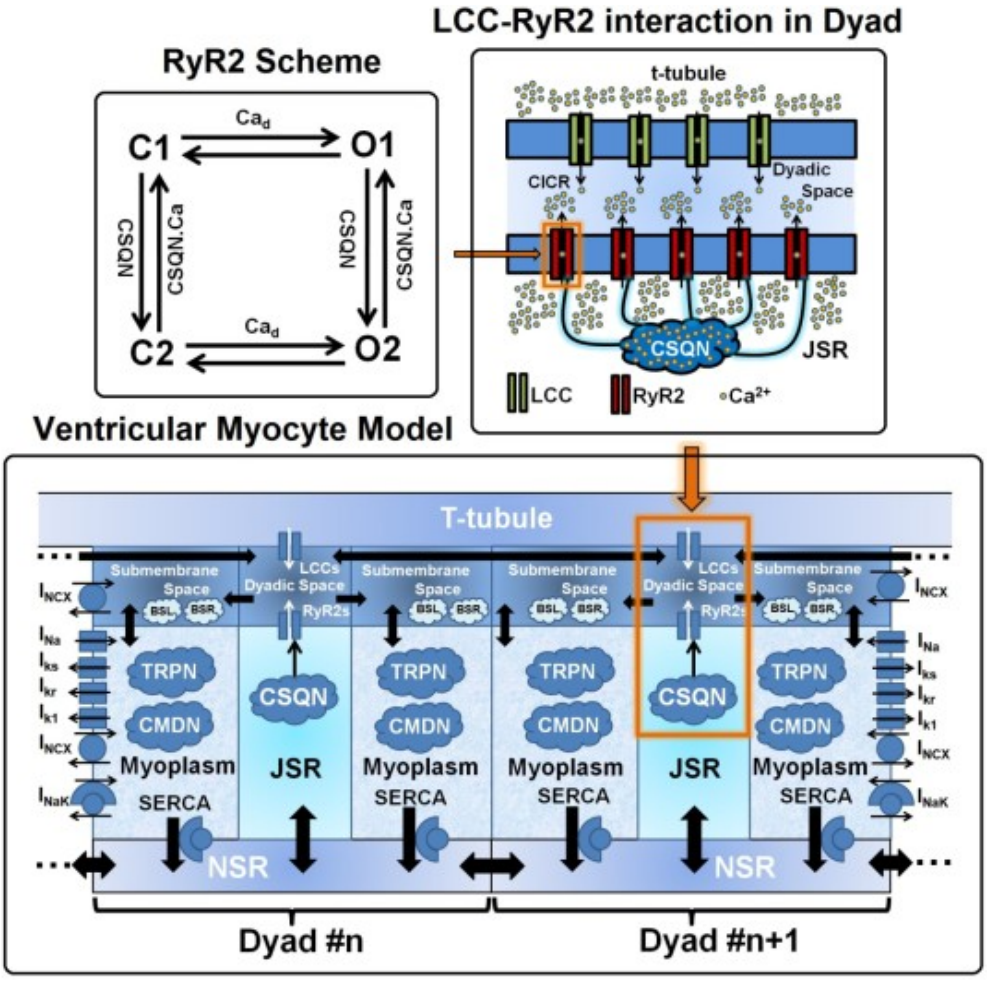

Figure 3-1 Schematic diagram of the multiscale ventricular myocyte model and its components. The model consists of 10,000 diffusively coupled Ca release units (CaRUs) also called dyads. Each dyad consists of five distinct Ca compartments: Network Sarcoplasmic Reticulum (NSR), Junctional Sarcoplasmic Reticulum (JSR), dyadic space, submembrane space and myoplasm. Ca concentration is assumed to be uniform in each compartment. The number of L-type Ca channels (LCCs) and SR Ca release channels (RyR2s) in a dyad is 15 and 100, respectively, and their states fluctuate stochastically. State diagram of the Ryanodine Receptor (RyR2) model is shown in the upper left corner. LCC-RyR2 interaction in a dyad is shown in the upper right corner. Ca release occurs in the dyadic space.

Calsequestrin (CSQN) is a Ca buffer that also regulates RyR2 openings. JSR is defined as domain of CSQN distribution so CSQN is in all of JSR. Sarcolemmal buffers (BSL) and SR buffers (BSR) are in the submembrane space. Calmodulin (CMDN) and troponin (TRPN) are Ca buffers in the myoplasm. All Ca-dependent membrane currents, pumps and exchangers sense Ca concentration in the compartment in which they reside. Important currents that determine membrane potential are shown. Diffusive Ca fluxes are indicated by solid thick arrows. Equations for the model are in Appendix B.

3.3.3 RyR2 Model

The Markov model of RyR2 (Figure 3-1) consists of 4 states and two tiers of modal gating (upper and lower). The upper tier is the activation tier and lower tier the refractory tier. K_m for Ca activation in the lower tier is 10 times higher than K_m in the upper tier (150 μM vs. 15 μM). The detailed description of the RyR2 model is presented in Appendix B.

3.3.4 CSQN Regulator (Luminal Ca Sensor)

Transition of RyR2 channel states between the activation tier and refractory tier depends upon CSQN. This dependence represents the luminal Ca sensor function of CSQN in the model. The detailed description of the luminal Ca sensor is presented in Appendix B.

3.3.5 CSQN Buffer

CSQN has a total capacity of absorbing 10 mM Ca with a half constant (K_d) of 0.8 mM. It is assumed that Ca binds instantaneously to CSQN.

3.4 Results

The multiscale model of the cardiac ventricular myocyte scales processes from stochastic single channel openings of RyR2s and LCCs to the whole-cell action potential (AP) and Calcium transient (CaT). In the first half of the results section, we present model simulations of normal physiological processes at both the local dyadic level and at

the whole-cell level and show their correspondence across scales. These simulations serve to evaluate and validate the model. In the second part of the Results section we discuss the macroscopic (whole-cell) consequences of changes in the microscopic properties of the dyad.

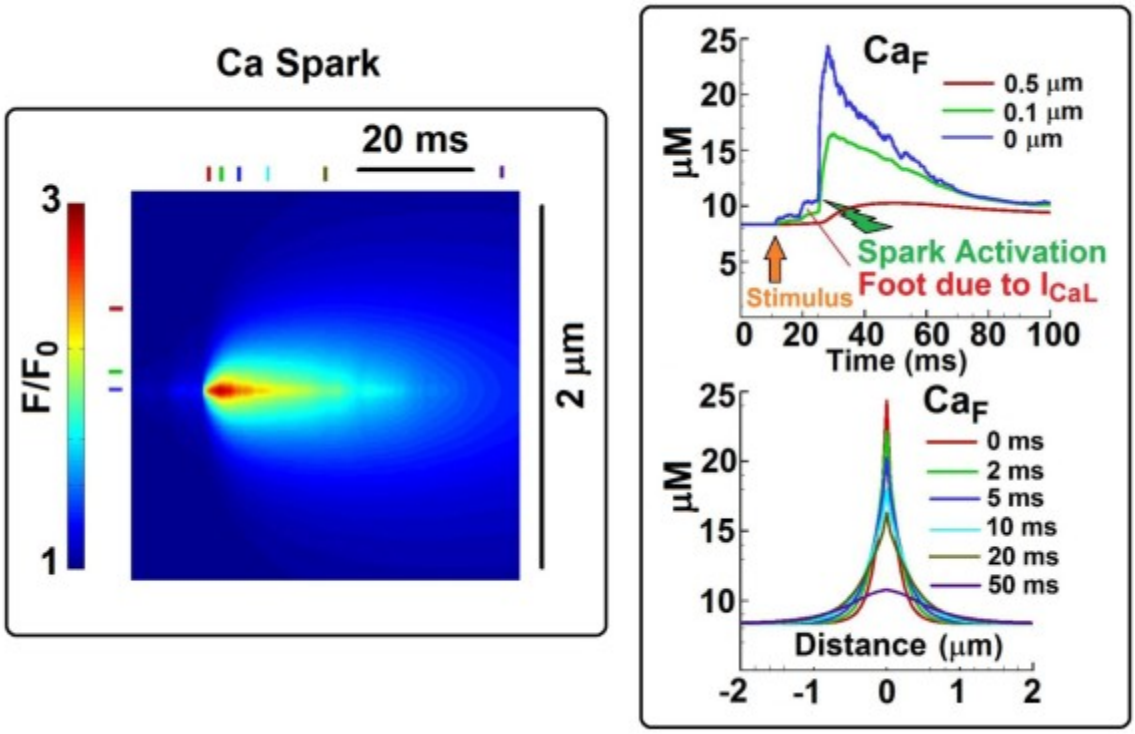

Figure 3-2 Simulated image of Ca spark. Left. Simulated Ca spark (line-scan). Ca_F indicates concentration of Ca-bound Fluo-3 dye. Right, Top. Temporal profile of Ca_F at three different locations: the spark center (blue), 0.1 μm (green) and 0.5 μm (red). Right, Bottom. Spatial profile of Ca spark at several time points after initiation. It is assumed that the line scan passes through the spark origin.

In particular, we are interested in whole-cell consequences of changes in structural properties of the dyad, including volume of the dyadic space and number of LCCs/RyR2s in the dyad. Pathologically, such changes may occur during detubulation in a failing heart (Song et al., 2006a). We are also interested in whole-cell consequences of impaired function of CSQN either as a buffer of Ca, or as a regulator of RyR2 function (or both). Impairment of CSQN function has been implicated in genetic mutations that

lead to cardiac arrhythmias (Dirksen et al., 2007; Rizzi et al., 2008). The model allows us to investigate separately the role of CSQN buffer and the role of CSQN regulator in these pathologies. In addition, we investigate the effects of inter-dyad coupling via Ca diffusion on whole-cell function when the above changes in dyadic properties are present.

3.4.1 Normal Physiological Function

3.4.1.1 Simulated Ca Spark

Figure 3-2 shows a simulated Ca spark during myocyte pacing at 1 Hz. Temporal profile of fluorescent-dye bound Ca (Ca_F) at 0, 0.1 and 0.5 μm from the spark center is shown (right top). Following the stimulus, a small "foot" of Ca increase due to I_{CaL} is seen before the Ca spark activates, similar to a sparklet-triggered spark observed in (Wang et al., 2001). The spatial profile of Ca spark at 0, 2, 5, 10, 20 and 50 ms after the initiation of the Ca spark is also shown (right bottom). The simulated Ca spark properties are consistent with experiments (Cheng et al., 1993) and with simulated Ca sparks generated with either a square pulse of Ca release (2 pA for 10 ms) (Smith et al., 1998) or by a square pulse of Ca trigger (0.5 pA for 0.5 ms) (Sobie et al., 2002a).

3.4.1.2 RyR2 Model Response to Cytosolic and SR Ca

Figure 3-3, left panel, shows simulated single channel RyR2 records for 15 μM Ca_d and for 100 μM and 2 mM Ca_{SR}. Experiments performed with native RyR2s in lipid bilayers (Gyorke and Gyorke, 1998) for *cis* Ca concentration of 1 μM, and *trans* Ca concentrations of 20 μM and 5 mM are shown on the right. Open probability of the channel at 15 μM Ca_d for different Ca_{SR} is shown in Figure 3-3B (left: model; right: experiment). The model behavior is similar to that seen in experiments. Quantitative

differences can be attributed to the different environment of RyR2 in the cell and in lipid bilayers.

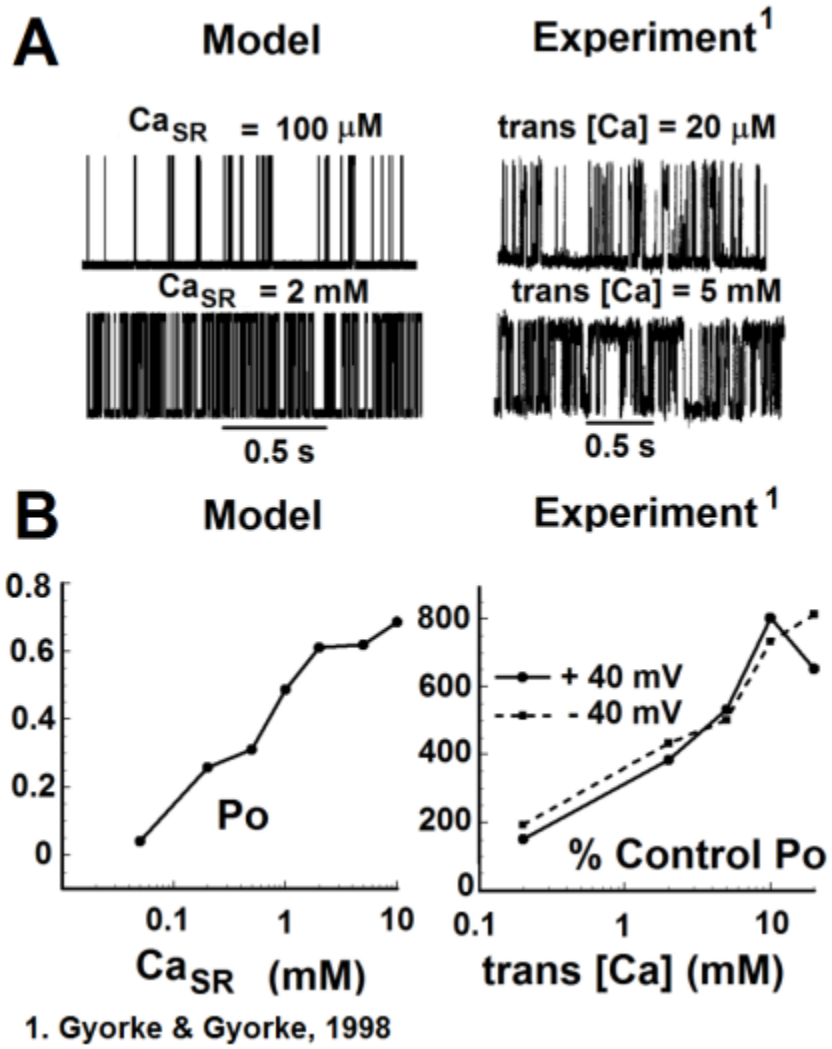

Figure 3-3 RyR2 model response. (A) Simulated (left) and experimentally measured (right) single channel current records of RyR2 in response to Ca. In the model, the dyadic space Ca (Ca_d) is held at 15μM and records are shown for two different SR Ca (Ca_{SR}): 100 μM and 2 mM. In experiments (Gyorke and Gyorke, 1998), *cis* [Ca] is held at 1 μM and traces are shown for two different *trans* [Ca]: 20 μM and 5 mM. (B) Open probability (Po) of RyR2 as a function of Ca_{SR} at 15 μM Ca_d. In the simulation (left) Po represents absolute open probability. In the experiments (right) Po is plotted relative to control conditions at 20 μM

trans [Ca] and 1 μM *cis* [Ca]. The solid line is for +40 mV voltage difference between the *cis* and *trans* (*cis* – *trans*) compartments of the lipid bilayer. The dashed line is for a voltage difference of -40 mV

3.4.1.3 Ca Currents and Ca Concentrations in a Single Dyad during Pacing

Simulated Ca currents and Ca concentrations in one of the dyads during an AP, when the cell is paced at 1 Hz, are shown in Figure 3-4. During pacing at 1 Hz in response to membrane voltage, Ca influx via I_{CaL}^{dyad} begins shortly after the AP upstroke. Peak I_{CaL}^{dyad} reaches -0.11 pA, and SR Ca release occurs 5 ms after peak I_{CaL}^{dyad} has been reached. Peak Ca release current reaches 4 pA and decays over 15 ms, consistent with reported values of elementary SR Ca release current and decay time course (Cheng et al., 1993). Following release termination, release channels become refractory for the remaining duration of the AP plateau. Ca_d^{dyad} peaks at 150 μM and decays over 20 ms, following the time course of SR Ca release. This result is consistent with the graded nature of ECC which states that under normal physiological conditions, a given Ca influx via LCCs triggers a much greater Ca release via RyR2s (Wier and Balke, 1999) and therefore Ca_d^{dyad} is governed by SR Ca release. Local SR Ca, Ca_{SR}^{dyad}, decays from 1.3 mM to a nadir of 1 mM and recovers in ~ 250 ms, consistent with the finding that diastolic Ca_{SR} is only partially depleted during contraction (Shannon et al., 2003). The results demonstrate that substantial differences in peak concentration and time course of Ca exist among different local Ca compartments within the dyad during ECC.

3.4.1.4 Whole-cell (macroscopic) Ca currents and Ca concentrations during pacing

Steady state action potential (AP) at 1 Hz together with whole-cell I_{CaL}^{cell} and J_{rel}^{cell} are shown in Figure 3-5, as are compartmental Ca concentrations. The duration of whole-cell Ca release flux, J_{rel}^{cell}, and of average dyadic space Ca transient, Ca_d^{cell}, is in the range

of 20-30 ms, similar to the duration of local Ca release events. However, the rise time of these whole-cell parameters is slower, and peak Ca_d^{cell} is lower than local Ca_d^{dyad}, reflecting slight temporal dispersion in the occurrence of local Ca release events.

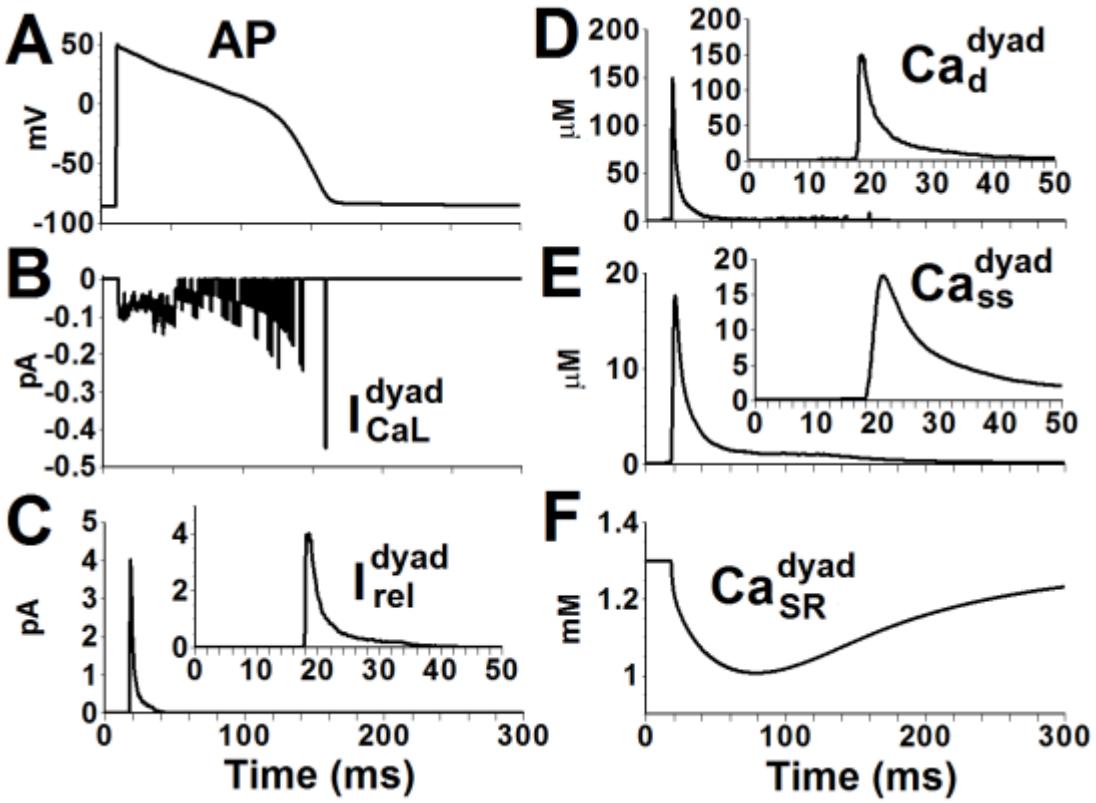

Figure 3-4 Ca currents and Ca concentrations in a single dyad during pacing. (A) Action Potential (AP). (B) L-type Ca current (I_{CaL}^{dyad}). (C) Ca release current (I_{rel}^{dyad}). (D) Dyadic space Ca concentration (Ca_d^{dyad}). (E) Submembrane Ca concentration (Ca_{ss}^{dyad}). (F) Free SR Ca concentration (Ca_{SR}^{dyad}). Insets in C, D and E show expanded time scale.

The global SR Ca depletion profile is similar to that of local SR Ca depletion (Ca_{SR}^{cell} *vs* Ca_{SR}^{dyad}), indicating that SR Ca depletion occurs uniformly throughout the cell. The different shape of I_{CaL}^{dyad} and I_{CaL}^{cell} can be attributed to the small number of LCCs in

the dyad.

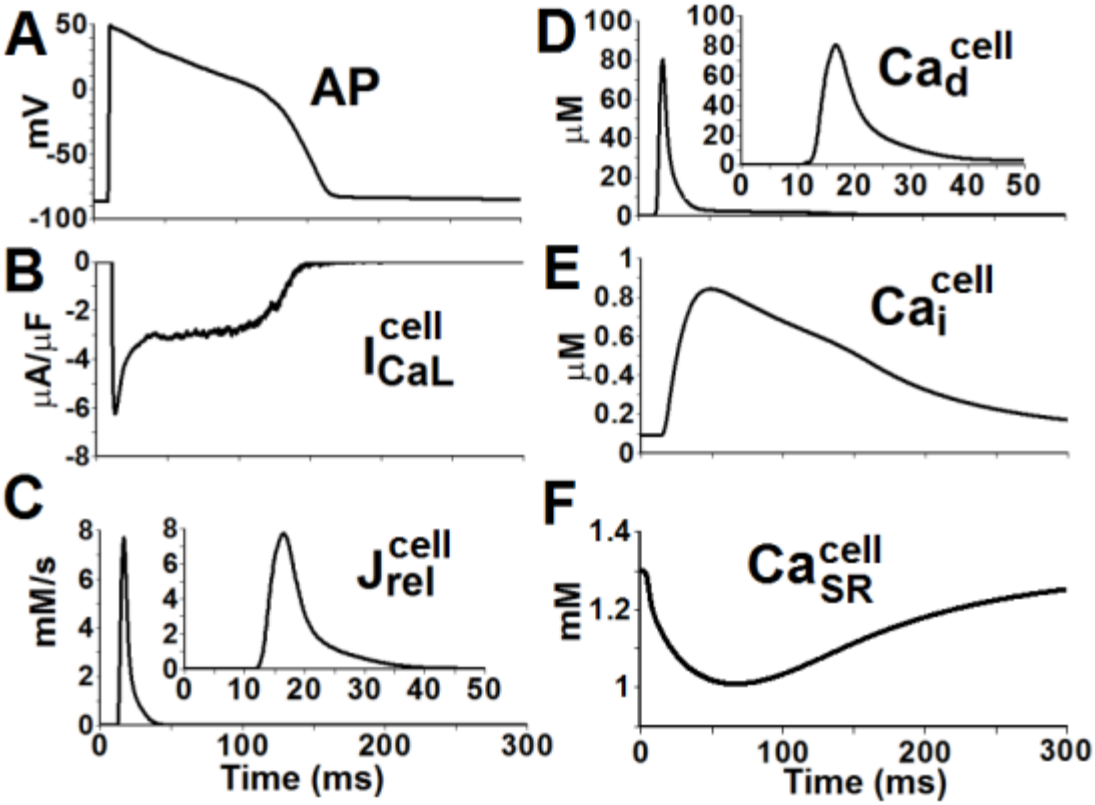

Figure 3-5 Whole-cell Ca currents and Ca concentrations during pacing. (A) AP. (B) L-type Ca current (I_{CaL}^{cell}). (C) Ca release flux from SR (J_{rel}^{cell}). (D) Average Ca concentration in the dyadic space (Ca_d^{cell}). (E) Ca transient in the myoplasm (Ca_i^{cell}). (F) Average free Ca concentration in the Sarcoplasmic Reticulum (Ca_{SR}^{cell}). Insets in C and D show expanded time scale.

3.4.1.5 Graded Release and Variable Gain and Rate Dependence of Myoplasmic Na and Ca

LCCs and RyR2s interact in local dyadic spaces and stochastic openings of local LCCs can trigger openings of local RyR2s. The magnitude of Ca entry via LCCs determines the number of RyR2 openings and therefore the magnitude of SR release. This phenomenon of graded release is reproduced by the model as demonstrated in Figure 3-6A, showing that peak RyR2 flux is a graded function of peak LCC flux.

Another property of a cardiac myocyte is variable gain. The ratio of Ca released from the SR to Ca entry into the myocyte, also known as gain, is a function of the transmembrane potential. The model

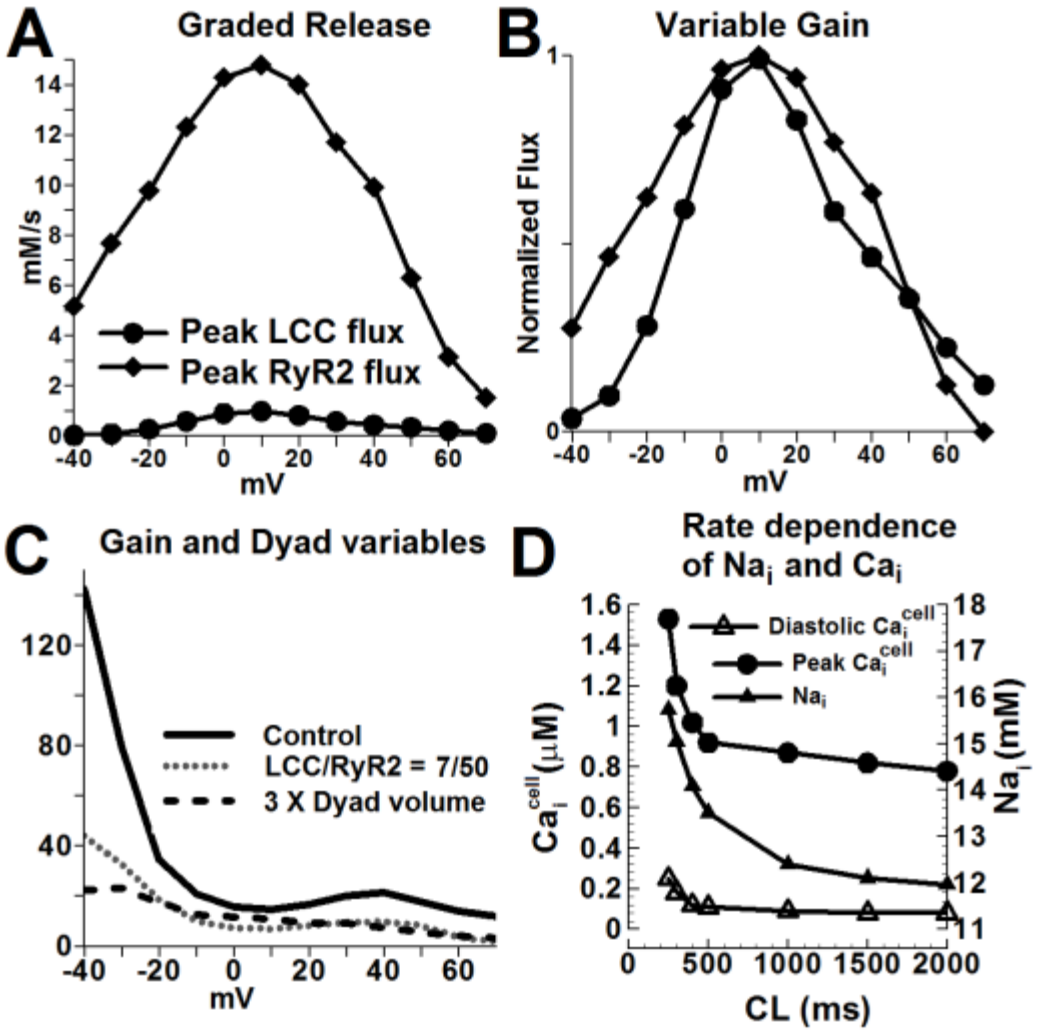

Figure 3-6 Graded release, variable gain, effect of dyad properties on ECC and rate dependence of myoplasmic Na_i and Ca_i. (A) Peak LCC Ca flux and peak Ca release flux as a function of transmembrane voltage. (B) Normalized peak LCC Ca flux and peak Ca release flux. (C) ECC Gain for three conditions: (i) Control (100/15 RyR2/LCC ratio, 2 X 10^{-19} L dyadic volume), (ii) 50/7 RyR2/LCC ratio, 2 X 10^{-19} L dyadic volume, (iii) 100/15 RyR2/LCC ratio, 6 X 10^{-19} L dyadic volume. Initial conditions were those of a paced myocyte at 1 Hz. After 5 ms the cell was clamped at the voltage indicated on the x-axis. (D)

Myoplasmic Na_i and Ca_i rate dependence. Steady-state (after 1000 beats of pacing) Na_i, peak Ca_i and diastolic Ca_i as a function of cycle length (CL).

reproduces this property. For example, in Figure 3-6B, for a different magnitude of peak LCC flux at transmembrane voltages of +50 mV and -20 mV, peak RyR2 flux is quite similar. Gain computed in the model as the ratio of peak RyR2 flux to peak LCC flux is a decreasing function of voltage (Figure 3-6C). Gain at 0 mV is 15.8, similar to the value of 16 measured in the rat (Wier et al., 1994).

Simulated Na_i, peak Ca_i^{cell} and diastolic Ca_i^{cell} as a function of pacing rate are shown in Figure 3-6D. Both Na and Ca ions accumulate increasingly in the cell as pacing frequency is increased, consistent with previous results (Faber et al., 2007).

3.4.2 Macroscopic Consequences of Changes in Microscopic Dyadic Function

3.4.2.1 Effects of Alterations of Dyadic Structure on ECC

Since ECC occurs at local domains of the dyad, changes in structural dyadic properties that alter the functional interaction between LCCs and RyR2s during CICR can have significant effects on the Ca release process. Such structural alterations are observed in failing or hypertrophic hearts (Gomez et al., 2001; Gomez et al., 1997). Figure 3-6C shows the ECC gain curve (defined as ratio of peak RyR2 Ca release flux to peak LCC Ca influx) when the dyadic space volume is increased by a factor of 3 (*solid line* is control) simulating increased separation between LCCs and RyR2s during tubular disarray. The *dotted line* shows the gain curve when the numbers of RyR2s/LCCs are reduced to 50/7 (from 100/15 in control), simulating structural derangement of channels in the dyad. Gain values are lower than control at all voltages. Taken together, the results support the hypothesis that reduced ECC gain of CICR in certain pathologies that involve

structural changes (e.g. hypertrophy), could be due to microscopic structural defects in the dyads (Gomez et al., 2001).

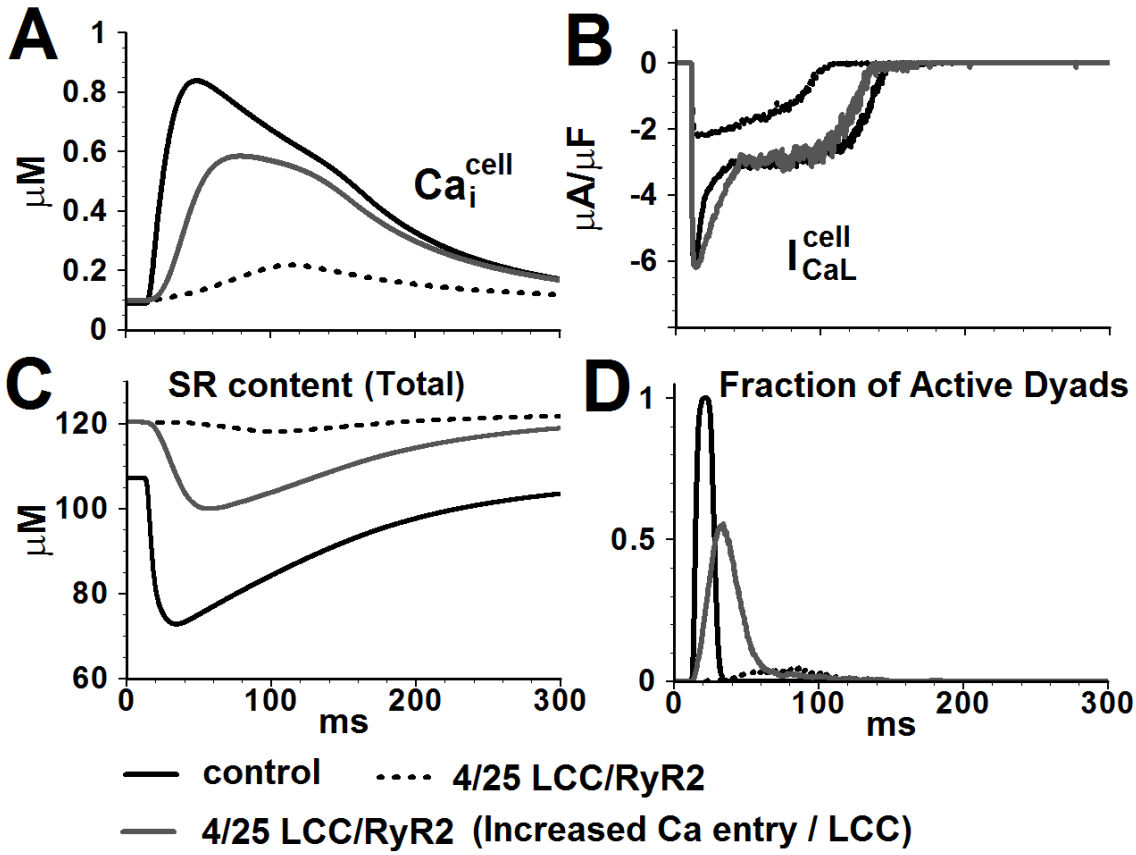

Figure 3-7 Effect of changing the number of functional RyR2s and LCCs in the dyad on whole-cell behavior. (A) Myoplasmic Ca transient (Ca_i^{cell}). (B) L-type Ca current (I_{CaL}^{cell}). (C) Total SR Ca content. (D) Fraction of active dyads.

Effects of structural derangement of channels in the dyad on the whole-cell Ca release process are investigated further in Figure 3-7. In the first set of simulations (*dashed line*; *solid black is control*) the number of functional channels in the dyad is reduced to 4/25 LCC/RyR2, while keeping Ca entry via individual LCC the same. During pacing, Ca transients are severely blunted, indicating near absence of SR Ca release and only few dyads are activated. The likely explanation for such impaired function is that the reduced

number of LCCs in the dyad reduces the functional coupling between LCCs and RyR2s during CICR. We then investigated if increasing Ca entry per LCC can rescue the impaired CICR, as suggested by the positive inotropic effect of Ca channel agonist BayK8644 (Thomas et al., 1985). The second set of simulations (*gray line*) shows a scenario where Ca entry through LCC is increased such that I_{CaL}^{cell} is similar to control conditions, while still keeping the number of channels in the dyad reduced to 4/25 LCC/RyR2. With this manipulation, Ca transients are rescued only partially, indicating that Ca release is still impaired due to asynchronous activation of dyads (panel D). This implies that the number of functional channels, via its effect on synchrony of release, has greater influence on global CaT than the magnitude of Ca entry. These results support the hypothesis that in a failing heart, despite similar whole cell I_{CaL}, smaller amplitude and slowed kinetics of CaT are due to asynchronous activation of Ca sparks (Litwin et al., 2000).

3.4.2.2 Role of Inter-Dyad Coupling in ECC

When the number of LCCs in the dyad was reduced to 7 (from 15 in control) and the inter-dyad coupling was impaired, SR Ca release became asynchronous (Figure 3-8, *black line*) resulting in smaller peak and slower time to peak of CaT. With intact inter-dyad coupling, SR Ca release became more synchronous (*gray line*), indicating that inter-dyad coupling had a synchronizing effect on SR Ca release in this simulated pathology. Similar results were obtained when the dyadic volume was increased 3-fold. Pathologic structural defects associated with heart failure, such as detubulation, may result in reduced number of functional LCCs or increased dyadic space volume. The simulation

results suggest that under such circumstances, SR Ca release becomes asynchronous and inter-dyad coupling serves as a compensatory mechanism that improves synchrony.

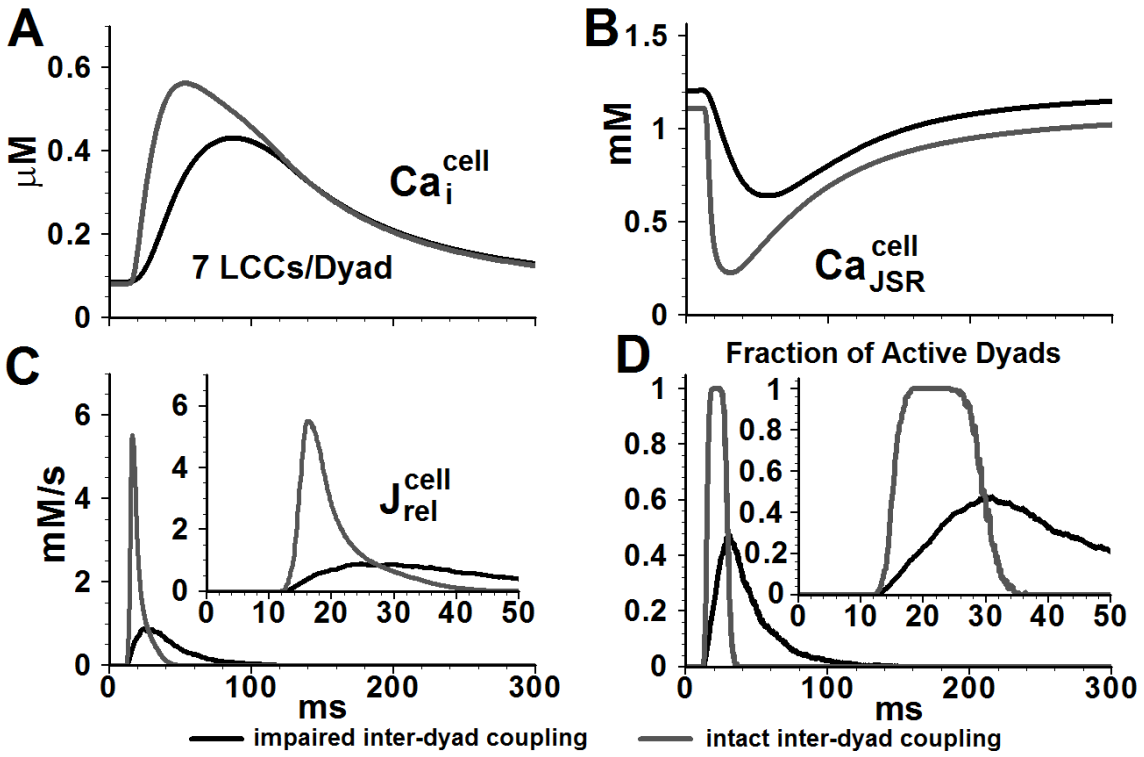

Figure 3-8 Effect of impaired inter-dyad coupling on whole-cell behavior. (A) Myoplasmic Ca transient (Ca_i^{cell}). (B) JSR Ca concentration (Ca_{JSR}^{cell}). (C) Ca release flux (J_{rel}^{cell}). (D) Fraction of active dyads. The myocyte model is paced at 1 Hz. Insets show J_{rel}^{cell} and fraction of active dyads on an expanded time scale.

3.4.2.3 Effects of Impaired CSQN Function

In SR, CSQN can function both as Ca buffer and as a regulator of RyR2 openings (Gyorke et al., 2004; MacLennan and Wong, 1971). Experimentally, it is very difficult, if not impossible, to isolate and study separately the effect of CSQN as a buffer or as a regulator on the SR Ca release process. The model allowed us to differentiate these effects in a controlled manner.

Simulated impaired CSQN *buffering ability* resulted in a smaller Ca release flux, smaller Ca transient and a higher diastolic JSR load (Figure 3-9). Recovery of JSR load after

release was faster. The reduced CICR was not associated with asynchronous activation of dyads (Figure 3-9D); it was reduced due to reduced amount of releasable Ca from SR. Diastolic Ca release events were not observed, despite faster recovery of JSR Ca load.

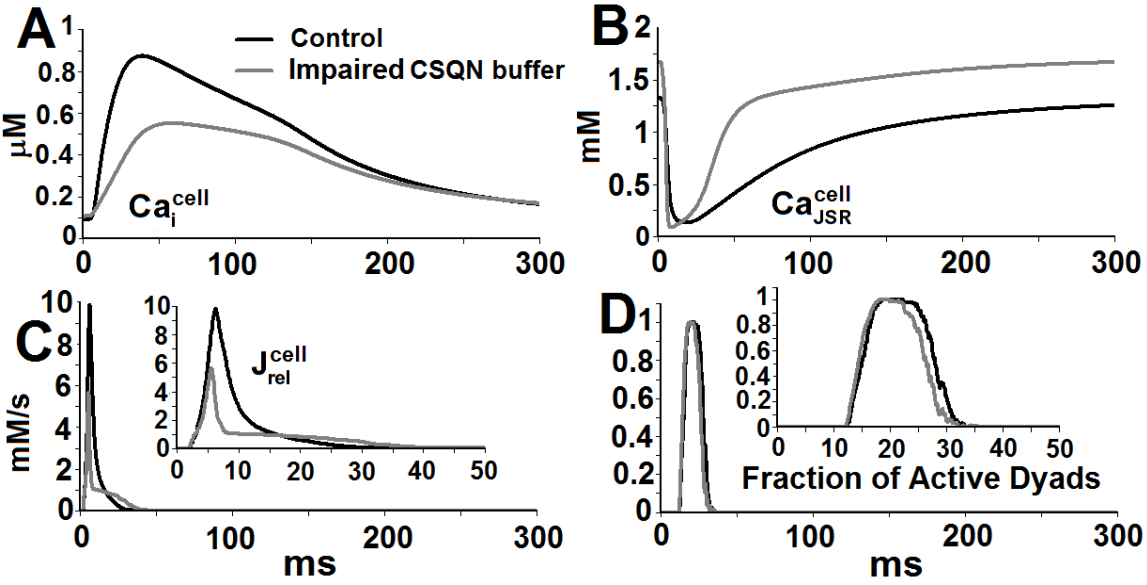

Figure 3-9 Effect of impaired CSQN buffering capacity on whole-cell behavior. (A) Myoplasmic Ca transient (Ca_i^{cell}). (B) JSR Ca concentration (Ca_{JSR}^{cell}). (C) Ca release flux (J_{rel}^{cell}). (D) Fraction of active dyads. The myocyte model is paced at 1 Hz. Insets show J_{rel}^{cell} and fraction of active dyads on an expanded time scale.

Figure 3-10 shows the effect on whole-cell behavior of impaired luminal Ca *sensor function*. In the simulation, the effect of CSQN on RyR2 openings was impaired in the presence of intact (Figure 3-10A-B) or impaired (Figure 3-10C-D) CSQN buffering function, in an attempt to separate the two processes. Multiple diastolic Ca release events in the form of Ca sparks (indicated by yellow arrows) and Ca waves (indicated by white arrows) occur when the CSQN buffer is intact (Figure 3-10 A). Panel B shows that the dyad reactivates during the AP (indicated by #) and activates spontaneously during diastole (indicated by *), indicating abnormal restitution of SR Ca release. In a paced control myocyte model, Ca sparks rarely occur in diastole, due to refractoriness of

RyR2s. In a quiescent myocyte, when RyR2s are in active state, spontaneous Ca spark frequency is calculated to be 40/cell/s, similar to the experimentally recorded frequency in guinea-pigs (Ogrodnik and Niggli, 2010).

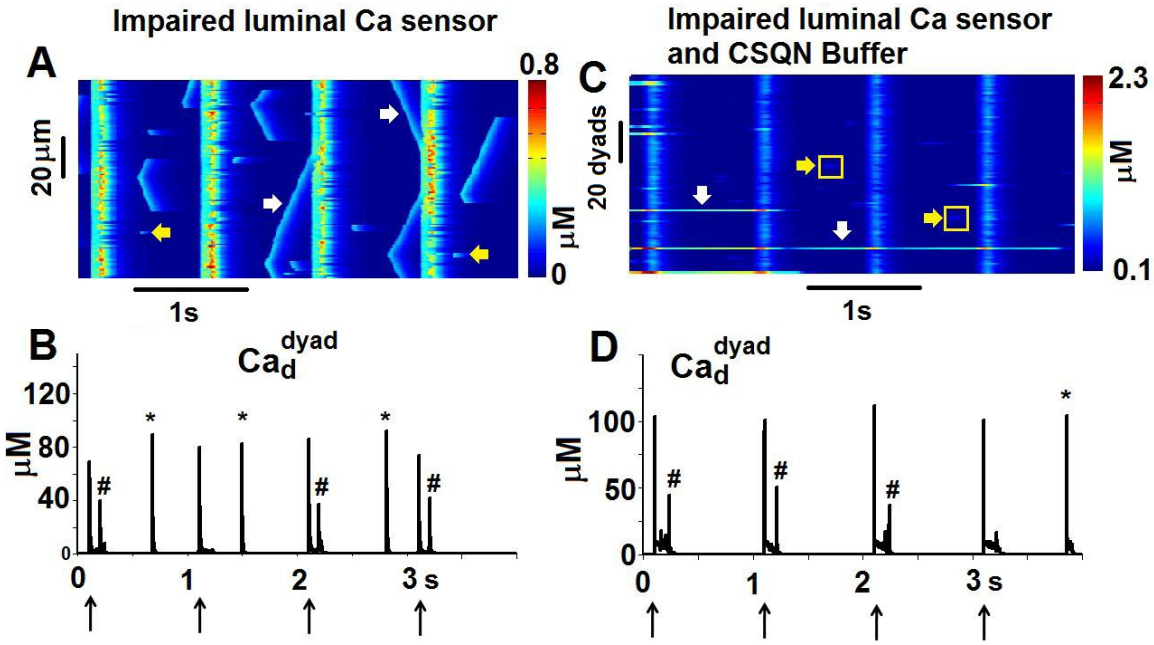

Figure 3-10 Effect of impaired luminal Ca sensor function on whole-cell behavior. (A, B) CSQN Buffer is intact. (C, D) CSQN Buffer is impaired. (A, C) Line scan image of Ca_i^{dyad} (B, D) Dyadic space Ca concentration (Ca_d^{dyad}) in one of the dyads. Arrows in bottom of panels B, D indicate pacing stimuli. Spontaneous diastolic Ca release events in the form of Ca sparks (yellow arrows) and waves (white arrows) are seen in Panel A. Long-lasting Ca release events in few of the dyads (white arrows) and dim Ca sparks (yellow arrows) are seen in panel C. Dyad reactivates during the paced AP (#) and spontaneously activates during diastole (*) in Panels B and D.

When CSQN buffer is also impaired, long-lasting Ca release events occur in few of the dyads, indicating defective termination process of Ca release (white arrows in Figure 3-10C). Ca sparks occur during diastole (yellow arrows). However, different from the case of impaired Ca sensor function alone (but with intact buffering), Ca waves do not develop, because in the absence of CSQN buffer the JSR Ca content and the amount of

released Ca is small and insufficient to trigger release from adjacent dyads to generate propagating waves. Ca_d^{dyad} in one of the dyads is plotted in panel D; the dyad reactivates during the AP (indicated by #) and can also activate spontaneously (indicated by *) during diastole, indicating that besides abnormal termination, there is abnormal restitution of Ca release at the dyadic level.

3.4.2.4 Role of inter-dyad coupling when CSQN function is impaired

When impaired inter-dyad coupling is present in addition to impaired luminal Ca sensor function (but CSQN buffering is intact), Ca waves no longer occur. However, dyads can still reactivate during the AP or spontaneously activate during diastole (results not shown). Thus, inter-dyad coupling promotes the formation of Ca waves when CSQN sensor function is impaired, but its buffering ability is intact. When CSQN is dysfunctional both as luminal Ca sensor and buffer, impaired inter-dyad coupling prevents formation of long-lasting release events. We conclude that abnormal patterns of Ca release due to impaired CSQN function are modulated by the interaction between CSQN as a buffer and inter-dyad coupling.

3.5 Discussion

In cardiac ventricular myocytes, Ca release occurs at local domains along t-tubules where LCCs and RyR2s interact via Ca in dyadic spaces. Pathologies such as heart failure may involve de-tubulation of the myocyte t-tubules system (Song et al., 2006b), changes in dyadic structure, and impaired functional coupling between LCCs and RyR2s (Gomez et al., 1997). These subcellular local changes can alter CICR and ECC, and disrupt normal whole-cell macroscopic behavior. Ca release can also occur spontaneously during diastole; impaired CSQN function, both as a regulator of RyR2 gating and as a buffer of

SR Ca (Dirksen et al., 2007; Rizzi et al., 2008), has been implicated in such aberrant Ca release events. At present, it is extremely difficult, if not impossible; to study microscopic processes in sub-cellular compartments experimentally. With experimental approaches, the ability to integrate across scales from microscopic processes to whole-cell behavior is very limited. To study these phenomena through computer modeling, a multiscale model of Ca cycling was constructed. It takes into account local dyadic Ca release activities and interactions between dyads via Ca diffusion.

3.5.1 Stochastic Model of Ca Cycling

Many existing models of Ca cycling in cardiac ventricular myocytes are deterministic, based on average, subcellular compartments representation (Faber et al., 2007; Jafri et al., 1998; Shannon et al., 2004). They are not stochastic and are not formulated at the microscopic scale of local dyadic interaction between LCCs and RyR2s. Several models were developed to investigate local stochastic Ca release at the level of the dyadic space (Cannell and Soeller, 1997; Sobie et al., 2002a; Tanskanen and Winslow, 2006). There have been fewer attempts to link these processes to the whole myocyte behavior. One of these models (Greenstein and Winslow, 2002) and its numerical simplification (Greenstein et al., 2006) described local control of Ca release during ECC. Other models (Restrepo and Karma, 2009; Restrepo et al., 2008) were used to study cardiac alternans. The task has proven arduous due to the large number of parameters involved and the large ratio of computing to simulation time. Our motivation for formulating the multiscale model of Ca release was to develop a computational framework for relating macroscopic whole-cell behavior to microscopic Ca release processes. This approach is needed for studying the stochastic nature of Ca release dysfunction in cardiac arrhythmias

such as Catecholaminergic Polymorphic Ventricular Tachycardia (CPVT) (Ylanen et al., 2010). With the stochastic model, one second simulated time required ~ 90 s of run time on Dell PowerEdge™ 2650 Dual Xeon Processor 2U Servers, with dual 2.8 GHz processors.

3.5.2 Effect of Structural Changes in Dyads on Whole-Cell Behavior

In normal cardiac myocytes, depolarization produces rapid rise in myoplasmic Ca as a consequence of coordination and summation of localized Ca release events (Wier and Balke, 1999). Disruption of coordinated Ca spark initiation may underlie abnormalities of Ca transients, as observed in myocytes from hearts with various pathologies. Several membrane factors can reduce synchrony of activation and summation of Ca sparks. These include depressed phase-1 AP notch due to reduced transient outward current, I_{to1} (Sah et al., 2002), which decreases the driving force for I_{CaL}, thereby affecting the trigger for SR Ca release. Changes in I_{CaL} due to mutations, remodeling, or drugs can also have a similar effect on Ca release synchrony. Intracellularly, altered Ca sensitivity and gating kinetics of RyR2s can affect synchrony of release (Kubalova et al., 2005). Besides such molecular changes, impaired coupling between LCCs and RyR2s (Gomez et al., 1997), or structural remodeling of t-tubules in failing hearts (Sobie et al., 2006) can result in Ca release asynchrony. In this work, we simulated several structural defects in the dyad and found support for the hypothesis that ECC gain is lower with such defects. Simulations also showed that even with normal level of whole-cell Ca entry via I_{CaL}, as might occur in failing or hypertrophic hearts (Gomez et al., 1997), reduced dyadic density of LCCs can alter CICR, resulting in smaller Ca transients due to asynchronous activation of dyads. In normal ventricular myocytes, Ca influx through LCCs is thought to be the primary synchronizing mechanism of Ca release (Bers, 2002). Our simulation results suggest that

propagated CICR via inter-dyad diffusive coupling increases synchronization of Ca release when Ca influx sensed by RyR2s is reduced due to decreased number of dyadic LCCs or increased dyadic volume. Such t-tubular or dyadic structural changes occur in failing hearts, and inter-dyad coupling may serve as a compensatory mechanism for rescuing ECC gain to improve contractility in these hearts.

3.5.3 Effects of Impaired CSQN Function

CSQN is a high-capacity Ca binding protein in the SR of cardiac myocytes. When CSQN buffering ability was impaired, SR Ca release flux was smaller in magnitude and duration, consistent with CSQN role as Ca buffer. This resulted in depressed CaT, which can suppress cardiac contractility. Impaired CSQN buffering ability caused little change in synchronization of Ca release. Ca_{JSR} recovery was faster; this could have led to premature recovery of RyR2s from luminal Ca dependent refractoriness (Gyorke et al., 2002) and diastolic release events. This possibility was not supported by our simulation results because restitution of Ca release was preserved by intact CSQN regulator function.

Multiple processes have been implicated in restitution of Ca release: cytosolic Ca-dependent or use-dependent inactivation of RyR2s, luminal Ca-dependent refractoriness of RyR2s, inactivation of LCCs and slower refilling of SR Ca following a previous SR Ca release event (Sobie et al., 2006). We found that in the presence of intact CSQN buffering ability, impaired luminal Ca sensor function of CSQN resulted in increased diastolic Ca release activity in the form of Ca waves. This suggests a potential role for luminal Ca-dependent refractoriness as a potent mechanism for restitution of Ca release.

When both CSQN buffering ability and luminal Ca sensor function are impaired, increased diastolic Ca sparks, but not Ca waves are present. Both the frequency of RyR2 openings and the SR Ca load are important factors in propagation of Ca waves, which are usually observed only in Ca overloaded cells (Cheng et al., 1993). In this case, despite increased frequency of diastolic Ca sparks, reduced SR load due to impaired CSQN buffer may have been insufficient to sustain Ca waves.

Our results indicate that impaired CSQN regulation function, but with preserved buffering ability, is necessary for formation of arrhythmogenic Ca waves. In CPVT, Ca-wave induced delayed after-depolarizations (DADs) and triggered activity (TA) have been implicated as the arrhythmogenic mechanism. The D307H missense mutation in CSQN, presumably leading to impaired CSQN buffering capacity (Dirksen et al., 2007), was implicated in CPVT. It is possible that the mutation also affects CSQN regulation of RyR2, and that the degree of buffering impairment is insufficient to prevent formation of Ca waves. It is also possible that compensatory mechanisms such as increased SR volume (Knollmann et al., 2006) and/or overexpression of the SR binding protein calreticulin (Song et al., 2007) may also preserve SR load to sustain propagated CICR in such mutants.

Ca sparks occur as brief, spatially restricted elevations of Ca, suggesting that a potent mechanism terminates Ca release. Depletion of SR Ca has been proposed as a key mechanism of release termination (Sobie et al., 2002a). Long-lasting Ca release events occurred in the simulations only when luminal Ca sensor function was impaired, indicating its role in signaling Ca release termination.

3.5.4 Inter-Dyad Coupling

In the model, inter-dyad coupling in the SR was implemented as rapid diffusion of Ca between NSRs of adjacent dyads ($\tau_{diff\_NSR\_NSR} = 1\ ms$) and slower diffusion of Ca between NSR and JSR in a given dyad ($\tau_{refill} = 10\ ms$). Recent reports have indicated rapid diffusion of Ca in the SR (Wu and Bers, 2006), suggesting a functionally continuous structure. Our choice to distinguish between NSR and JSR is based on two considerations: (i) CSQN localizes only at the terminal cisternae of the SR; we define JSR as the volume (compartment) of CSQN distribution. (ii) structural considerations can restrict connectivity between JSR and NSR (Brochet et al., 2005). Experiments have also indicated that some junctions are better connected to the rest of the SR than others (Zima et al., 2008). During global Ca-induced-Ca-release, the simulated local SR Ca depletion in individual dyads (including contributions from JSR and NSR) is 47% (computed as ratio of Ca released to free SR Ca before release), 33% (computed as ratio of Ca released to total SR Ca before release), or 23% (computed as ratio of free SR Ca depletion to free SR Ca before release, Figure 3-4F). The whole-cell SR Ca depletion (contributed from JSR and NSR) during a global Ca transient constitutes a similar percentage of diastolic Ca_{SR} content. These numbers are consistent with measurements indicating that diastolic Ca_{SR} is only partially depleted (24 to 63%) during contraction (Shannon et al., 2003). Ca waves and long-lasting Ca release events are not present when inter-dyad coupling is impaired. Local Ca release disturbances still remain in the form of dyad reactivation during the AP and spontaneous Ca release during diastole. These results demonstrate that inter-dyad coupling can amplify local stochastic Ca release disturbances. This deleterious amplification can occur at the level of the dyad, causing long-lasting Ca release events, or

across the dyads to form Ca waves in the whole-cell. On the other hand, under pathological conditions when the dyadic structure is impaired, inter-dyad coupling may be a beneficial mechanism to maintain normal synchronization of Ca release. Thus, in a functioning cardiac ventricular myocyte, optimal tuning of inter-dyad coupling may be a factor in maintaining proper systolic function without amplification of local Ca release events during diastole.

3.5.5 Limitations

The stochastic multiscale model presented here goes beyond previous efforts of constructing a myocyte Ca cycling model that captures the spatial dynamics of Ca release and CSQN mediated regulation of RyR2 gating. However, it has important limitations that should be considered. The model represents the complex 3D spatial organization of dyads and their distribution in the myocyte by simplified linear geometry. Inter-dyad coupling in the cytoplasm was implemented by diffusion of Ca between adjacent dyadic spaces. Although phenomenological, this implementation is consistent with the experimental observation that Ca waves occur in Ca overloaded cells (Cheng et al., 1993). Finally, luminal Ca regulation of RyR2 gating is assumed to occur exclusively via CSQN. Alternative regulation mechanisms of RyR2 gating, such as luminal Ca feed-through or Ca inactivation sites (Laver, 2009), were not considered.

Chapter 4 Spontaneous Ca Release and Ca Waves Underlie Early and Delayed Afterdepolarizations, and Triggered Activity, In Ryanodine Receptor Mutations Associated With Catecholaminergic Polymorphic Ventricular Tachycardia

4.1 Abstract

Cardiac ryanodine receptor (RyR) mutations are associated with autosomal dominant catecholaminergic polymorphic ventricular tachycardia (CPVT). Spontaneous sarcoplasmic reticulum (SR) Ca release mediated afterdepolarizations is the proposed mechanism of arrhythmogenesis in these mutants, yet the underlying molecular and ionic mechanisms remain unclear, impairing rational approach to therapy. The main objective of this study is to investigate the mechanisms of cellular arrhythmia in CPVT and suggest therapeutic strategies using a multiscale stochastic simulation model of Ca cycling and the action potential (AP) in a human ventricular myocyte. Each of the proposed molecular mechanisms of the disease was simulated. Increased RyR sensitivity to cytosolic Ca, as occurs during weakened interaction between the N-terminus and central domain of RyR (domain unzipping), resulted in increased propensity of spontaneous SR Ca release, Ca waves, delayed afterdepolarizations (DADs), early afterdepolarizations (EADs) and triggered activity (TA). DADs occurred due to I_{NaCa} activation by Ca waves. TA was supported by I_{CaL}, without contributions from I_{Na}. EADs occurred due to reactivation of I_{CaL} during AP prolongation by I_{NaCa}, secondary to synchronous spontaneous SR Ca release. Partial block of I_{CaL} or I_{NaCa} abolished TA, but Ca waves-mediated DADs persisted. Partial block of RyR or SERCA abolished spontaneous Ca waves and arrhythmic activity. Flecainide suppressed TA, but did not abolish spontaneous Ca waves and DADs. It exerted its antiarrhythmic effect by targeting RyR.

Impaired FKBP12.6-RyR interaction or impaired luminal Ca sensitivity increased spontaneous Ca spark frequency (CaSPF) but did not generate Ca waves and arrhythmic activity. In conclusion, RyR impaired domain interactions underlie cellular arrhythmogenecity in CPVT due to its effect of increased RyR sensitivity to cytosolic Ca. The antiarrhythmic effect of flecainide in CPVT is due to RyR block (not I_{Na} block); it is not associated with abolishment of Ca waves.

4.2 Introduction

Catecholaminergic Polymorphic Ventricular Tachycardia (CPVT) is a highly malignant arrhythmogenic disorder, triggered by exertion or emotional-stress(Priori and Chen, 2011). Mutations in the Ryanodine Receptor (RyR) have been reported in families affected by the disorder. The bidirectional ventricular tachycardia (VT) that is the phenotypic manifestation of the disease, suggests that spontaneous Ca-mediated delayed afterdepolarizations (DADs) and triggered activity (TA) is the most likely electrophysiological mechanism for arrhythmia initiation in CPVT(Cerrone et al., 2009). Although it is known that Sarcoplasmic Reticulum (SR) Ca release is disrupted by the disease, the molecular mechanisms that lead to the disruption are unclear. In particular, three different arrhythmogenic mechanisms have been proposed for CPVT-RyR mutants: (1) Increased sensitivity of the mutant RyR to SR Ca content(Jiang et al., 2005) can result in abnormal diastolic Ca release events, leading to increased frequency of spontaneous Ca sparks, Ca waves, DAD and TA. (2) RyR mutants have been shown to have reduced binding affinity for FKBP12.6(Wehrens et al., 2003). Studies have demonstrated that FKBP12.6 dissociation from RyR destabilizes the closed conformation of the channel(Chelu et al., 2004). This can result in abnormal openings of RyRs during diastole, possibly causing arrhythmogenic Ca waves, DADs and TA. (3) It has also been shown that the mutation weakens the interaction between the N terminus and central domains of RyR (domain-unzipping), causing greater propensity for abnormal SR Ca leak (Uchinoumi et al., 2010) and associated arrhythmias.

Using a multiscale Ca cycling model(Gaur and Rudy, 2011) that scales processes from single L-type Ca channel (LCC), RyR openings and Ca sparks to whole-cell Ca cycling

and electrophysiology in a human ventricular myocyte, we simulate these CPVT-RyR mutant effects and explore their arrhythmogenic consequences during β-adrenergic stimulation (βAS) in the presence of Isoproterenol (ISO). Interventions that target membrane ionic currents, including Na current (I_{Na}), L-type Ca current (I_{CaL}), Na-Ca exchange current (I_{NaCa}), or the Ca cycling system (RyR, Sarcoplasmic endoplasmic reticulum Ca^{2+} ATPase (SERCA)) are explored as potential anti-arrhythmic therapy.

4.3 Methods

4.3.1 The multiscale Ca cycling model of a ventricular myocyte with stochastic Ca release processes

Our previously published model of Ca cycling in a ventricular myocyte provides the basis for the simulations in this study(Gaur and Rudy, 2011). The model consists of 10,000 diffusively-coupled dyads in which Ca release occurs stochastically within a dyad. Each dyad comprises the following Ca distribution compartments: myoplasm, network sarcoplasmic reticulum (NSR), junctional SR (JSR), dyadic space and submembrane space. The number of LCCs and SR Ca release channels (RyRs) in a dyad is 7 and 50, respectively, and their states fluctuate stochastically. RyR kinetics are simulated by a Markov model, described in detail elsewhere(Gaur and Rudy, 2011). All other ionic currents, pumps and exchangers are formulated from the O'Hara-Rudy (ORd) computer model of the human ventricular myocyte action potential(O'Hara et al., 2011).

4.3.2 The model of effects of the RyR-FKBP12.6 interaction on the SR Ca release process

Physical association among RyRs in a dyadic cluster results in a coordinated gating behavior, known as coupled gating(Marx et al., 2001). Coupled gating was implemented

in the model by assuming that the activation rate of RyR increases with the number of neighboring RyRs in the open state within a dyadic cluster. Similarly, the deactivation rate of RyR increases with the number of RyRs in the closed state in the cluster. Coupled gating can be a function of RyR-FKBP12.6 interaction(Marx et al., 2001). FKBP12.6-RyR interaction can be regulated by Protein Kinase A (PKA) phosphorylation of RyR during βAS(Marx et al., 2000). PKA phosphorylation can cause depletion of FKBP12.6 from the channel macromolecular complex, weakening the interaction between RyR and FKBP12.6, resulting in a lower degree of coupled gating and consequently less synchronized openings of individual RyRs ("leaky RyRs"). To determine the arrhythmic consequences of impaired RyR-FKBP12.6 interaction if RyR-FKBP12.6 interaction played an important role in Ca cycling, the SR Ca release process was implemented by making the degree of coupled gating a function of RyR-FKBP12.6 interaction.

4.3.3 ISO model

Steady-state PKA phosphorylation effects of βAS due to ISO on its targets: I_{CaL}, slow delayed rectifier K^+ current (I_{Ks}), background K^+ current (I_{Kb}), Fast Na^+ current (I_{Na}) and Ca uptake via SERCA were simulated using the β-adrenergic cascade model of Heijman et al (Heijman et al., 2011) as adapted by O'Hara and Rudy(O'Hara and Rudy, 2012). In addition, RyR-FKBP12.6 interaction within a dyadic cluster was simulated as a function of ISO.

4.3.4 CPVT-RyR mutant models

(1) Increased unzipping of the interaction between the N-terminus domain and the central domain of RyR ("domain unzipping"(Ikemoto and Yamamoto, 2002)) was implemented as an increase (~2.5 fold) in cytosolic Ca sensitivity of RyR compared to control. (2)

Increased luminal Ca sensitivity of RyR was simulated by doubling the rate of transition from a CSQN-dependent RyR refractory mode to an active mode after a previous episode of Ca release in the dyad. (3) Decreased binding affinity of FKBP12.6 to a CPVT-RyR mutant channel was implemented by assuming that RyR-FKBP12.6 interaction is lower at all concentrations of ISO.

4.4 Results

4.4.1 Arrhythmogenic events in a CPVT-RyR mutant with increased domain-unzipping.

We simulated the effects of ISO in a control cell and a CPVT-RyR mutant cell with increased domain unzipping. The cell was paced to steady state at 1 Hz, followed by a pause. Figure 4-1 shows the response of the mutant cell. DADs and/or TA did not occur in the control cell. Under basal (without ISO) conditions, very low amplitude DAD occurred in the mutant cell (indicated by #). During ISO application, DADs and TA (indicated by *) occurred after cessation of pacing (the last paced beat is indicated by vertical arrow). These results are consistent with the CPVT clinical phenotype, where βAS in the form of exercise and/or emotional stress may unmask the underlying defect to cause triggered arrhythmias (Priori and Chen, 2011).

To identify the mechanisms of DADs and TA, we plot the relevant currents in Figure 4-2. Panel A shows the last paced beat at 1 Hz, followed by one DAD and one triggered action potential (AP) after a pause. The computed line scan image of myoplasmic Ca

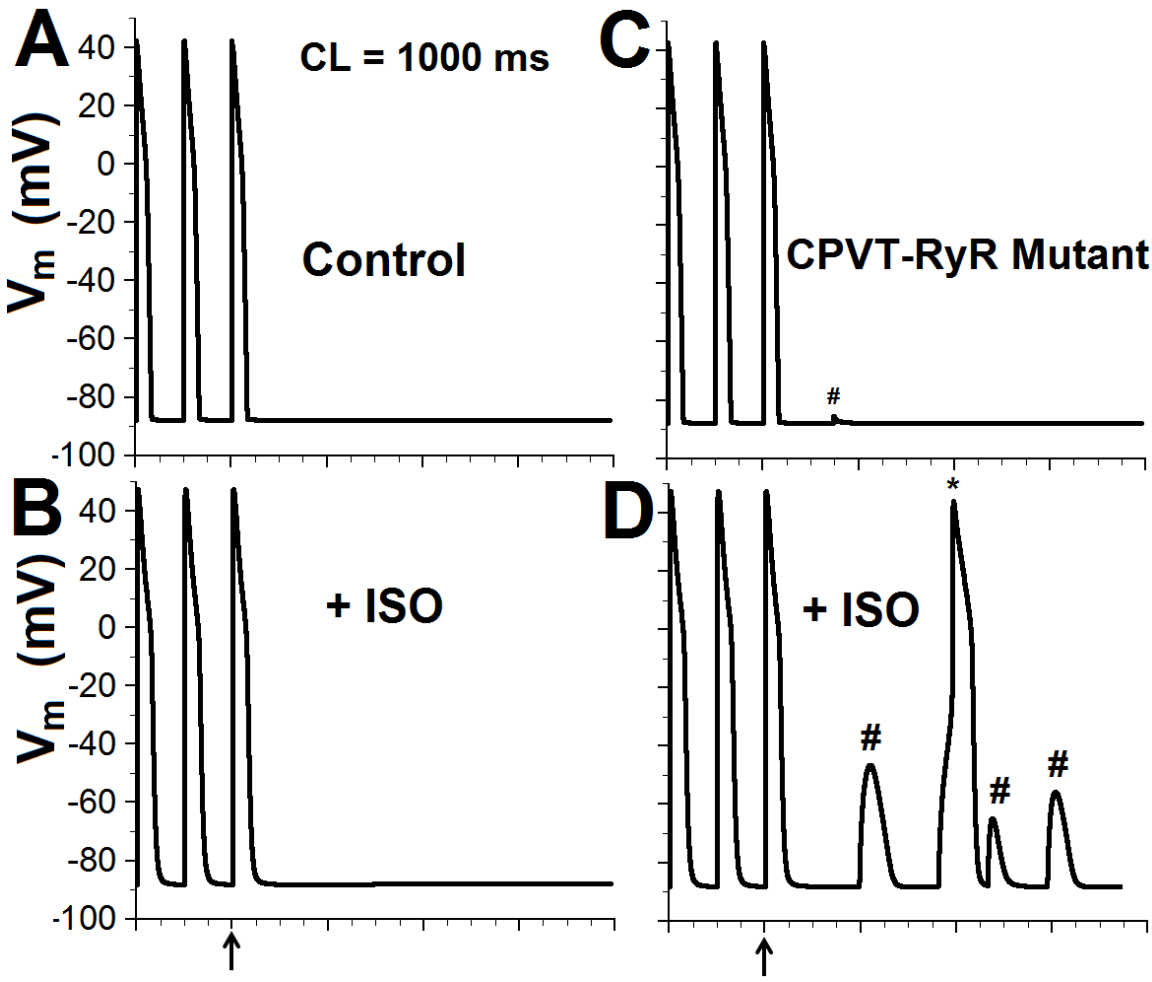

Figure 4-1 Effect of Isoproterenol (ISO) on CPVT-RyR mutant with domain –unzipping. **A**, Representative simulated membrane potential in a control myocyte. **B**, Membrane potential in a control myocyte in the presence of ISO. **C**, Representative membrane potential in mutant myocyte. **D**, Membrane potential in a mutant myocyte in the presence of ISO. In a control (wild type) ventricular myocyte, DADs or TA are not observed. DAD (indicated by #) and TA (indicated by *) are observed in the mutant with ISO. Arrow indicates the last paced beat.

shows that the initiation of a spontaneous diastolic Ca wave corresponds with the initiation of the DAD, as indicated by a vertical time line. The spontaneous Ca wave activated I_{NaCa}, which then depolarized the membrane to generate a DAD.

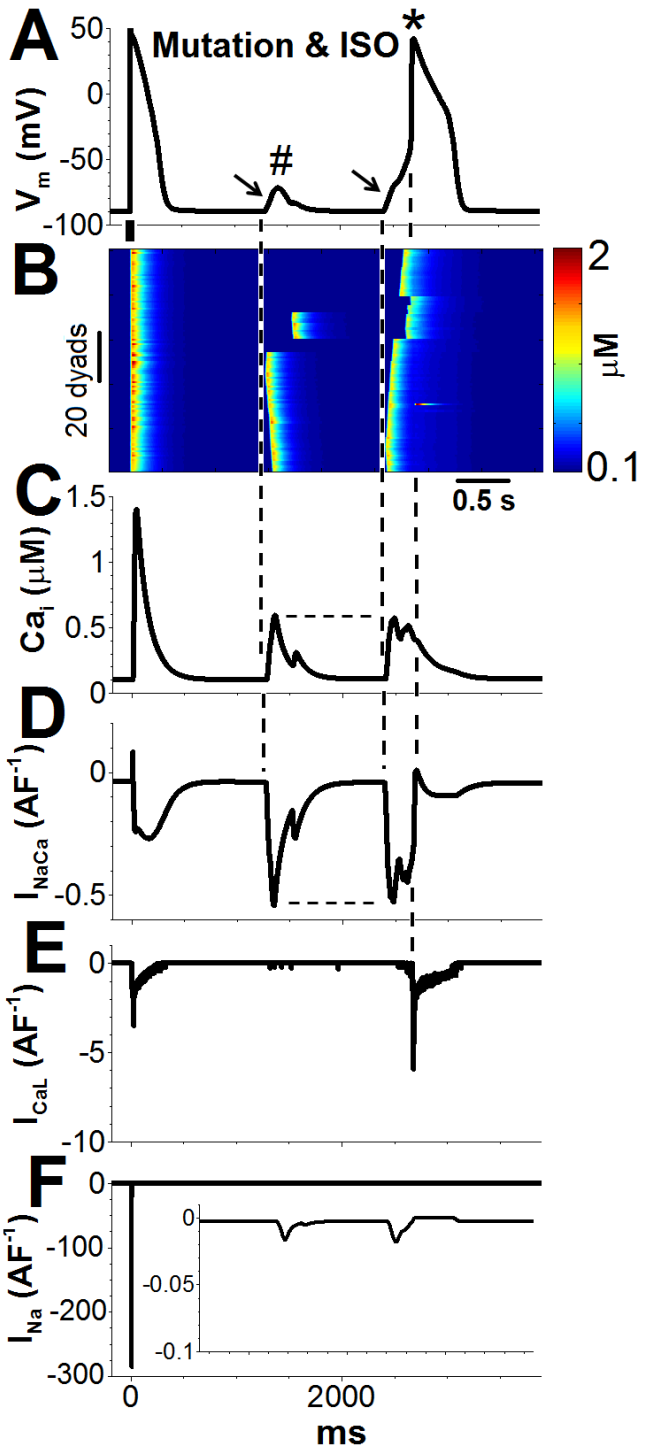

Figure 4-2 Mechanisms of DAD and TA in CPVT. DAD **(A**; indicated by #**)** is initiated by a spontaneous Ca wave **(B)**, **(C)** which activates the depolarizing current I_{NaCa} **(D)**. When the DAD has reached the threshold for activation of I_{CaL} **(E)**, TA occurs (**A**; indicated by *). TA is not due to I_{Na} **(F)**; the slow rising foot of the DAD (indicated by arrows in panel A) inactivates I_{Na} almost completely before I_{CaL} activation.

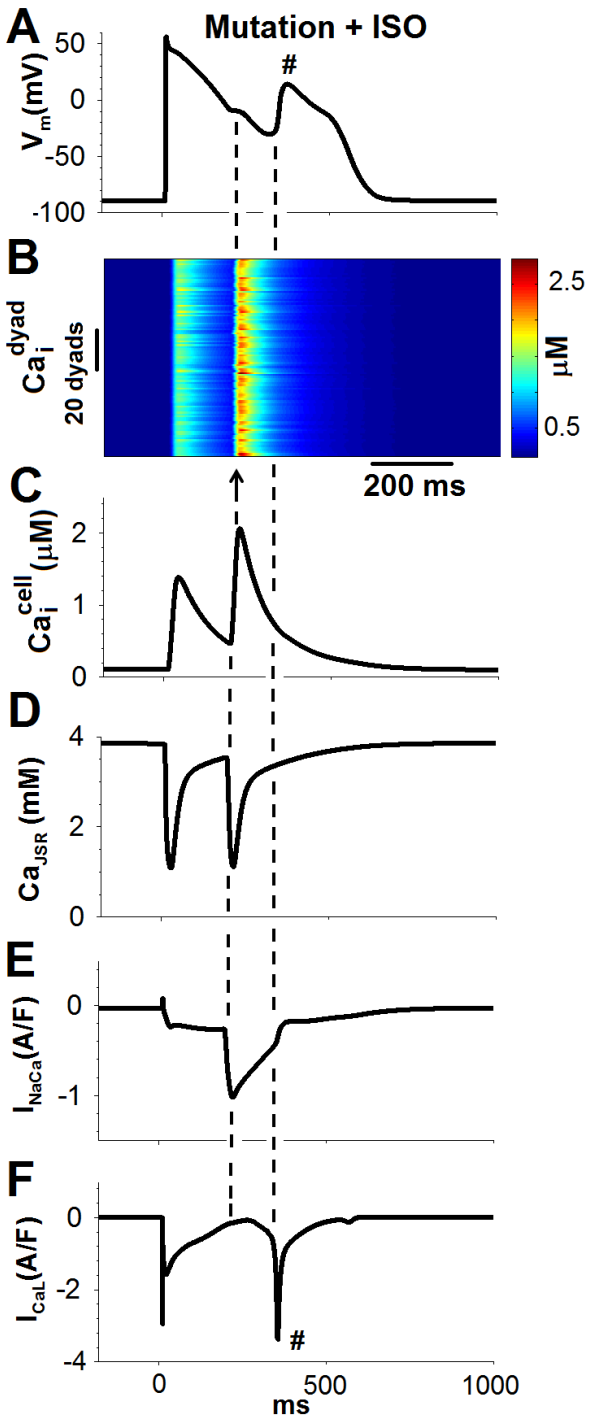

Figure 4-3 Mechanism of EAD in CPVT. EAD (indicated by #) **(A)** follows spontaneous Ca release **(B, C, D)** during the AP plateau. It activates depolarizing I_{NaCa} **(E)** which slows the AP repolarization rate to prolong the AP. Prolongation of the AP at plateau potentials provides time for reactivation of I_{CaL} **(F**; indicated by #**)**, which generates the depolarizing charge for EAD formation. Arrow indicates spontaneous Ca release.

In this case, the first spontaneous Ca wave was aborted, followed by a smaller Ca wave. The cumulative SR Ca release during these two episodes was unable to activate I_{NaCa} sufficiently to depolarize the membrane to its threshold for TA. The second DAD was also initiated by a spontaneous Ca wave that activated the I_{NaCa} to provide the depolarizing charge. In this case, the first spontaneous Ca wave was followed by two smaller spontaneous Ca waves. Although the peak of the spontaneous Ca transient (Ca_i) and I_{NaCa} (indicated by horizontal dashed lines) were similar to the values during the release causing the first DAD, this time the cumulative SR Ca release was sufficient to activate I_{NaCa} that depolarized the membrane to its threshold for TA. Note that the I_{NaCa}-supported depolarization to threshold is relatively slow (arrow), followed by a faster upstroke above threshold. The vertical time line indicates that I_{CaL} was activated to support the above-threshold upstroke of the triggered AP. In both episodes of spontaneous Ca release, I_{Na} was activated only marginally (< 0.02 A/F in magnitude compared to 280 A/F for a paced AP).

During pacing at 1 Hz, EADs developed (Figure 4-3) when spontaneous SR Ca release occurred after RyR recovery from refractoriness during phase-2 of the AP (arrow in panel B). The spontaneous SR Ca release occurred synchronously and not as a propagating Ca wave. Due to incomplete sequestration of the systolic Ca transient by SERCA and a small residual I_{CaL} (0.2 A/F) at the time of RyR recovery, cytosolic Ca was sufficiently high to activate SR Ca release simultaneously across the dyads. Because of the higher cytosolic Ca, the resulting spontaneous Ca transient was of greater magnitude than that during the previous paced AP. When coupling between the dyads was eliminated in the cell, spontaneous SR Ca release and EADs still occurred during the AP, but Ca waves and

associated DADs/TA were abolished although spontaneous diastolic Ca sparks were still present.

To elucidate the mechanism of the EADs, we plot the relevant currents, I_{NaCa} and I_{CaL}. The spontaneous SR Ca release activated depolarizing I_{NaCa} (first dashed vertical line), which in turn slowed the repolarization rate and prolonged the AP. Prolongation of the AP at plateau potentials provided time for reactivation of I_{CaL} (indicated by the second dashed vertical line). I_{CaL} provided the depolarizing charge for the upstroke of the EAD, consistent with the previously identified mechanism of EADs in human ventricular myocytes (O'Hara et al., 2011). Thus, both depolarizing currents, I_{NaCa} and I_{CaL}, are involved in EAD formation. However, I_{NaCa} provides the current for prolongation of the AP and I_{CaL} is the actual depolarizing charge carrier for EAD formation. This differs from the role of these currents in DAD and TA. In the case of DAD, I_{NaCa} activation by a Ca wave depolarizes the membrane to generate the DAD, without contribution from I_{CaL}. During TA, I_{NaCa} provides the initial charge for membrane depolarization to the threshold of I_{CaL} activation, which then provides the depolarizing charge for the upstroke of the triggered AP. The results demonstrate that increased sensitivity of RyR to cytosolic Ca in CPVT-RyR mutants with increased domain unzipping can provide conditions for arrhythmic cellular activity in the form of DAD, TA and EAD.

4.4.2 Role of increased sensitivity of RyR to luminal (SR) Ca.

Increased sensitivity of RyR to luminal Ca has been implicated as one of the causes of CPVT(Jiang et al., 2004). The functional consequence of such an effect could be faster recovery from luminal Ca dependent refractoriness as JSR Ca increases via SERCA uptake and Ca translocation from NSR to JSR. Theoretically, faster recovery of JSR Ca

can lead to earlier sensitization of RyR to cytosolic Ca, which may then lead to increased frequency of Ca sparks, Ca waves, DAD and TA(Gyorke, 2009). We tested this hypothesis by increasing the rate of RyR recovery from luminal Ca-dependent refractoriness with no other changes. The frequency of spontaneous Ca sparks (Ca spark frequency, CaSPF) was increased by 75% (from 40/cell/s to 70/cell/s) relative to control under basal (no ISO) conditions (Figure 4-4B, 4-4E). In the presence of ISO, CaSPF was increased by 130% relative to control (from 70/cell/s to 160/cell/s). Although CaSPF was increased, spontaneous Ca release in the form of Ca waves did not develop.

4.4.3 Role of impaired FKBP12.6-RyR binding affinity.

Studies have suggested that CPVT mutations are associated with impaired binding of FKBP12.6 to RyR(Wehrens et al., 2003). FKBP12.6 is believed to stabilize the RyR, and its dissociation as a result of RyR phosphorylation by PKA during β-adrenergic stimulation can increase the sensitivity of the channel to cytosolic Ca activation. Impaired FKBP12.6 binding to RyR can then result in leaky RyRs, leading to diastolic Ca release mediated TA. We tested this hypothesis by simulating impaired RyR-FKBP12.6 interaction (Figure 4-4C, 4-4E). Under basal conditions (no ISO), CaSPF was increased by 75% relative to control in the simulated impaired FKBP12.6-RyR case (70/cell/s *vs* 40/cell/s) and with ISO it was greater by 240% (240/cell/s *vs* 70/cell/s). Once again, although CaSPF was increased, spontaneous Ca waves did not occur. For comparison, CaSPF in the RyR mutant with domain-unzipping increased by 175% without ISO (110/cell/s *vs* 40/cell/s) and dramatically by 630% with ISO (510/cell/s *vs* 70/cell/s) compared to control (Figure 4-4D, 4-4E), consistent with the possibility that Ca wave-mediated triggered beats underlie arrhythmogenesis in this mutant.

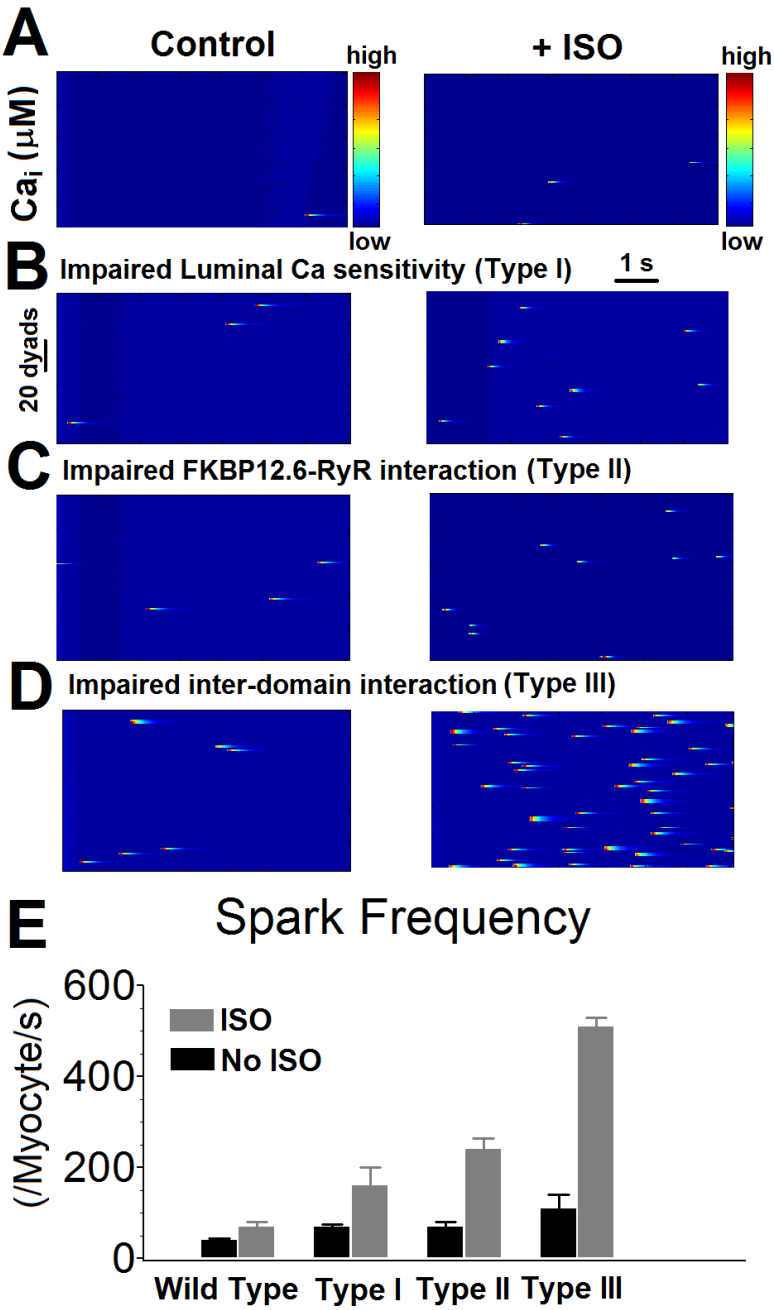

Figure 4-4 Ca sparks in CPVT-RyR mutants. Representative simulated linescan image of myoplasmic Ca in a control myocyte **(A)**, CPVT-RyR mutant with impaired luminal Ca sensitivity **(B)**, impaired FKBP12.6-RyR interaction **(C),** or impaired inter-domain interaction between the N terminus and central domain of RyR ("domain unzipping") **(D)**. Mutation + ISO increases the spark frequency most dramatically in the mutant with domain unzipping. **(E)**, Summary result of Ca spark frequency (CaSPF) in these mutants. Data are shown as mean ± SEM for n=20 different simulation runs in a quiescent myocyte.

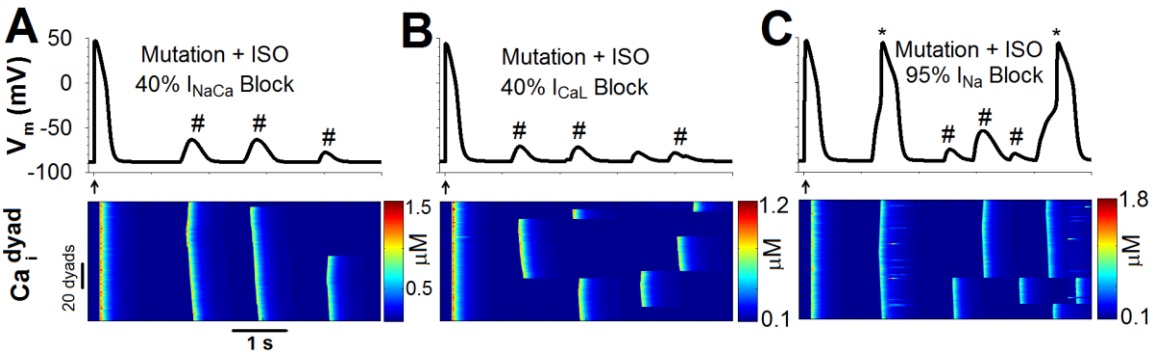

Figure 4-5 Effect of I_{CaL} and I_{NaCa} block on CPVT-RyR mutant with domain unzipping with ISO. Effects of 40% block of I_{NaCa} **(A)**, 40% block of I_{CaL} **(B)** or 95% block of I_{Na} **(C)** on membrane potential (V_m). Myoplasmic Ca (Ca_i) is also shown of each intervention. TA (indicated by *) is abolished with block of I_{CaL} and I_{NaCa}, but not by block of I_{Na}. Arrow indicates the last paced beat. Spontaneous Ca-wave induced DADs (indicated by #) are not abolished by any of the interventions.

4.4.4 Pharmacological targets for prevention of CPVT

The use of β-blockers has met with limited success in the prevention of arrhythmias in patients with CPVT mutations (Rosso et al., 2007). In an attempt to determine other possible therapeutic targets that can prevent spontaneous Ca waves and arrhythmogenic DAD/TA, we conducted systematic upregulation/downregulation of protein functions that affect electrophysiologic and/or Ca cycling components of the human ventricular myocyte such that TA was abolished. The study was performed in a CPVT-RyR mutant with impaired inter-domain interaction in which spontaneous Ca release-mediated DADs/TA occurred. 40% block of I_{CaL} or 40% block of I_{NaCa} abolished TA, but spontaneous Ca release and DADs were not abolished (as indicated by # in Figure 4-5). When I_{NaCa} was reduced, depolarizing I_{NaCa} during spontaneous Ca waves could not reach threshold of V_m for I_{CaL} activation. When I_{CaL} was reduced, it was unable to support the upstroke of triggered APs. 95% block of I_{Na} did not abolish TA (Figure 4-5C), consistent with the result that TA is supported by I_{CaL} in human ventricular myocytes.

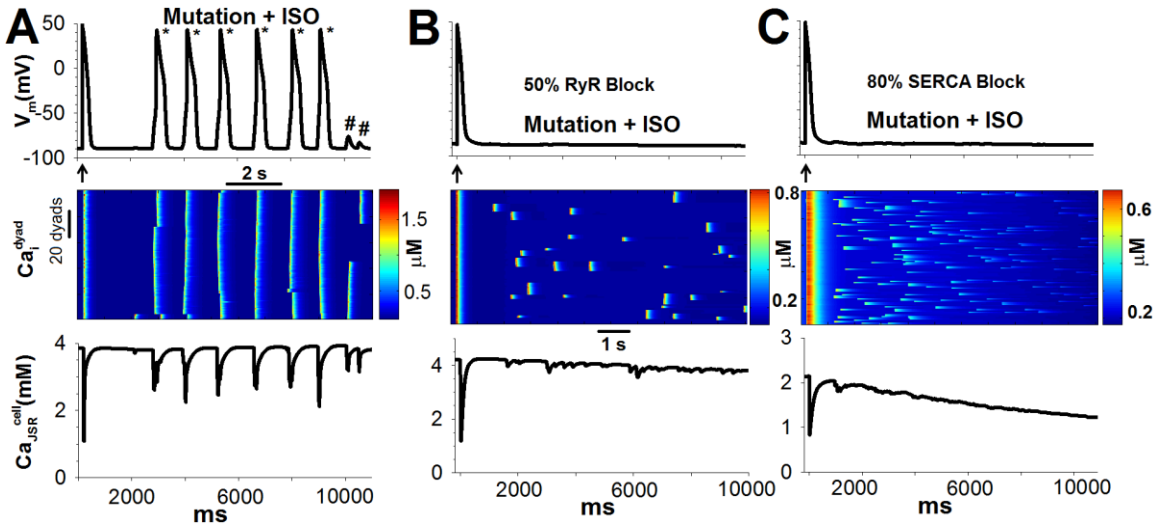

Figure 4-6 Effect of block of Ca cycling processes in a CPVT-RyR mutant with domain unzipping with ISO. Effects of 50% block of RyR **(B)** or 80% block of SERCA **(C)**. These were the minimum levels of block that abolished Ca waves and DADs/TA. Block of SERCA reduced SR content, but increased Ca spark frequency due to high diastolic cytosolic Ca.

We next investigated if block of flux through proteins that are critically involved in Ca cycling, including RyR and SERCA, may lead to abolition of spontaneous Ca waves and associated DADs/TA. A minimum of 50% RyR block or 80% SERCA block was needed to abolish spontaneous Ca waves and DADs/TA (Figure 4-6). SERCA block was effective in suppressing spontaneous Ca wave by reducing the diastolic JSR from 3.8 mM in mutant+ISO to 2.2 mM. Diastolic Ca_i was higher and resulted in increased CaSPF. When RyR was blocked 50%, JSR Ca increased from 3.8 mM to 4.2 mM. In this case, spontaneous Ca waves were suppressed due to inhibition of CICR across dyads. The diastolic Ca_i was smaller compared to the case with SERCA block, resulting in a smaller CaSPF.

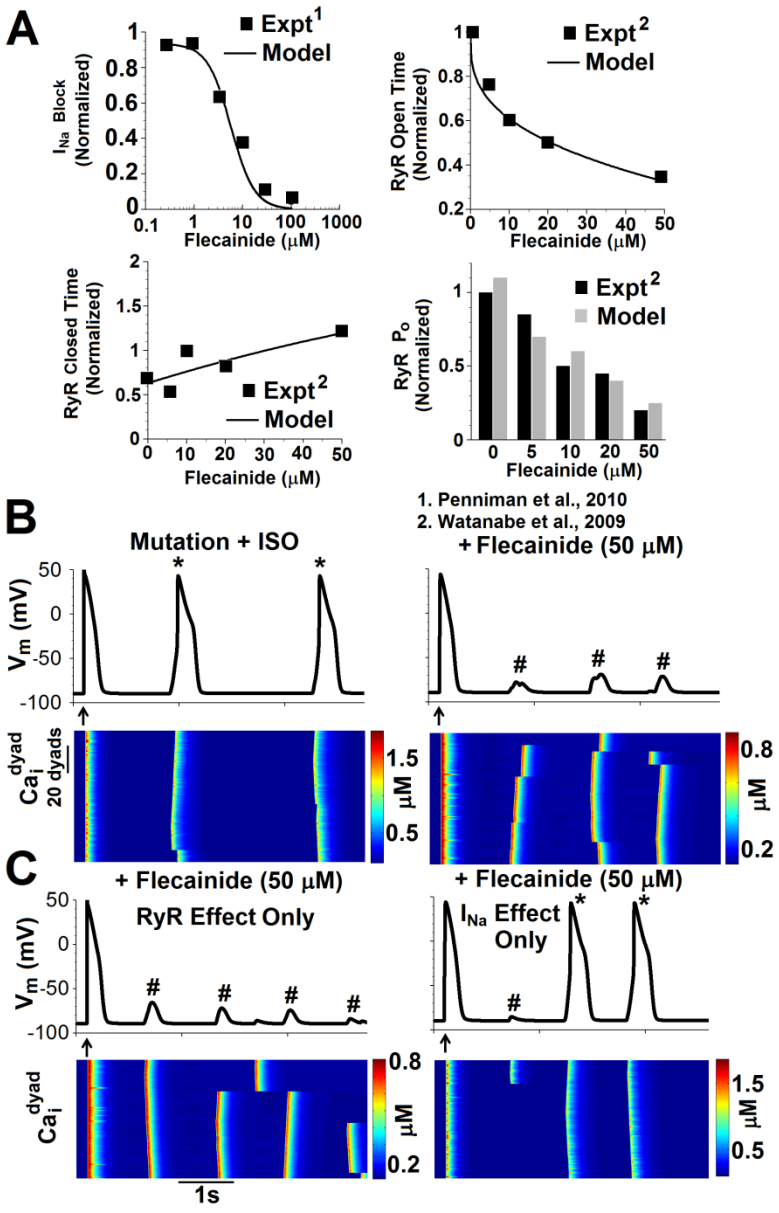

Figure 4-7 Antiarrhythmic effects of flecainide. (**A**), Dose-dependence of I_{Na} block(Penniman et al., 2010) and of mean open and closed time of RyR(Watanabe et al., 2009) were used to develop a model of flecainide dose-dependent effects. Simulated open probability (P_o) of RyR matches experimental values(Watanabe et al., 2009). (**B**), Left, Mutant+ISO exhibits TA (triggered APs marked with *). Right, when flecainide application is simulated (at 50 μM), the cell does not generate TA after cessation of pacing. Spontaneous Ca release still occurs, leading to DADs (marked by #). (**C**), Isolated effect of RyR block (left) and of I_{Na} block (right). TA suppression by flecainide is due to its effect on RyR alone (left panel), and not on I_{Na} (right panel). Arrows indicate last paced beat.

Recently, flecainide (a class 1C anti-arrhythmic drug) has been shown to prevent arrhythmias in calsequestrin knockout mice (Hilliard et al., 2010), CPVT patients(Watanabe et al., 2009) and a mouse model of CPVT(Liu et al., 2011). Flecainide is known to have dose-dependent effects on availability of I_{Na} (Penniman et al., 2010) and was shown to cause open state block of RyRs in a dose-dependent manner (Watanabe et al., 2009). However, the mechanism by which flecainide inhibits arrhythmias in CPVT is not known. Theoretically, such inhibition could depend on reduced excitability due to I_{Na} inhibition effects, or on suppression of Ca waves due to RyR block and therefore suppression of Ca-wave mediated DADs and TA. We developed a model of the dose-dependent effects of flecainide on I_{Na} conductance and on RyR mean open/closed time by fitting experimental data (Figure 4-7A). The model simulated open probability of RyR as a function of flecainide concentration is similar to experiments (Figure 4-7A, bottom right). We then explored the possible anti-arrhythmic effect of flecainide in the context of the whole myocyte. As the dose was increased, flecainide suppressed triggered beats in a CPVT-RyR mutant with domain-unzipping at 50 μM (Figure 4-7B right). Such suppression required RyR open/closed state block by flecainide, as effects of flecainide on I_{Na} alone did not result in abolition of triggered beats (Figure 4-7C). However, the combined suppression of I_{Na} and RyR flux that abolished TA was not associated with abolition of spontaneous Ca waves (Figure 4-7B right). Taken together, these results suggest that arrhythmia suppression by flecainide in CPVT patients is mainly due to its effect on RyR, but is not necessarily associated with abolition of spontaneous Ca waves. Spontaneous Ca waves caused low-amplitude DADs due to smaller amount of Ca release (Figure 4-7B right, #), but the DADs did not develop into TA.

4.5 Discussion

In this chapter, we studied possible mechanisms underlying CPVT in patients with heterozygous RyR mutations. We also examined possible therapeutic targets for prevention of CPVT.

There are currently three hypothetical molecular mechanisms underpinning the impaired function of RyR in this mutation-induced pathology. It has been proposed that mutations in the RyR gene result in impaired inter-domain interaction between the N terminus and central domain region of RyR. Such impaired interaction can result in loss of conformational constraints, the so called domain switch hypothesis(Ikemoto and Yamamoto, 2002), resulting in increased sensitivity of RyR openings to agonists such as Ca. The second hypothesis suggests that CPVT-RyR mutations increase sensitivity of RyR to luminal SR Ca. Such RyR CPVT mutants are associated with decreased threshold for SR Ca release when expressed in HEK cells(Jiang et al., 2005; Jiang et al., 2004). The third suggested mechanism is impaired binding of the channel-stabilizing protein FKBP12.6 to RyR(Wehrens et al., 2003). This impairment is associated with increased incidence of SR diastolic Ca leak. β-adrenergic stimulation (βAS) can exacerbate the functional consequences of the underlying molecular defects of RyR in CPVT. This can occur by increasing the Ca loading of the cell via both increased SR Ca uptake and increased Ca influx through I_{CaL}. βAS can also induce PKA phosphorylation of RyR, resulting in increased dissociation of FKBP12.6 from the channel complex, which further exacerbates the effects of impaired RyR-FKBP12.6 binding in the mutant. A functional consequence of CPVT-RyR mutations is increased probability of RyR openings, resulting in increased frequency of spontaneous Ca release events which can be in the form of

invisible Ca leak, Ca sparks and/or Ca waves. In this work, we simulated the functional consequences of each of the proposed mechanisms of CPVT mutations and found that spontaneous Ca release in the form of Ca waves occurred only for the case of impaired inter-domain interactions and that βAS was necessary to induce Ca waves. The Ca waves were associated with arrhythmogenic DADs and TA during ISO application, indicating that spontaneous Ca release in the form of Ca waves was the source of arrhythmogenic behavior. In agreement with Fernandez-Velasco et al (Fernandez-Velasco et al., 2009), the simulations suggest that increased cytosolic Ca activation of RyR associated with domain-unzipping can explain the increased frequency of Ca waves, DADs and TA in mutant cells.

Several groups developed knock-in mouse models with different point mutations corresponding to CPVT mutations found in patients (Fernandez-Velasco et al., 2009; Kannankeril et al., 2006; Uchinoumi et al., 2010). The phenotypes were identical regardless of the mutation location on RyR, indicating that the functional end-point of the mutations is increased sensitivity of RyR to agonists such as caffeine, cytosolic Ca, or luminal Ca. This observation is supported by the results of the present simulation studies; the simulated arrhythmic behavior includes EADs, DADs and TA.

A DAD is defined as a depolarizing afterpotential that begins after normal repolarization is complete (Cranefield and Aronson, 1988). The proposed mechanism of DAD formation in CPVT is spontaneous Ca release and activation of I_{NaCa}(Priori and Chen, 2011). The simulations support this hypothesis; DADs were associated with spontaneous Ca waves and membrane depolarization by I_{NaCa}. If sufficiently large, I_{NaCa}-supported depolarization reached the threshold for I_{CaL} activation, which then supported

the upstroke of a triggered AP (TA). Due to inactivation during the slow rising I_{NaCa}-supported foot, I_{Na} did not contribute to the triggered AP. Note that increased mutant sensitivity to cytosolic Ca is key to the development of Ca waves and in turn DADs and TA.

The simulations also suggest the possibility of an additional arrhythmogenic mechanism in CPVT, namely EADs. An EAD is defined as a depolarizing afterpotential that begins before the completion of repolarization of an AP(Cranefield and Aronson, 1988). Consistent with this definition, EAD occurred for mutant+ISO conditions when synchronous spontaneous Ca release occurred during the AP plateau. Faster recovery of mutant RyR and its increased sensitivity to cytosolic Ca compared to wild type caused such spontaneous release. The spontaneous Ca transient activated I_{NaCa} to slow the repolarization rate. This provided time at the appropriate voltage for reactivation of I_{CaL}, which provided depolarizing charge for EAD generation (Zeng and Rudy, 1995). EADs can provide both the arrhythmic substrate by increasing dispersion of repolarization, and arrhythmic trigger by local depolarization. This could be an arrhythmogenic mechanism in CPVT, in addition to DADs and TA. To the best of our knowledge, this predictive simulation result has not been observed in experimental models of CPVT and warrants further investigation.

Several groups have demonstrated that CPVT RyR mutations (Jiang et al., 2005; Uchinoumi et al., 2010) have no effect on RyR-FKBP12.6 binding. Moreover, PKA phosphorylation of RyR has been shown to have no effect on diastolic SR Ca release(Ai et al., 2005; Curran et al., 2010; Curran et al., 2007) or on FKBP12.6 binding to RyR (Guo et al., 2010). The link between RyR PKA phosphorylation and cardiac dysfunction

(Bers, 2012) has also been questioned. In addition, it was estimated that the concentration of FKBP12.6 in a cardiac myocyte is much smaller that of RyR (Guo et al., 2010). Thus, inspite of the high affinity of RyR-FKBP12.6 binding (Guo et al., 2010), the interaction between RyR and FKBP12.6 may be negligible and not have a noticeable effect on RyR gating. Our simulations were designed to answer the question what would the arrhythmic consequences of RyR mutations be if RyR-FKBP12.6 interaction did play a role in Ca cycling, and if RyR PKA phosphorylation can modulate this interaction. The results indicate that CPVT-RyR mutations with impaired RyR-FKBP12.6 interaction increased the diastolic SR Ca leak in the form of Ca sparks. However, arrhythmogenic Ca waves, DADs and TA fail to occur.

Several RyR mutations were shown to preferentially increase the sensitivity of single channel activation by luminal Ca in lipid bilayers(Jiang et al., 2005). These mutations were also associated with increased frequency of Ca waves in HEK or HL-1 cells(Jiang et al., 2005; Jiang et al., 2004). Based on these observations, Jiang et al(Jiang et al., 2005) proposed that CPVT RyR mutations caused Ca waves by increasing RyR sensitivity to luminal Ca. In our work, the functional effect of increased RyR activation by luminal Ca was simulated as faster recovery from luminal Ca-dependent refractoriness. Although faster recovery resulted in increased frequency of Ca sparks, Ca waves did not occur. Planar lipid bilayer studies have shown distinct regulation of RyR by cytosolic or luminal Ca (Gyorke and Gyorke, 1998). However, due to inherent interdependence of the luminal and cytosolic environments in ventricular myocytes, it is difficult to assign distinct roles to cytosolic and luminal Ca in situ(Laver, 2009). Whether Ca wave generation is determined by opening of RyR in response to luminal

Ca(MacLennan and Chen, 2009), or is an integral part of enhanced calcium-induced-calcium-release (CICR)(Prosser et al., 2010), is a subject of debate. Our results indicate that Ca waves can be generated by enhanced CICR due to increased cytosolic Ca sensitivity of RyR with impaired-domain-domain interaction.

The arrhythmic mechanism of TA induced by spontaneous Ca release suggests at least two strategies for suppression of CPVT: (1) Abolition of TA (2) Abolition of spontaneous Ca release. Partially blocking I_{CaL} and I_{NaCa} suppressed TA (Figure 4-5) without abolition of DADs and spontaneous Ca release. Although reducing the incidence of premature ventricular beats is a beneficial strategy, spontaneous Ca release in the form of Ca waves are arrhythmogenic in ways other than promoting TA. They can give rise to discordant alternans, EADs, or sudden repolarization changes that promote dispersion of repolarization(Xie and Weiss, 2009). Thus, this strategy may not be optimal for treating CPVT. SERCA block prevented spontaneous Ca release, DADs and TA. But this block was associated with a low SR load and high diastolic Ca in cytosol, possibly impairing contractility. RyR block resulted in only slightly higher SR load and abolition of Ca waves, DADs and TA, suggesting it as a desirable therapeutic approach. Recently, flecainide has attracted attention as a treatment possibility for CPVT(Hilliard et al., 2010; van der Werf et al., 2011; Watanabe et al., 2009). Flecainide, a known class 1C antiarrhythmic drug, blocks both I_{Na} and RyR flux. Whether the antiarrhythmic activity of flecainide is due to RyR open/closed state blockade(Hilliard et al., 2010) or sodium channel blockade is not clear(Liu et al., 2011). We found that a dose of 50 μM flecainide was necessary for suppression of TA. Incidentally, this intervention failed to prevent occurrence of Ca waves; rather, the TA suppression was due to reduced amount of Ca

released during episodes of Ca waves. The reduced amount activated a smaller I_{NaCa}, which generated DADs but was not sufficient to cause TA. In contrast, partial block of RyR was able to abolish Ca waves and DADs, suggesting that drugs blocking the pore of RyR may provide a better therapeutic strategy than those altering the RyR gating kinetics. The effect of flecainide on I_{Na} was not necessary for suppression of TA, consistent with the simulation result that TA is supported by I_{CaL}, without contribution from I_{Na}, in human ventricular myocytes.

Limitations

Recent studies indicated that the mechanism of invisible leak from the SR may be through stochastic openings of a single or few RyRs (Brochet et al., 2011; Zima et al., 2010). At present at physiological SR load, the model does not distinguish between SR leak via concerted openings of multiple RyRs (Ca sparks) or via openings of single or few RyRs (invisible leak). The effects of flecainide on RyR and I_{Na} were investigated at a resting heart rate of 1 Hz and during a post-pacing pause. Smaller effects on other currents (I_{K1}) and use dependence of I_{Na} block as a function of rate were not considered.

Chapter 5. Summary and future directions

In this study, we developed a multiscale model of Ca cycling and action potential (AP) of a cardiac ventricular myocyte. The model takes into account local interactions of LCCs and RyRs in restricted dyadic spaces and simulates the stochastic activity of these channels as a function of time, Ca and voltage. In addition, a kinetic model of RyR that includes regulation of its opening via CSQN was implemented. 10,000 Ca release units are simulated and integrated into a myocyte model of the AP based on membrane ionic currents of either guinea-pig (Faber and Rudy, 2000) or human ventricular myocytes (O'Hara et al. 2011). The multiscale model was used to simulate macroscopic (whole-cell) consequences of changes at the microscopic (dyadic) level that may occur during various pathophysiological conditions as described in Chapter 3.

In Chapter 4, the model was used to investigate causative mechanisms of initiation and therapeutic interventions for prevention of arrhythmias arising from RyR mutations and Ca cycling disturbances in Catecholaminergic Polymorphic Ventricular Tachycardia (CPVT). Simulation results indicated that increased sensitivity to Ca of RyR activation, as may occur during impaired domain-domain interaction between N terminus and central domains of RyR, can result in increased frequency of arrhythmogenic cellular activity in the form of DADs, EADs and TA. Model results indicated that the underlying mechanisms of such triggers for arrhythmias were impaired Ca handling in the ventricular myocyte. Increased frequency of Ca sparks and Ca waves was associated with these arrhythmogenic triggers. DADs occurred when Ca waves activated the depolarizing Na-Ca exchange current. When the magnitude of this current was sufficient to elevate membrane potential to the threshold for activation of I_{CaL}, TA occurred. Spontaneous SR

Ca release during phase-2 of the AP also activated the Na-Ca exchange current and prolonged the AP at plateau potentials. The prolongation of the AP resulted in reactivation of I_{CaL}, which acted as the depolarizing charge carrier for EAD generation. Simulations demonstrated that flecainide can abolish TA, suggesting that it can play a potential role as an anti-arrhythmic agent in the prevention of CPVT, as shown recently (Hong et al., 2012; van der Werf et al., 2011). Based on the simulations, the anti-arrhythmic effect of flecainide was due to reduction of the mean open time of RyR, not due to its blocking effect on I_{Na}.

Chapter 2 discusses the implications of hypoxia on arrhythmogenesis. The major conclusion from this study was that increased sensitivity of activation of I_{CaL} to β-adrenergic stimulation during hypoxia can result in cellular arrhythmogenic behavior in the form of EADs and/or TA. EADs occurred by reactivation of I_{CaL}. I_{CaL} increased the Ca content of the cell leading to spontaneous beats. Upstroke of spontaneous beat was due to I_{CaL}.

The multiscale model of Ca cycling and the AP represents an advancement in our understanding of Ca dynamics in the context of cell electrophysiology at several different levels. (1) The model simulates stochastic interactions of LCCs and RyRs in dyadic spaces. (2) The model includes a realistic number of Ca release units in computing whole-cell Ca dynamics and the AP. (3) The model includes diffusion of Ca across the cytosol and the SR, representing inter-dyad coupling. However, important limitations and avenues for future directions must be considered. The multiscale model is compartmental in nature and does not account for the actual three-dimensional spatial distribution of Ca release units in a ventricular myocyte. Neither does it consider the precise structure and

detailed geometric arrangements of compartments of Ca flow. Future models describing Ca cycling in a ventricular myocyte should consider these structural issues. Detailed cell signaling pathways, including adrenergic and CaMKII pathways, can modulate cardiac cell electrophysiology and it is important that they be incorporated in future studies using the model. Such models were developed in our laboratory (Heijman et al., 2011; Hund and Rudy, 2004) but not yet applied to the dyads-based stochastic model presented here. Ca diffusion in both the cytosol and SR is a subject of very intense investigations (Picht et al., 2011; Sobie and Lederer, 2012), as diffusion can be a complex function of buffering and tortuousity of SR network and myofibril space. As new data emerge, these properties should be included in the model as the formation of Ca waves and its role in causing arrhythmias is critically dependent on these parameters. Similarly, factors governing restitution of Ca release is a topic of active investigation(Kornyeyev et al., 2012; Sobie et al., 2005, 2006) and has been implicated in the formation of arrhythmogenic cellular behavior. Therefore new emerging data should be incorporated in future versions of the model.

Besides genetic mutations of RyR leading to CPVT, mutations in CSQN have been identified that can also cause CPVT(di Barletta et al., 2006; Lahat et al., 2001; Terentyev et al., 2008; Terentyev et al., 2006; Valle et al., 2008; Viatchenko-Karpinski et al., 2004). An understanding of how mutations in CSQN affect RyR gating to cause CPVT can lead to mechanistic insights on intracellular Ca handling and possible therapeutic targets that are not addressed in this work, but the multiscale model developed under this thesis provides a useful tool to study their effects.

Appendix A

Definitions and Abbreviations

ISO	Concentration of Isoproterenol (nmol/L)
K_{50}^{ISO}	$K_{0.5}$ of activation of L-type Ca channel current (I_{CaL}) or slowly activated delayed rectifier potassium current (I_{Ks}) in response to ISO
$Isofactor$	Change factor of I_{CaL} or I_{Ks}due to ISO
I_{CaL}	Calcium (Ca^{2+}) current through L-type channels (μA/μF)
I_{CaNa}	Sodium (Na^{+}) current through L-type channels (μA/μF)
I_{CaK}	Potassium (K^{+}) current through L-type channels (μA/μF)
d	Voltage dependent activation gate of I_{CaL}
f	Voltage dependent inactivation of I_{CaL}
f_{Ca}	Ca^{2+} dependent inactivation gate of I_{CaL}
$\overline{I_{Ca}}$	Max. Ca^{2+} current through L-type channels (μA/μF)
$\overline{I_{CaNa}}$	Max. Na^{+} current through L-type channels (μA/μF)
$\overline{I_{CaK}}$	Max. K^{+} current through L-type channels (μA/μF)
I_{Ks}	Current through slowly activated delayed rectifier K^{+} channels (μA/μF)
G_{Ks}	Max. conductance of I_{Ks} (mS/μF)
x_{s1}	Fast activation gate of I_{Ks}
x_{s2}	Slow activation gate of I_{Ks}
E_{Ks}	Reversal potential of I_{Ks} (mV)
I_{Nap}	Late Na^{+} current (μA/μF)

a_{Na}	Rate of activation of late Na^+ current (I_{Nap}) (ms^{-1})
b_{Na}	Rate of deactivation of late Na^+ current (I_{Nap}) (ms^{-1})
p	Activation gate of I_{Nap}
p_{ss}	Steady state value of activation gate of I_{Nap}
τ_p	Time constant of activation gate of I_{Nap}
G_{Na}	Max. conductance of fast Na^+ current ($mS.\mu F^{-1}$)
I_{Na}	Fast Na+ current ($\mu A.\mu F^{-1}$)
V_m	Membrane potential (mV)
E_{Na}	Reversal potential of Na^+ current (mV)
I_{up}	Ca^{2+} uptake from myoplasm to network sarcoplasmic reticulum (NSR) ($mmol.L^{-1}.ms^{-1}$)
$\overline{I_{up}}$	Max. Ca^{2+} uptake from myoplasm to NSR ($mmol.L^{-1}.ms^{-1}$)
K_{mup}	Half saturation concentration of I_{up} ($mmol.L^{-1}$)
Ca_i	Myoplasmic Ca^{2+} concentration ($\mu mol.L^{-1}.\mu F^{-1}$)
I_{K1}	Current through inward rectifier K^+ channels ($\mu A.\mu F^{-1}$)
G_{K1}	Max. conductance of I_{K1} ($mS.\mu F^{-1}$)
E_{K1}	Reversal potential of K^+ currents (mV)
k_{in}	Inactivation gate of I_{K1}

Model Equations

L-Type Calcium Current, I_{CaL}

Control Conditions

$K_{50}^{ISO} = 5.3$

$$Isofactor = 1 + \frac{3}{1 + 10^{\log_{10}(K_{50}^{ISO}) - \log_{10}(ISO)}}$$

Hypoxic Conditions

$K_{50}^{ISO} = 1.6$

$$Isofactor = 0.75 + \frac{3}{1 + 10^{\log_{10}(K_{50}^{ISO}) - \log_{10}(ISO)}}$$

$$I_{CaL} = Isofactor \cdot d \cdot f \cdot f_{Ca} \cdot \overline{I_{Ca}}$$

$$I_{CaNa} = Isofactor \cdot d \cdot f \cdot f_{Ca} \cdot \overline{I_{CaNa}}$$

$$I_{CaK} = Isofactor \cdot d \cdot f \cdot f_{Ca} \cdot \overline{I_{CaNa}}$$

<u>Slow Delayed Rectifier Potassium Current</u>, I_{Ks}

Control Conditions

$K_{50}^{ISO} = 15$

$$Isofactor = 0.3 + \frac{0.6}{1 + 10^{\log_{10}(K_{50}^{ISO}) - \log_{10}(ISO)}}$$

Hypoxic Conditions

$K_{50}^{ISO} = 1.5$

$$Isofactor = 0.3 + \frac{0.6}{1 + 10^{\log_{10}(K_{50}^{ISO}) - \log_{10}(ISO)}}$$

$$I_{Ks} = Isofactor \cdot G_{Ks} \cdot x_{S1} \cdot x_{S2} \cdot (V_m - E_{Ks})$$

<u>Late Sodium Current</u>, I_{NaL}

$$a_{Na} = 19 \cdot exp\left(\frac{V_m}{16.5}\right)$$

$$b_{Na} = 0.2 \cdot exp\left(\frac{-V_m}{20}\right)$$

$$p_{ss} = \left(\frac{a_{Na}}{a_{Na} + b_{Na}}\right)$$

$$\tau_p = \left(\frac{1}{a_{Na} + b_{Na}}\right)$$

$$p = p_{ss} - (p_{ss} - p) \cdot exp\left(\frac{-dt}{\tau_p}\right)$$

Control Conditions

$$I_{NaL} = 0.00007 \cdot G_{Na} \cdot p^3 \cdot (V_m - E_{Na})$$

Hypoxic Conditions

$$I_{NaL} = 0.00018 \cdot G_{Na} \cdot p^3 \cdot (V_m - E_{Na})$$

<u>Fast Sodium Current</u>, I_{Na}

Control Conditions

$$G_{Na} = 16$$

Hypoxic Conditions

$$G_{Na} = 14.4$$

<u>SR Ca^{2+} Uptake</u>

β-adrenergic stimulation (βAS) conditions

$$I_{up} = 1.5 \cdot \overline{I_{up}} \cdot \left(\frac{Ca_i}{Ca_i + K_{mup}}\right)$$

Non- βAS conditions

$$I_{up} = \overline{I_{up}} \cdot \left(\frac{Ca_i}{Ca_i + K_{mup}}\right)$$

<u>Inward Rectifier Potassium Current</u>, I_{K1}

Non- βAS conditions

$$I_{K1} = G_{K1} \cdot K_{in} \cdot (V_m - E_{K1})$$

βAS conditions

Experiments (Koumi et al., 1995) indicate that the open probability of I_{K1} channels decreases to 21±4% of its normal value during exposure to ISO. We incorporate this effect in the model by reducing I_{K1} to 25% of its normal value.

$I_{K1} = 0.25 \cdot G_{K1} \cdot K_{in} \cdot (V_m - E_{K1})$

Time-dependent changes of I_{CaL} and I_{Ks} due to βAS

For less than 50 paced beats

$Isofactor = Isofactor \cdot \left(\frac{i}{50}\right)$, where *i* is the beat number

For more than 50 beats

$Isofactor = Isofactor$

Appendix B

Definitions and Abbreviations

Cell Geometry

V_{cell}	Volume of the cell (μL)
A_{cap}	Capacitive membrane area (cm^2)
V_i	Volume of the myoplasm (μL)
V_{NSR}	Volume of the network sarcoplasmic reticulum (NSR) (μL)
V_{JSR}	Volume of the junctional sarcoplasmic reticulum (JSR) (μL)
V_{ss}	Volume of the submembrane space (μL)
N_{total_dyads}	Total number of dyads in the cell
v_i^n	Volume of the nth dyadic myoplasm (μL)
v_{ss}^n	Volume of the nth dyadic submembrane space (μL)
v_{NSR}^n	Volume of the nth dyadic NSR (μL)
v_{JSR}^n	Volume of the nth dyadic JSR (μL)
v_{ds}^n	Volume of the nth dyadic space volume (μL)
N_{LCC}^n	Number of L-type channels (LCCs) in the nth dyad
N_{RyR2}^n	Number of Ryanodine Receptors (RyR2s) in the nth dyad

Currents

I_{ion}	Total ionic current ($\mu A/\mu F$)
I_{Na}	Fast Na current ($\mu A/\mu F$)
I_{CaL}^{cell}	Whole-cell L-type Ca current ($\mu A/\mu F$)
I_{CaNa}	Na current through LCCs ($\mu A/\mu F$)
I_{CaK}	K current through LCCs ($\mu A/\mu F$)

I_{Cat}^{cell}	Whole-cell T-type Ca current ($\mu A/\mu F$)
I_{Kr}	Rapid delayed rectifier K current ($\mu A/\mu F$)
I_{Ks}	Slow delayed rectifier K current ($\mu A/\mu F$)
I_{K1}	Inward rectifier K current ($\mu A/\mu F$)
I_{NaCa}^{cell}	Whole-cell myoplasmic Na-Ca exchanger current ($\mu A/\mu F$)
$I_{NaCa,ss}^{cell}$	Whole-cell submembrane Na-Ca exchanger current ($\mu A/\mu F$)
I_{NaK}	Na-K pump current ($\mu A/\mu F$)
I_{Nab}	Background Na current ($\mu A/\mu F$)
I_{pCa}^{cell}	Whole-cell current through sarcolemmal Ca pump ($\mu A/\mu F$)
I_{Cab}^{cell}	Whole-cell background Ca current ($\mu A/\mu F$)
I_{Kp}	Plateau K current ($\mu A/\mu F$)
$\overline{I_{Ca}}$	Maximum Ca current through LCCs ($\mu A/\mu F$)
I_{CaL}^{n}	L-type Ca current in the nth dyad ($\mu A/\mu F$)
I_{Cab}^{n}	Background Ca current in the nth dyad ($\mu A/\mu F$)
I_{Cat}^{n}	T-type Ca current in the nth dyad ($\mu A/\mu F$)
I_{pCa}^{n}	Sarcolemmal pump current in the nth dyad ($\mu A/\mu F$)
I_{NaCa}^{n}	Na-Ca exchanger current in the myoplasm in the nth dyad ($\mu A/\mu F$)
$I_{NaCa,ss}^{n}$	Na-Ca exchanger current in the submembrane space in the nth dyad ($\mu A/\mu F$)
$\bar{I}_{CaNa}$	Maximum Na current through LCCs ($\mu A/\mu F$)
$\bar{I}_{CaK}$	Maximum K current through LCCs ($\mu A/\mu F$)
I_{st}	Stimulus current ($\mu A/\mu F$)

Gates

m	Activation gate of Na current
h	Fast inactivation gate of Na current
j	Slow inactivation gate of Na current
x_r	Activation gate of I_{Kr}
r_{kr}	Time-independent rectification gate of I_{Kr}
x_{s1}	Fast activation gate of I_{Ks}
x_{s2}	Slow activation gate of I_{Ks}
K_1	Inactivation gate of I_{K1}
K_p	Fast activation gate of I_{Kp}
b	Activation gate of T-type Ca current
g	Inactivation gate of T-type Ca current

Conductances and Permeability

G_{Na}	Maximum conductance of I_{Na} $(mS/\mu F)$
G_{Nab}	Maximum conductance of I_{Nab} $(mS/\mu F)$
G_{Kr}	Maximum conductance of I_{Kr} $(mS/\mu F)$
$P_{Na,K}$	Permeability ratio of Na ion to K ion
G_{Ks}	Maximum conductance of I_{Ks} $(mS/\mu F)$
G_{K1}	Maximum conductance of I_{K1} $(mS/\mu F)$
G_{Kp}	Maximum conductance of I_{Kp} $(mS/\mu F)$
G_{NaK}	Maximum conductance of I_{NaK} $(mS/\mu F)$
P_{Ca}	Permeability of membrane to Ca (cm/s)
P_{Na}	Permeability of membrane to Na (cm/s)
P_K	Permeability of membrane to K (cm/s)

Concentrations

Na_o	Extracellular Na concentration (mM)
Na_i	Intracellular Na concentration (mM)
K_i	Intracellular K concentration (mM)
K_o	Extracellular K concentration (mM)
Ca_o	Extracellular Ca concentration (mM)
Ca_{JSR}^n	Free JSR Ca concentration in the nth dyad (mM)
Ca_{NSR}^n	Free NSR Ca concentration in the nth dyad (mM)
Ca_d^n	Dyadic space Ca concentration in the nth dyad (μM)
Ca_{ss}^n	Submembrane Ca concentration in the nth dyad (mM)
Ca_i^n	Myoplasmic Ca concentration in the nth dyad (mM)
Ca_i^{cell}	Whole-cell Ca concentration in the myoplasm (mM)
Ca_{ss}^{cell}	Whole-cell Ca concentration in the submembrane space (mM)
Ca_d^{cell}	Whole-cell Ca concentration in the dyadic space (μM)
Ca_{NSR}^{cell}	Whole-cell Ca concentration in the NSR (mM)
Ca_{JSR}^{cell}	Whole-cell Ca concentration in the JSR (mM)
$\overline{NSR}$	Maximum Ca concentration in the NSR (mM)

Fluxes

J_{CaL}^n	Ca flux through LCCs in the nth dyad $(\mu M/ms)$
J_{rel}^n	Ca release flux in the nth dyad $(\mu M/ms)$
J_{Cadiff}^n	Diffusive Ca flux into the nth dyadic space from adjacent dyadic spaces $(\mu M/ms)$

$J^n_{NSRdiff}$	Diffusive Ca flux into the nth dyadic NSR from adjacent dyadic NSRs (mM/ms)
$J^n_{Cadiff\_ds\_ss}$	Diffusive Ca flux from dyadic space into submembrane space $(\mu M/ms)$
$J^n_{Cadiff\_ss\_i}$	Diffusive Ca flux from submembrane space into the myoplasm $(\mu M/ms)$
$J^n_{Cadiff\_NSR\_JSR}$	Translocation Ca flux from NSR to JSR (mM/ms)
J^n_{up}	Uptake Ca flux into NSR from the myoplasm in the nth dyad $(\mu M/ms)$
$\overline{I_{up}}$	Maximum rate of Ca uptake into NSR (mM/ms)
J^n_{leak}	SR leak into NSR in the nth dyad (mM/ms)

Buffers

$csqn$	Free calsequestrin (CSQN) concentration (mM)
$csqn.ca$	Ca-bound CSQN concentration (mM)
K_{mcsqn}	Half-saturation constant of Ca binding of CSQN (mM)
$\overline{csqn}$	Total concentration of CSQN (mM)
B_{ss}	Instantaneous buffering factor in submembrane space
B_{JSR}	Instantaneous buffering factor in JSR
B_{myo}	Instantaneous buffering factor in myoplasm
$\overline{TRPN}$	Maximum concentration of Troponin C buffer (mM)
$\overline{CMDN}$	Maximum concentration of Calmodulin (mM)
K_{mTRPN}	Half-saturation constant of Ca binding of Troponin C (mM)
K_{mCMDN}	Half-saturation constant of Ca binding of Calmodulin (mM)

Rates and Time Constants

k_{xy}	Transition rate between state x and y in LCC or in RyR2 (ms^{-1})
τ_{efflux}	Time-constant of Ca diffusion from the dyadic space into the submembrane space (ms)
τ_{refill}	Time-constant of Ca translocation from NSR to JSR (ms)
$\tau_{diff\_ds\_ds}$	Time-constant of Ca diffusion between dyadic spaces (ms)
$\tau_{diff\_NSR\_NSR}$	Time-constant of Ca diffusion between dyadic NSRs (ms)
d_{ryr}	Diffusion rate of Ca through open RyR2 (ms^{-1})

Reversal Potentials

E_{Na}	Reversal potential of Na current (mV)
E_K	Reversal potential of I_{Kr} and I_{K1} current (mV)
E_{Ks}	Reversal potential of I_{Ks} (mV)
E_{Ca}^{n}	Reversal potential of Ca in the nth dyad (mV)

Others

C_m	Total cellular membrane capacitance $(\mu F/cm^2)$
V_m	Transmembrane potential (mV)
F	Faraday constant (C/mol)
R	Gas constant $(J/kmol/K)$
T	Temperature (K)
BCL	Basic Cycle Length (ms)
$K_{m,Nai}$	Half saturation constant of Na for I_{NaK}
$K_{m,Ko}$	Half saturation constant of K for I_{NaK}
K_{mpCa}	Half saturation concentration for sarcolemmal Ca pump (mM)

K_{mup}	Half-saturation constant of SR Ca uptake into NSR (mM)
σ	Na_o - dependent factor of f_{NaK}
f_{NaK}	Voltage-dependent factor of I_{NaK}
$\gamma_{Cai},\ \gamma_{Cao}$	Activity coefficient of Ca
γ_s	Position of energy barrier controlling voltage-dependence of Na-Ca exchanger current
$\gamma_{Nai},\ \gamma_{Nao}$	Activity coefficient of Na
$\gamma_{Ki},\ \gamma_{Ko}$	Activity coefficient of K
z_{Ca}	Valence state of Ca
z_{Na}	Valence state of Na
z_K	Valence state of K
$N^n_{open\ LCC}$	Number of open LCCs in a dyad
$N^n_{open\ RyR2}$	Number of open RyR2s in the nth dyad
LCC	L-type channel
RyR2	Type 2 isoform of Ryanodine Receptor

Model Parameters

Cell Geometry

$V_{cell} = 38 \cdot 10^{-6}\ \mu L$

$A_{cap} = 1.534 \cdot 10^{-4}\ cm^2$

$V_i = 25.84 \cdot 10^{-6}\ \mu L$

$V_{NSR} = 2.098 \cdot 10^{-6}\ \mu L$

$V_{JSR} = 0.182 \cdot 10^{-6}\ \mu L$

$V_{ss} = 0.76 \cdot 10^{-6}\ \mu L$

$N_{total\_dyads} = 10{,}000$

$v_i^n = \frac{V_i}{N_{total\_dyads}}$

$v_{ss}^n = \frac{V_{ss}}{N_{total\_dyads}}$

$v_{NSR}^n = \frac{V_{NSR}}{N_{total\_dyads}}$

$v_{JSR}^n = \frac{V_{JSR}}{N_{total\_dyads}}$

$v_{ds}^n = 2 \cdot 10^{-13}\ \mu L$

$N_{LCC}^n = 15$

$N_{RyR2}^n = 100$

External Concentrations

$Na_o = 140\ mM$

$Ca_o = 2\ mM$

$K_o = 4.5\ mM$

Initial Conditions

$V_m = -86.364\ mV$

$m = 0.001231$

$h = 0.988864$

$j = 0.992842$

$xs_1 = 0.00611$

$xs_2 = 0.029537$

$xr = 0.000175$

$b = 0.001229$

$g = 0.991057$

$Na_i = 12.6233\ mM$

$K_i = 124.383\ mM$

$Ca_i^n = 8.83 \cdot 10^{-5}\ mM$

$Ca_{ss}^n = 8.04 \cdot 10^{-5}\ mM$

$Ca_d^n = 8.04 \cdot 10^{-2}\ \mu M$

$Ca_{JSR}^n = 1.29871\ mM$

$Ca_{NSR}^n = 1.29892\ mM$

Monte Carlo simulations determine the initial state of each LCC and RyR2 based on transition rates determined by the initial conditions.

Stimulus

A stimulus current (I_{st}) of -80 A/F amplitude for a duration of 0.5 ms is used to pace the cell. The current is assumed to be K current (Hund et al., 2001).

Model Currents

Fast Sodium Current, I_{Na}

$G_{Na} = 16$

$F = 96500$

$R = 8310$

$T = 310$

$$E_{Na} = \left(\frac{R \cdot T}{F}\right) \cdot ln\left(\frac{Na_o}{Na_i}\right)$$

$$\alpha_m = \frac{\left(0.32 \cdot (V_m + 47.13)\right)}{\left(1 - exp\left(-0.1 \cdot (V_m + 47.13)\right)\right)}$$

$$\beta_m = 0.08 \cdot exp\left(\frac{-V_m}{11}\right)$$

If (V_m< -40)

$$\alpha_j$$

$$= \frac{\left(\left(-127140 \cdot exp(0.2444 \cdot V_m) - 3.474 \cdot 10^{-5} \cdot exp(-0.04391 \cdot V_m)\right)(V_m + 37.78)\right)}{\left(1 + exp\left(0.311 \cdot (V_m + 79.23)\right)\right)}$$

$$\beta_j = \frac{(0.1212 \cdot exp(-0.01052 \cdot V_m))}{\left(1 + exp\left(-0.1378 \cdot (V_m + 40.14)\right)\right)}$$

$$\alpha_h = 0.135 \cdot exp\left(\frac{80 + V_m}{-6.8}\right)$$

$$\beta_h = 3.56 \cdot exp(0.079 \cdot V_m) + 3.1 \cdot 10^5 \cdot exp(0.35 \cdot V_m)$$

If (V_m ≥-40)

$$\alpha_h = \alpha_j = 0$$

$$\beta_h = \frac{1}{\left(0.13 \cdot \left(1 + exp\left(\frac{(V_m + 10.66)}{-11.1}\right)\right)\right)}$$

$$\beta_j = \frac{0.3 \cdot exp(-0.0000002535 \cdot V_m)}{1 + exp\left(-0.1 \cdot (V_m + 32)\right)}$$

$$\frac{dm}{dt} = \alpha_m \cdot m - \beta_m \cdot (1 - m)$$

$$\frac{dh}{dt} = \alpha_h \cdot h - \beta_h \cdot (1 - h)$$

$$\frac{dj}{dt} = \alpha_j \cdot j - \beta_j \cdot (1 - j)$$

$$I_{Na} = G_{Na} \cdot m^3 \cdot h \cdot j \cdot (V_m - E_{Na})$$

Fast Delayed Rectifier Potassium Current, I_{Kr}

$$G_{Kr} = 0.02614 \cdot \sqrt{\frac{K_o}{5.4}}$$

$$E_K = \left(\frac{R \cdot T}{F}\right) \cdot ln\left(\frac{K_o}{K_i}\right)$$

$$x_{rss} = \frac{1}{\left(1 + exp\left(-\frac{(V_m + 21.5)}{7.5}\right)\right)}$$

$$\tau_{xr} = \frac{1}{\frac{1.38 \cdot 10^{-3} \cdot (V_m + 14.2)}{1 - exp\left(-0.123 \cdot (V_m + 14.2)\right)} + \frac{6.1 \cdot 10^{-4} \cdot (V_m + 38.9)}{exp\left(0.145 \cdot (V_m + 38.9)\right) - 1}}$$

$$r_{kr} = \frac{1}{1 + exp\left(\frac{V_m + 9}{18.4}\right)}$$

$$\frac{dx_r}{dt} = \frac{x_{rss} - x_r}{\tau_{xr}}$$

$$I_{kr} = G_{kr} \cdot x_r \cdot r_{kr} \cdot (V_m - E_K)$$

Slow Delayed Rectifier K Current, I_{Ks}

$$P_{Na,K} = 0.01833$$

$$G_{Ks} = 0.3031 \cdot \left(1 + \frac{0.6}{1 + \left(\frac{3.8 \cdot 10^{-5}}{Ca_i^{cell}}\right)^{1.4}}\right)$$

$$E_{Ks} = \left(\frac{R \cdot T}{F}\right) \cdot ln\left(\frac{K_o + P_{Na,K} \cdot Na_o}{K_i + P_{Na,K} \cdot Na_i}\right)$$

$$x_{s1ss} = x_{s2ss} = \frac{1}{1 + exp\left(\frac{1.5 - V_m}{16.7}\right)}$$

$$\tau_{xs1} = \frac{1}{\frac{7.19 \cdot 10^{-5} \cdot (V_m + 30)}{1 - exp\left(-0.148 \cdot (V_m + 30)\right)} + \frac{1.31 \cdot 10^{-4} \cdot (V_m + 30)}{exp\left(0.0687 \cdot (V_m + 30)\right) - 1}}$$

$$\tau_{xs2} = 4 \cdot \tau_{xs1}$$

$$\frac{dx_{s1}}{dt} = \frac{x_{s1ss} - x_{s1}}{\tau_{xs1}}$$

$$\frac{d_{xs2}}{dt} = \frac{x_{s2ss} - x_{s2}}{\tau_{xs2}}$$

$$I_{Ks} = G_{ks} \cdot x_{s1} \cdot x_{s2} \cdot (V_m - E_{Ks})$$

Inward Rectifier K Current, $\boldsymbol{I_{K1}}$

$$G_{K1} = 0.75 \cdot \sqrt{\frac{K_o}{5.4}}$$

$$E_K = \left(\frac{R \cdot T}{F}\right) \cdot ln\left(\frac{K_o}{K_i}\right)$$

$$\alpha_{K1} = \frac{1.02}{1 + exp\left(0.2385 \cdot (V_m - E_K - 59.215)\right)}$$

$$\beta_{K1}$$

$$= \frac{0.49124 \cdot exp\left(0.08032 \cdot (V_m - E_K + 5.476)\right) + exp\left(0.06175 \cdot (V_m - E_K - 594.31)\right)}{1 + exp\left(-0.5143 \cdot (V_m - E_K + 4.753)\right)}$$

$$K_1 = \frac{\alpha_{K1}}{\alpha_{K1} + \beta_{K1}}$$

$$I_{K1} = G_{K1} \cdot K_1 \cdot (V_m - E_K)$$

Sodium Potassium Pump Current, $\boldsymbol{I_{NaK}}$

$$G_{NaK} = 2.25$$

$$\sigma = \frac{exp\left(\frac{Na_o}{67.3}\right) - 1}{7}$$

$$f_{NaK} = \frac{1}{1 + 0.1245 \cdot exp\left(\frac{-0.1 \cdot V_m \cdot F}{R \cdot T}\right) + 0.0365 \cdot \sigma \cdot exp\left(\frac{-V_m \cdot F}{R \cdot T}\right)}$$

$$K_{m,Nai} = 10$$

$$K_{m,Ko} = 1.5$$

$$I_{NaK} = G_{NaK} \cdot \frac{f_{NaK}}{1 + \left(\frac{K_{m,Nai}}{Na_i}\right)^2} \cdot \left(\frac{K_o}{K_o + K_{m,Ko}}\right)$$

Background Sodium Current, I_{Nab}

$$G_{Nab} = 0.004$$

$$E_{Na} = \left(\frac{R \cdot T}{F}\right) \cdot ln\left(\frac{Na_o}{Na_i}\right)$$

$$I_{Nab} = G_{Nab} \cdot (V_m - E_{Na})$$

Plateau K Current, I_{Kp}

$$G_{Kp} = 5.52 \cdot 10^{-3}$$

$$E_K = \left(\frac{R \cdot T}{F}\right) \cdot ln\left(\frac{K_o}{K_i}\right)$$

$$K_p = \frac{1}{1 + exp\left(\frac{7.488 - V_m}{5.98}\right)}$$

$$I_{Kp} = G_{Kp} \cdot K_p \cdot (V_m - E_K)$$

L-type Ca Current

The LCC scheme is same as in (Faber et al., 2007). Kinetic state of every single LCC in the model is monitored. Monte-Carlo simulations determine the state of LCC in the next time step based on transition rates shown below.

Transition Rates Between States

$$\alpha = 0.925 \cdot exp\left(\frac{V_m}{30}\right)$$

$$\beta = 0.39 \cdot exp\left(\frac{-V_m}{40}\right)$$

$$k_{C1C2} = 4 \cdot \alpha$$

$$k_{C2C3} = 3 \cdot \alpha$$

$$k_{C3C4} = 2 \cdot \alpha$$

$$k_{C4O} = \alpha$$

$$k_{OC4} = 4 \cdot \beta$$

$$k_{C4C3} = 3 \cdot \beta$$

$$k_{C3C2} = 2 \cdot \beta$$

$$k_{C2C1} = \beta$$

$$k_{C3IVs} = 0.005 \cdot exp\left(\frac{-V_m}{40}\right)$$

$$k_{C3IVf} = 0.245 \cdot exp\left(\frac{V_m}{10}\right)$$

$$k_{OIVs} = 0.03 \cdot exp\left(\frac{-V_m}{280}\right)$$

$$k_{OIVf} = 0.02 \cdot exp\left(\frac{V_m}{500}\right)$$

$$k_{IVsO} = 0.0011 \cdot exp\left(\frac{V_m}{500}\right)$$

$$k_{IVfO} = 0.035 \cdot exp\left(\frac{-V_m}{300}\right)$$

$$k_{IVsIVf} = \frac{k_{IVsO} \cdot k_{OIVf}}{k_{IVfO}}$$

$$k_{IVfIVs} = k_{OIVs}$$

$$k_{IVsC3} = \frac{k_{OC3} \cdot k_{IVsO} \cdot k_{C3IVs}}{k_{C3O} \cdot k_{OIVs}}$$

$$k_{IVfC3} = \frac{k_{OC3} \cdot k_{IVfO} \cdot k_{C3IVf}}{k_{C3O} \cdot k_{OIVf}}$$

<u>Ca-dependent Inactivation Transition Rates</u>

$$k_{Mode\,V-Mode\,Ca} = \frac{1}{1 + \frac{1}{Ca_d^n \cdot 10^{-3}}}$$

$$k_{Mode\,Ca-Mode\,V} = 0.01$$

$$\bar{I}_{Ca} = P_{Ca} \cdot z_{Ca}^2 \cdot \frac{V_m \cdot F^2}{R \cdot T} \cdot \frac{\gamma_{Cai} \cdot Ca_d^n \cdot 10^{-3} \cdot exp\left(\frac{z_{Ca} \cdot V_m \cdot F}{R \cdot T}\right) - \gamma_{Cao} \cdot Ca_o}{exp\left(\frac{z_{Ca} \cdot V_m \cdot F}{R \cdot T}\right) - 1}$$

$$P_{Ca} = 6.075 \cdot 10^{-4}$$

$$\gamma_{Cai} = 0.01$$

$$\gamma_{Cao} = 0.341$$

$$z_{Ca} = 2$$

$$I_{CaL}^n = \bar{I}_{Ca} \cdot \left(\frac{N_{open\,LCC}^n}{N_{LCC}^n}\right)$$

$$I_{CaL}^{cell} = \frac{\sum_{n=1}^{n=N_{total\_dyads}} I_{CaL}^n}{N_{total\_dyads}}$$

$$J_{CaL}^n = \frac{-I_{CaL}^n}{2 \cdot v_{ds}^n \cdot F} \cdot \left(\frac{A_{cap}}{N_{total\_dyads}}\right) \cdot 1000$$

The transition rate into Ca-dependent inactivation tier, $k_{Mode\,V-Mode\,Ca}$ and P_{Ca} were modified to reproduce I_{CaL}^{cell} during pacing in a guinea pig ventricular myocyte.

<u>Sodium (Na) Current through L-type Channels</u>

$$\bar{I}_{CaNa} = P_{Na} \cdot z_{Na}^2 \cdot \frac{V_m \cdot F^2}{R \cdot T} \cdot \frac{\gamma_{Nai} \cdot Na_i \cdot exp\left(\frac{z_{Na} \cdot V_m \cdot F}{R \cdot T}\right) - \gamma_{Nao} \cdot Na_o}{exp\left(\frac{z_{Na} \cdot V_m \cdot F}{R \cdot T}\right) - 1}$$

$P_{Na} = 1.518 \cdot 10^{-6}$

$\gamma_{Nai} = 0.75$

$\gamma_{Nao} = 0.75$

$z_{Na} = 1$

$$I_{CaNa} = \bar{I}_{CaNa} \cdot \sum_{n=1}^{n=N_{total\_dyads}} \frac{N_{open\ LCC}^n}{N_{LCC}^n}$$

<u>Potassium (K) Current through L-type Channels</u>

$$\bar{I}_{CaK} = P_K \cdot z_K^2 \cdot \frac{V_m \cdot F^2}{R \cdot T} \cdot \frac{\gamma_{Ki} \cdot K_i \cdot exp\left(\frac{z_K \cdot V_m \cdot F}{R \cdot T}\right) - \gamma_{Ko} \cdot K_o}{exp\left(\frac{z_K \cdot V_m \cdot F}{R \cdot T}\right) - 1}$$

$P_K = 4.34 \cdot 10^{-7}$

$\gamma_{Ki} = 0.75$

$\gamma_{Ko} = 0.75$

$z_K = 1$

$$I_{CaK} = \bar{I}_{CaK} \cdot \sum_{n=1}^{n=N_{total\_dyads}} \frac{N_{open\ LCC}^n}{N_{LCC}^n}$$

<u>Background Ca Current</u>

$$E_{Ca}^n = \left(\frac{R \cdot T}{2 \cdot F}\right) \cdot ln\left(\frac{Ca_o}{Ca_i^n}\right)$$

$I_{Cab}^n = 0.003016 \cdot (V_m - E_{Ca})$

$$I_{Cab}^{cell} = \frac{\sum_{n=1}^{n=N_{total\_dyads}} I_{Cab}^n}{N_{total\_dyads}}$$

T-type Ca Current

$$b_{ss} = \frac{1}{1 + exp\left(\frac{-(V_m + 14)}{10.8}\right)}$$

$$\tau_b = 3.7 + \frac{6.1}{1 + exp\left(\frac{V_m + 25}{4.5}\right)}$$

$$g_{ss} = \frac{1}{1 + exp\left(\frac{V_m + 60}{5.6}\right)}$$

$$\tau_g = -0.875 \cdot V_m + 12 \ (V_m < 0);\ \tau_g = 12 \ (V_m \geq 0)$$

$$\frac{db}{dt} = \frac{b_{ss} - b}{\tau_b}$$

$$\frac{dg}{dt} = \frac{g_{ss} - g}{\tau_g}$$

$$I_{Cat}^n = 0.05 \cdot b \cdot b \cdot g \cdot (V_m - E_{Ca}^n)$$

$$I_{Cat}^{cell} = \frac{\sum_{n=1}^{n=N_{total\_dyads}} I_{Cat}^n}{N_{total\_dyads}}$$

Sarcolemmal Ca Pump Current

$$I_{pCa}^n = \frac{1.15 \cdot Ca_i^n}{Ca_i^n + K_{mpCa}}$$

$$K_{mpCa} = 0.0005$$

$$I_{pCa}^{cell} = \frac{\sum_{n=1}^{n=N_{total\_dyads}} I_{pCa}^n}{N_{total\_dyads}}$$

Na-Ca Exchange Current in the Myoplasm

$$c_1 = 0.00025$$

$$c_2 = 0.0001$$

$$c_3 = 1$$

$$\gamma = 0.15$$

$$z_{Ca} = 2$$

$$I_{NaCa}^{n} = \frac{c_1 \cdot exp\left(\frac{(\gamma - 1) \cdot V_m \cdot F}{R \cdot T}\right) \cdot \left(exp\left(\frac{V_m \cdot F}{R \cdot T}\right) \cdot Na_i^3 \cdot Ca_o - c_3 \cdot Na_o^3 \cdot Ca_i^n\right)}{1 + c_2 \cdot exp\left(\frac{(\gamma - 1) \cdot V_m \cdot F}{R \cdot T}\right) \cdot \left(exp\left(\frac{V_m \cdot F}{R \cdot T}\right) \cdot Na_i^3 \cdot Ca_o + c_3 \cdot Na_o^3 \cdot Ca_i^n\right)}$$

$$I_{NaCa}^{cell} = \frac{\sum_{n=1}^{n=N_{total\_dyads}} I_{NaCa}^{n}}{N_{total\_dyads}}$$

Na-Ca Exchange Current in the Submembrane Space

$$I_{NaCa,ss}^{n}$$

$$= \frac{0.25 \cdot c_1 \cdot exp\left(\frac{(\gamma - 1) \cdot V_m \cdot F}{R \cdot T}\right) \cdot \left(exp\left(\frac{V_m \cdot F}{R \cdot T}\right) \cdot Na_i^3 \cdot Ca_o - c_3 \cdot Na_o^3 \cdot Ca_{ss}^n\right)}{1 + c_2 \cdot exp\left(\frac{(\gamma - 1) \cdot V_m \cdot F}{R \cdot T}\right) \cdot \left(exp\left(\frac{V_m \cdot F}{R \cdot T}\right) \cdot Na_i^3 \cdot Ca_o + c_3 \cdot Na_o^3 \cdot Ca_{ss}^n\right)}$$

$$I_{NaCa,ss}^{cell} = \frac{\sum_{n=1}^{n=N_{total\_dyads}} I_{NaCa,ss}^{n}}{N_{total\_dyads}}$$

Voltage

$$C_m = 1$$

$$I_{ion} = I_{Na} + I_{CaL}^{cell} + I_{CaNa} + I_{CaK} + I_{Cat}^{cell} + I_{Kr} + I_{Ks} + I_{K1} + I_{NaCa}^{cell} + I_{NaCa,ss}^{cell} + I_{NaK} + I_{Nab} + I_{pCa}^{cell} + I_{Cab}^{cell} + I_{Kp} + I_{st}$$

$$\frac{dV_m}{dt} = \frac{-I_{ion}}{C_m}$$

Ca fluxes

SR Ca release

Luminal Ca Sensor

CSQN can act both as SR Ca buffer (CSQN buffer) (MacLennan and Wong, 1971) and as a regulator of RyR2 openings (CSQN regulator) (Gyorke et al., 2004). The model

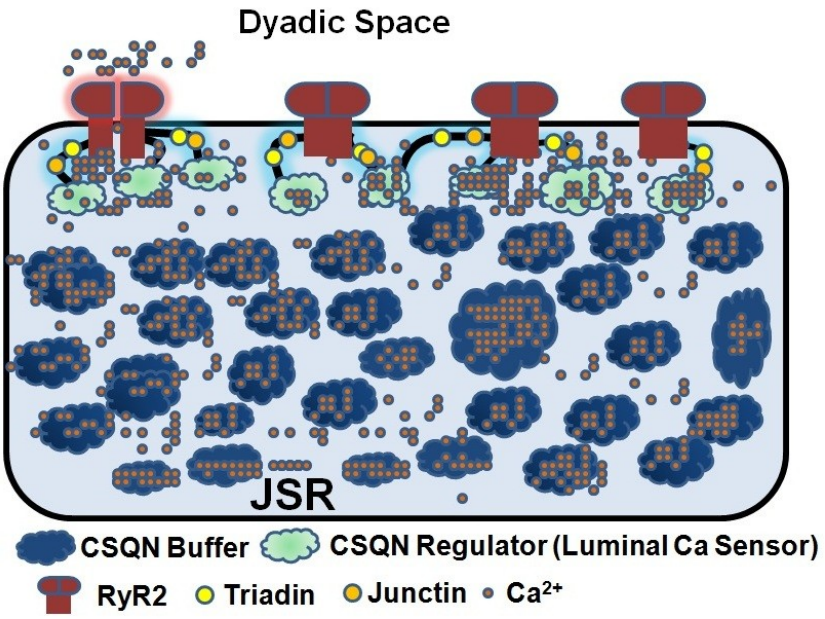

Figure B-1. Schematic diagram of CSQN function as represented in the model. Each RyR2 senses a proximal portion of CSQN network in its vicinity (CSQN Regulator). The majority of CSQN acts as CSQN Buffer. Junctional Sarcoplasmic Reticulum (JSR) is defined as the domain of CSQN distribution. The Ca buffering properties of CSQN are assumed to be identical throughout the CSQN network. Impaired CSQN buffering capacity was implemented by setting total CSQN to 0.01 mM, thus simulating the role of CSQN as RyR2 regulator only. Impaired luminal Ca sensor regulation was simulated by setting the transition rates between activation and recovery tiers of RyR2 (k_{C1C2}, k_{C2C1}, k_{O1O2} and k_{O2O1}) to zero. To simulate complete impairment of CSQN function (as might occur in a knock-out mouse), both total CSQN concentration and the above transition rates were set to zero.

of CSQN function can be interpreted biophysically as follows. Both free and Ca-bound CSQN form a relatively immobile network of protomers near RyR2s (CSQN network in Figure B-1), consistent with the scheme presented in (Royer and Rios, 2009). Diffusion of SR free Ca can occur readily in this network, thereby ensuring that the relative concentration of Ca-bound and free CSQN is spatially uniform in this network. Each RyR2 senses a proximal portion of the CSQN network in its vicinity (CSQN regulator in Figure B-1). In the RyR2 model (Figure 3-1A), transition rate from the activation to the

refractory tier is proportional to the concentration of free CSQN in the CSQN regulator domain, and the transition from the refractory to the activation tier is proportional to Ca-bound CSQN in this domain. In the CSQN network, the majority of CSQN acts as CSQN buffer (Figure B-1). This functional modeling scheme of luminal RyR2 regulation is based on the schemes depicted in (Qin et al., 2009) and (Gyorke et al., 2004). In the scheme presented in (Qin et al., 2009), the bulk of CSQN acts as SR Ca buffer. Single CSQN monomer binds to the Triadin/Junctin/RyR2 complex and modulates cytosolic Ca activation of RyR2. In the scheme presented in (Gyorke et al., 2004) CSQN binds to the Triadin/Junctin/RyR2 complex, making the channel refractory, and Ca-bound CSQN relieves this inhibition. The model was validated by comparing simulated open probability (P_o) of RyR2 at various SR and cytosolic Ca levels to single channel records measured in lipid bilayers (Figure 3-3). The cell model was then fine-tuned to insure robust termination and appropriate restitution of SR Ca release in the whole cell, and accurate global Ca transients at all rates.

RyR2 Model

The RyR2 model scheme is shown in Figure 3-1A. The kinetic state of every single RyR2 in the model is monitored. Monte-Carlo simulations determine the state of each individual RyR2 in the next time step based on transition rates provided below. The activation and deactivation rates (k_{C1O1}, k_{O1C1}) and RyR2 channel conductance (d_{ryr}) were adapted from (Sobie et al., 2002b). The activation rate reflects the fact that Ca binds instantaneously to each of the subunits of the RyR2 tetramer before a slower Ca-independent transition to the open state occurs. The deactivation rate implies that the mean open time of the RyR2 channel is ~ 2 ms ($1/k_{O1C1}$). Considerations for inclusion of

activation and refractory tiers in the RyR2 model are discussed in the "Luminal Ca Sensor" section. The transition rates between RyR2 tiers were constrained to reproduce accurately the local and global Ca concentrations and Ca currents in a guinea-pig myocyte during pacing at all rates.

Transition Rates

$$k_{C1O1} = \frac{3 \cdot (Ca_d^n)^4}{(Ca_d^n)^4 + (15)^4}$$

$$k_{O1C1} = 0.48$$

$$k_{C2O2} = \frac{3 \cdot (Ca_d^n)^4}{(Ca_d^n)^4 + (150)^4}$$

$$k_{O2C2} = 0.48$$

$$k_{C1C2} = 0.1 \cdot \left(\frac{csqn}{\overline{csqn}}\right)$$

$$k_{C2C1} = 0.1 \cdot \left(\frac{csqn.ca}{\overline{csqn}}\right) \cdot \frac{1}{1 + exp(0.9 \cdot BCL + t_{rel} - t)}$$

$$k_{O2O1} = k_{C2C1}$$

$$k_{O1O2} = k_{C1C2}$$

The dyad is considered active when the open fraction of RyR2s in the dyad is more than 0.2. t_{rel} is the time of last Ca release in the dyad, determined as the time at which open fraction of RyR2s in the dyad exceeds 0.2 upon activation of Ca release from the dyad.

$$J_{rel}^n = d_{ryr} \cdot N_{open\ RyR2}^n \cdot \left(1000 \cdot Ca_{JSR}^n - Ca_d^n\right)$$

$$d_{ryr} = 4$$

$$csqn = \frac{\overline{csqn} \cdot K_{mcsqn}}{\left(Ca_{jsr}^n + K_{mcsqn}\right)}$$

$csqn.ca = \overline{csqn} - csqn$

$\overline{csqn} = 10$

$K_{mcsqn} = 0.8$

Ca Diffusion fluxes

Inter-dyad coupling

In ventricular myocytes, Ca diffusion can occur in both the cytosol and the SR (Wu and Bers, 2006). Under conditions of Ca overload, Ca released in a dyad can diffuse and trigger Ca release in adjacent dyads, forming traveling Ca waves (Cheng et al., 1993); this provides evidence of cytosolic inter-dyad coupling. Model inter-dyad coupling in the cytosol was implemented by Ca diffusion between adjacent dyadic spaces. The parameters of diffusion were chosen so that Ca waves occur only under conditions of high SR load (with all other model parameters at control values). Simulated Ca release activity in a quiescent myocyte is shown in Figure B-2. With this choice of parameters, spontaneous Ca release activity in the form of Ca sparks, but not Ca waves, occurs when the initial SR load is low at 0.2 mM. Ca waves occur when the initial SR load is high at 5 mM.

Recent evidence suggests rapid diffusion of Ca in SR (Wu and Bers, 2006). Therefore, inter-dyad coupling in SR is implemented by fast Ca diffusion (time constant, $\tau_{diff\_NSR\_NSR}$ = 1 ms) between dyadic NSRs.

For $n > 1$ and $n < N_{total\_dyads}$

$$J^n_{Cadiff} = \frac{Ca_d^{n+1} - 2Ca_d^n + Ca_d^{n-1}}{\tau_{diff\_ds\_ds}}$$

$\tau_{diff\_ds\_ds} = 15$

$$J^{n}_{NSRdiff} = \frac{Ca^{n+1}_{NSR} - 2Ca^{n}_{NSR} + Ca^{n-1}_{NSR}}{\tau_{diff\_NSR\_NSR}}$$

$$\tau_{diff\_NSR\_NSR} = 1$$

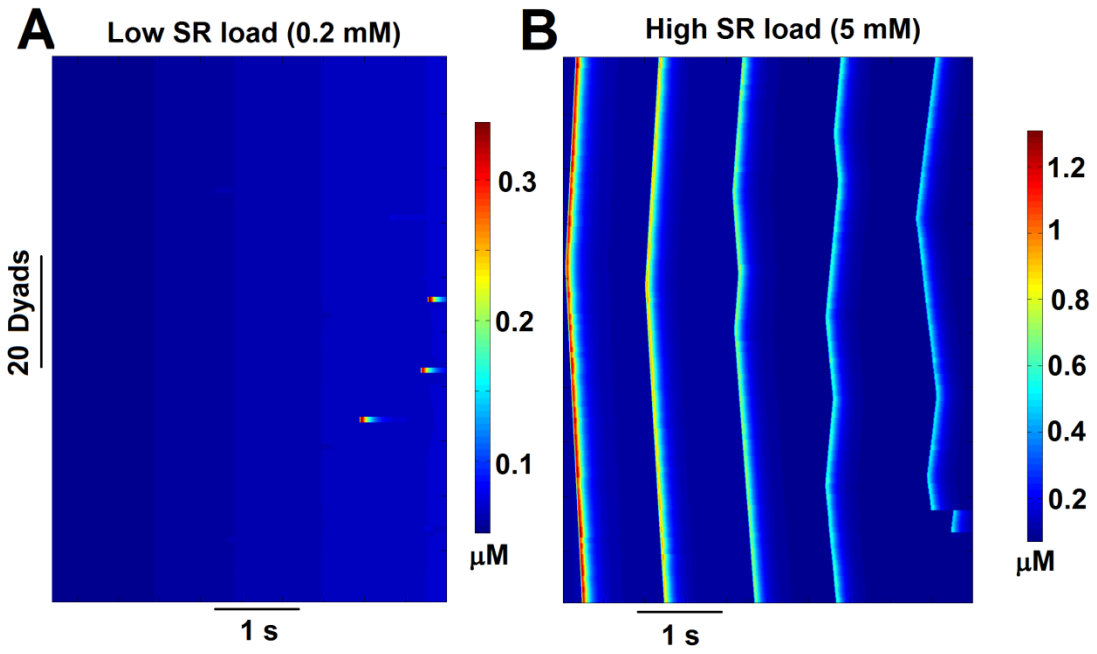

Figure B-2. Effect of SR Ca load on spontaneous Ca release activity in a quiescent myocyte. (A) Few Ca sparks are seen when the initial SR load was set to a low value of 0.2 mM. (B) Ca waves occur when initial SR load was set to a high value of 5 mM. The duration of simulation is 5 seconds. Ca waves occur during condition of high SR load, similar to experimental observation of Ca waves in Ca overloaded cells.

For $n = 1$

$$J^{1}_{Cadiff} = \frac{Ca^{2}_{d} - Ca^{1}_{d}}{\tau_{diff\_ds\_ds}}$$

$$J^{1}_{NSRdiff} = \frac{Ca^{2}_{NSR} - Ca^{1}_{NSR}}{\tau_{diff\_NSR\_NSR}}$$

For $n = N_{total\_dyads}$

$$J^{N_{total\_dyads}}_{Cadiff} = \frac{Ca_{d}^{N_{total\_dyads}} - Ca_{d}^{N_{total\_dyads}-1}}{\tau_{diff\_ds\_ds}}$$

$$J_{NSRdiff}^{N_{total\_dyads}} = \frac{Ca_{NSR}^{N_{total\_dyads}} - Ca_{NSR}^{N_{total\_dyads}-1}}{\tau_{diff\_NSR\_NSR}}$$

Ca Diffusion from Dyadic Space into Submembrane Space

$$J_{Cadiff\_ds\_ss}^{n} = \frac{Ca_{ds}^{n} - Ca_{ss}^{n}}{\tau_{efflux}}$$

$$\tau_{efflux} = 7 \cdot 10^{-4}$$

Ca Diffusion from the Submembrane Space into the Myoplasm

$$J_{Cadiff\_ss\_i}^{n} = \frac{Ca_{ss}^{n} - Ca_{i}^{n}}{\tau_{diff\_ss\_i}}$$

$$\tau_{diff\_ss\_i} = 0.1$$

Ca Translocation from NSR to JSR

$$J_{Cadiff\_NSR\_JSR}^{n} = \frac{Ca_{NSR}^{n} - Ca_{JSR}^{n}}{\tau_{refill}}$$

$$\tau_{refill} = 10$$

SERCA Ca Uptake in the SR

$$J_{up}^{n} = \frac{\overline{I_{up}} \cdot Ca_{i}^{n}}{Ca_{i}^{n} + K_{mup}}$$

$$\overline{I_{up}} = 0.00875;\ K_{mup} = 0.00092$$

Ca Leak from SR

$$J_{leak}^{n} = \frac{\overline{I_{up}} \cdot Ca_{NSR}^{n}}{\overline{NSR}}$$

$$\overline{NSR} = 15$$

Concentrations and Buffers

Ca Concentration in the Dyadic Space

$$Ca_d^n = J_{Cadiff}^n + \left(J_{rel}^n + J_{CaL}^n + \frac{Ca_{ss}^n}{\tau_{efflux}}\right) \cdot \tau_{efflux};\ \tau_{efflux} = 7.10^{-4}$$

$$Ca_d^{cell} = \frac{\sum_{n=1}^{n=N_{total\_dyads}} Ca_{ds}^n}{N_{total\_dyads}}$$

Note that we use the quasi-equilibrium approximation of Ca_d^n (Hinch, 2004) since the time-scale over which Ca_d^n equilibrates with Ca_{ss}^n is much faster than other processes such as channel gating and Ca diffusion from adjacent dyads.

Ca Concentration in the Submembrane Space

$$B_{ss} = \frac{1}{1 + \frac{\overline{B_{SR}} \cdot K_{mSR}}{(Ca_{ss}^n + K_{mSR})^2} + \frac{\overline{B_{SL}} \cdot K_{mSL}}{(Ca_{ss}^n + K_{mSL})^2}}$$

$\overline{BSR} = 0.047$

$\overline{BSL} = 1.124$

$K_{mSR} = 0.00087$

$K_{mSL} = 0.0087$

$$\frac{dCa_{ss}^n}{dt} = -B_{ss} \cdot \left(-2I_{NaCa,ss}^n \cdot \left(\frac{A_{cap}}{N_{total\_dyads} \cdot z_{Ca} \cdot F \cdot v_{ss}^n}\right) + J_{Cadiff\_ss\_i}^n - 10^{-3} \cdot J_{Cadiff\_ds\_ss}^n \cdot \left(\frac{v_{ds}^n}{v_{ss}^n}\right)\right)$$

$$Ca_{ss}^{cell} = \frac{\sum_{n=1}^{n=N_{total\_dyads}} Ca_{ss}^n}{N_{total\_dyads}}$$

Ca Concentration in the JSR

$$B_{JSR} = \frac{1}{1 + \frac{\overline{csqn} \cdot K_{mcsqn}}{\left(Ca_{JSR}^n + K_{mcsqn}\right)^2}}$$

$$\frac{dCa_{JSR}^{n}}{dt} = B_{JSR} \cdot \left(-10^{-3} \cdot J_{rel}^{n} \cdot \left(\frac{v_{ds}^{n}}{v_{JSR}^{n}} \right) + J_{Cadiff\_NSR\_JSR}^{n} \right)$$

$$Ca_{JSR}^{cell} = \frac{\sum_{n=1}^{n=N_{total\_dyads}} Ca_{JSR}^{n}}{N_{total\_dyads}}$$

Ca Concentration in the NSR

$$\frac{dCa_{NSR}^{n}}{dt} = J_{NSRdiff}^{n} + \left(J_{up}^{n} - J_{leak}^{n} - J_{Cadiff\_NSR\_JSR}^{n} \cdot \left(\frac{v_{JSR}^{n}}{v_{NSR}^{n}} \right) \right)$$

$$Ca_{NSR}^{cell} = \frac{\sum_{n=1}^{n=N_{total\_dyads}} Ca_{NSR}^{n}}{N_{total\_dyads}}$$

Ca Concentration in the Myoplasm

$$B_{myo} = \frac{1}{1 + \frac{\overline{TRPN} \cdot K_{mTRPN}}{(Ca_i^n + K_{mTRPN})^2} + \frac{\overline{CMDN} \cdot K_{mCMDN}}{(Ca_i^n + K_{mCMDN})^2}}$$

$\overline{TRPN} = 0.07$

$K_{mTRPN} = 0.0005$

$\overline{CMDN} = 0.05$

$K_{mCMDN} = 0.00238$

$$\frac{dCa_i^n}{dt} = -B_{myo} \cdot \left(\left(I_{Cab}^n + I_{Cat}^n + I_{pCa}^n - 2 \cdot I_{NaCa}^n \right) \cdot \left(\frac{A_{cap}}{N_{total\_dyads} \cdot z_{Ca} \cdot F \cdot v_i^n} \right) + \left(J_{up}^n - J_{leak}^n \right) \cdot \left(\frac{v_{NSR}^n}{v_{cyt}^n} \right) - J_{Cadiff\_ss\_i}^n \cdot \left(\frac{v_{ss}^n}{v_{cyt}^n} \right) \right)$$

$$Ca_i^{cell} = \frac{\sum_{n=1}^{n=N_{total\_dyads}} Ca_i^n}{N_{total\_dyads}}$$

Na Concentration in the Myoplasm

$$\frac{dNa_i}{dt} = -\left(I_{Na} + I_{Nab} + I_{CaNa} + 3 \cdot I_{NaK} + 3 \cdot I_{NaCa}^{cell} + 3 \cdot I_{NaCa,ss}^{cell}\right) \cdot \left(\frac{A_{cap}}{F \cdot V_i \cdot z_{Na}}\right)$$

K Concentration in the Myoplasm

$$\frac{dK_i}{dt} = -\left(I_{Kr} + I_{Ks} + I_{K1} + I_{Kp} + I_{CaK} - 2 \cdot I_{NaK} + I_{st}\right) \cdot \left(\frac{A_{cap}}{F \cdot V_i \cdot z_K}\right)$$

Additional Methods

Simulation Methods

A global time step of 0.1 ms is used in the simulations. At each time step, the channel states of the entire population of RyR2 and LCC, and the Ca concentration in each of the dyadic compartments are tracked. The transition rates between LCC and RyR2 states in every dyad are calculated based on the local dyadic Ca concentration. Monte Carlo simulations using these transition rates determine the state of individual LCCs and RyR2s in the dyad. The Ca fluxes through LCCs and RyR2s are calculated based on the number of open LCCs and RyR2s, respectively, and are used to update local dyadic Ca concentrations. The Ca currents in all individual dyads are added to determine the whole-cell Ca current for a given time step. One second simulated time during pacing at 1 Hz, implemented on a 164 processor Linux cluster for high-performance computing, takes about 900 seconds of computing time.

Fraction of active dyads and time of Ca release from the dyad

A dyad is assumed to be active when at least 20% of the RyR2s in the dyad are open indicating that a significant amount of Ca release is occurring in the dyad. Start time of Ca release from the dyad is determined as the time at which 20% of RyR2s open.

Ca Spark model

A simulated Ca spark is generated by using Ca efflux from the dyadic space as an input to the buffering and diffusion model of Ca sparks described previously (Smith et al., 1998), with the exception that we do not take into account optical blurring by confocal microscope.

Impairment of function

In the results section, effects of *complete* impairment of CSQN buffering capacity, luminal sensor function, or inter-dyad coupling are shown, unless stated otherwise. Impaired CSQN buffering capacity was implemented by setting total CSQN to 0.01 mM, thus simulating the role of CSQN as RyR2 regulator only. Impaired luminal Ca sensor regulation was simulated by setting the transition rates between activation and recovery tiers of RyR2 (k_{C1C2}, k_{C2C1}, k_{O1O2} and k_{O2O1}) to zero. To simulate complete impairment of CSQN function (as might occur in a knock-out mouse), both total CSQN concentration and the above transition rates were set to zero.

Appendix C

Definitions and Abbreviations

ISO	Isoproterenol concentration (nM)
$CSQN$	Calsequestrin
LCC	L-type Ca channel
$FKBP126$	Normalized degree of FKBP12.6-RyR interaction relative to control, no ISO conditions.
$Flecainide$	Flecainide concentration, μM
I_{CaL}	L-type Ca current, A/F
$d_{ss,PKA}$	Steady-state activation gate value of PKA phosphorylated LCC
V_m	Membrane potential, mV
I_{Na}	Fast Na current, A/F
G_{Na}	Conductance of I_{Na}, mS/mF
$k_{coopopen}$	Cooperativity factor of opening of RyRs
$k_{coopclose}$	Cooperativity factor of closing of RyRs
k_{C1O1}	Transition rate between state C1 and O1 of RyR, ms^{-1}
k_{O1C1}	Transition rate between state O1 and C1 of RyR, ms^{-1}
k_{C2O2}	Transition rate between state C2 and O2 of RyR, ms^{-1}
k_{O2C2}	Transition rate between state O2 and C2 of RyR, ms^{-1}
k_{C2C1}	Transition rate between state C2 and C1 of RyR, ms^{-1}
k_{C1C2}	Transition rate between state C1 and C2 of RyR, ms^{-1}
Ca_d^n	Dyadic space Ca concentration in the n^{th} dyad, μM
Ca_{JSR}^n	Dyadic JSR Ca concentration in the n^{th} dyad, mM

K_m	Half-saturation constant of cytosolic Ca activation of RyR when CSQN-unbound, μM
K_{mCSQN}	Half-saturation constant of cytosolic Ca activation of RyR when CSQN-bound, μM
N_{RyR}	Number of RyRs in a dyad
$N_{RyRopen}$	Number of open RyRs in a dyad
$csqn$	Free CSQN concentration, mM
$csqn.ca$	Ca bound CSQN concentration, mM
$\overline{csqn}$	Total concentration of CSQN, mM
K_{csqn}	Half-saturation constant of Ca binding to CSQN, mM
t_{rel}	Time of last Ca release in the dyad

Additional Methods

The multiscale Ca cycling model of a ventricular myocyte(Gaur and Rudy, 2011) and the recently published model of the human ventricular action potential(O'Hara et al., 2011) form the basis of the simulations. Below are details of the model and equations that were modified from the original publications for the purpose of this study.

Sarcoplasmic Reticulum (SR) Ca release

The RyR model is modified to include the effect of coupled gating of RyRs in a dyadic cluster (Marx et al., 2001). Coupled gating was implemented based on the assumption that the activation rate of RyR increases with the number of neighboring RyRs in the open state within a dyadic cluster. Similarly, the deactivation rate of RyR increases with the number of RyRs in the closed state in the cluster. An analogous scheme was described in the sticky cluster model of RyR (Sobie et al., 2002b). Coupled gating can be

a function of RyR-FKBP12.6 interaction (Marx et al., 2001), a property that was incorporated in the model. We assumed that for the maximum possible degree of RyR-FKBP12.6 interaction, $FKBP126 = 1$ (control conditions, no ISO), while for minimum interaction $FKBP126 = 0$.

Equations

$$k_{minC1O1} = 0.5 + 0.5 \cdot (1 - FKBP126)$$

$$k_{maxC1O1} = 1 - (1 - FKBP126)$$

$$k_{coopopen} = k_{minC1O1} + k_{maxC1O1} \cdot \frac{N_{RyRopen}}{N_{RyR}}$$

$$k_{minO1C1} = 0.5 + 0.5 \cdot (1 - FKBP126)$$

$$k_{maxO1C1} = 1 - (1 - FKBP126)$$

$$k_{coopclose} = k_{minO1C1} + k_{maxO1C1} \cdot \frac{N_{RyR} - N_{RyRopen}}{N_{RyR}}$$

$$k_{C1O1} = k_{coopopen} \cdot \left(3 \cdot \frac{(Ca_d^n)^4}{(Ca_d^n)^4 + (K_m)^4}\right);\ K_m = 12$$

$$k_{O1C1} = k_{coopclose} \cdot 0.48$$

$$k_{C2O2} = k_{coopopen} \cdot \left(3 \cdot \frac{(Ca_d^n)^4}{(Ca_d^n)^4 + \left(K_{mCSQN}\right)^4}\right); K_{mCSQN} = 150$$

$$k_{O2C2} = k_{coopclose} \cdot 0.48$$

$$\frac{csqn.ca}{\overline{csqn}} = \frac{\left(Ca_{JSR}^n\right)^8}{\left(Ca_{JSR}^n\right)^8 + K_{csqn}}$$

$$K_{csqn} = 0.8$$

$$k_{C1C2} = 10 \cdot \left(\frac{csqn}{\overline{csqn}}\right)$$

$$k_{C2C1} = 10 \cdot \left(\frac{csqn.ca}{\overline{csqn}}\right) \cdot \frac{1}{1 + exp(950 + t_{rel} - t)}$$

Isoproterenol (ISO) Effects

Parameters affected by PKA phosphorylation due to ISO are identical to those described by O'Hara and Rudy(O'Hara and Rudy, 2012), except for the changes indicated in Equations below. Maximum phosphorylation changes, corresponding to saturating dose of ISO, are considered in the study.

Equations

a. I_{CaL}

$$d_{ss,PKA} = \frac{1}{1 + exp\left(\frac{-(V_m + 16.94)}{4.23}\right)}$$

b. SR Ca release

$$FKBP126 = 0.5$$

CPVT-RyR Mutant Models

RyR mutation with impaired domain-domain interaction between N and central domains, also known as "domain unzipping"

It is proposed that the N-terminal domain and the central domain of RyR interact to act as a switch that opens or closes the channel. This interacting domain pair is named "domain switch"(Ikemoto and Yamamoto, 2002). In the resting state, the N terminal and central domain make contact at several sub-domains, stabilizing the closed state of RyR. With agonist stimulation (*eg*. cytosolic Ca), the subdomain contacts are weakened, leading to channel opening.

A mutation in either domain can cause impaired domain-domain interaction (domain-unzipping) (Uchinoumi et al., 2010) making the channel hyper-sensitive to agonist activation. Accordingly, we simulate the effect of domain-unzipping in CPVT-RyR

mutations as 2.4 fold increase in sensitivity of RyR to cytosolic Ca, from 12 μM in control to 5 μM in the mutant ($K_m = 5$).

RyR mutation with increased SR luminal Ca sensitivity

Increased sensitivity of RyR to SR luminal Ca was simulated by increasing the rate of transition from a CSQN-dependent RyR refractory mode to the active state of the molecule, following a dyadic Ca release event. The functional consequence of such a scheme is shortened refractoriness of RyR, as has been proposed(Gyorke, 2009).

Equations

$$k_{C2C1} = 20 \cdot \left(\frac{csqn.ca}{\overline{csqn}}\right) \cdot \frac{1}{1 + exp(500 + t_{rel} - t)}$$

$$k_{C2C1} = k_{O2O1}$$

RyR mutation with impaired RyR-FKBP12.6 binding affinity

^{35}S-labeled FKBP12.6 binding to microsomes from HEK23 cells containing wild type (WT) or CPVT mutant indicated decreased FKBP12.6 affinity for mutant RyR(Wehrens et al., 2003). PKA phosphorylation increased significantly the open probability of both WT mutant channels; the open probability being higher in mutant than in WT(Wehrens et al., 2003). It was shown that PKA phosphorylation of RyR at Ser^{2809} dissociates FKBP12.6 from the channel complex, providing a mechanism for upregulating RyR activity to increase SR Ca release in response to stress(Marx et al., 2000). To simulate this proposed mechanism, we assume that the RyR-FKBP12.6 interaction is weaker in mutant under basal (no ISO) conditions. With increase in PKA RyR phosphorylation (increased dose of ISO), the RyR-FKBP12.6 interaction is decreased in both WT and mutant channels, but more so in mutants.

Equations

$FKBP126 = 0.8$; No ISO conditions

$FKBP126 = 0$; ISO conditions

Flecainide Effect on I_{Na} and RyR

Equations

$$G_{Na} = 75 \cdot \frac{1}{1 + \left(\frac{Flecainide}{5.7}\right)^{1.8}}$$

$$k_{O1C1} = k_{O1C1} \cdot \frac{1.0037}{1.0037 - 0.165 \cdot Flecainide^{0.3575}}$$

$$k_{C1O1} = \frac{k_{C1O1}}{\left(1 + \frac{Flecainide}{50}\right)}$$

References

Ai, X., Curran, J.W., Shannon, T.R., Bers, D.M., and Pogwizd, S.M. (2005). Ca2+/calmodulin-dependent protein kinase modulates cardiac ryanodine receptor phosphorylation and sarcoplasmic reticulum Ca2+ leak in heart failure. Circ Res *97*, 1314-1322.

Bers, D.M. (2002). Cardiac excitation-contraction coupling. Nature *415*, 198-205.

Bers, D.M. (2012). Ryanodine receptor s2808 phosphorylation in heart failure: smoking gun or red herring. Circ Res *110*, 796-799.

Brochet, D.X., Xie, W., Yang, D., Cheng, H., and Lederer, W.J. (2011). Quarky calcium release in the heart. Circ Res *108*, 210-218.

Brochet, D.X., Yang, D., Di Maio, A., Lederer, W.J., Franzini-Armstrong, C., and Cheng, H. (2005). Ca2+ blinks: rapid nanoscopic store calcium signaling. Proc Natl Acad Sci U S A *102*, 3099-3104.

Cannell, M.B., and Soeller, C. (1997). Numerical analysis of ryanodine receptor activation by L-type channel activity in the cardiac muscle diad. Biophys J *73*, 112-122.

Casey, T.M., Pakay, J.L., Guppy, M., and Arthur, P.G. (2002). Hypoxia causes downregulation of protein and RNA synthesis in noncontracting Mammalian cardiomyocytes. Circulation Research *90*, 777-783.

Cerrone, M., Colombi, B., Santoro, M., di Barletta, M.R., Scelsi, M., Villani, L., Napolitano, C., and Priori, S.G. (2005). Bidirectional ventricular tachycardia and fibrillation elicited in a knock-in mouse model carrier of a mutation in the cardiac ryanodine receptor. Circ Res *96*, e77-82.

Cerrone, M., Napolitano, C., and Priori, S.G. (2009). Catecholaminergic polymorphic ventricular tachycardia: A paradigm to understand mechanisms of arrhythmias associated to impaired Ca(2+) regulation. Heart Rhythm *6*, 1652-1659.

Chelu, M.G., Danila, C.I., Gilman, C.P., and Hamilton, S.L. (2004). Regulation of ryanodine receptors by FK506 binding proteins. Trends Cardiovasc Med *14*, 227-234.

Cheng, H., Cannell, M.B., and Lederer, W.J. (1994). Propagation of Excitation-Contraction Coupling into Ventricular Myocytes. Pflug Arch Eur J Phy *428*, 415-417.

Cranefield, P.F., and Aronson, R.S. (1988). Torsade de pointes and other pause-induced ventricular tachycardias: the short-long-short sequence and early afterdepolarizations. Pacing Clin Electrophysiol *11*, 670-678.

Curran, J., Brown, K.H., Santiago, D.J., Pogwizd, S., Bers, D.M., and Shannon, T.R. (2010). Spontaneous Ca waves in ventricular myocytes from failing hearts depend on Ca(2+)-calmodulin-dependent protein kinase II. J Mol Cell Cardiol *49*, 25-32.

Curran, J., Hinton, M.J., Rios, E., Bers, D.M., and Shannon, T.R. (2007). Beta-adrenergic enhancement of sarcoplasmic reticulum calcium leak in cardiac myocytes is mediated by calcium/calmodulin-dependent protein kinase. Circ Res *100*, 391-398.

di Barletta, M.R., Viatchenko-Karpinski, S., Nori, A., Memmi, M., Terentyev, D., Turcato, F., Valle, G., Rizzi, N., Napolitano, C., Gyorke, S., Volpe, P., and Priori, S.G. (2006). Clinical phenotype and functional characterization of CASQ2 mutations associated with catecholaminergic polymorphic ventricular tachycardia. Circulation *114*, 1012-1019.

Dirksen, W.P., Lacombe, V.A., Chi, M., Kalyanasundaram, A., Viatchenko-Karpinski, S., Terentyev, D., Zhou, Z., Vedamoorthyrao, S., Li, N., Chiamvimonvat, N., Carnes, C.A., Franzini-Armstrong, C., Gyorke, S., and Periasamy, M. (2007). A mutation in calsequestrin, CASQ2D307H, impairs Sarcoplasmic Reticulum Ca2+ handling and causes complex ventricular arrhythmias in mice. Cardiovasc Res *75*, 69-78.

Dorian, P. (2005). Antiarrhythmic action of beta-blockers: potential mechanisms. J Cardiovasc Pharmacol Ther *10 Suppl 1*, S15-22.

Eisner, D.A., Kashimura, T., Venetucci, L.A., and Trafford, A.W. (2009). From the ryanodine receptor to cardiac arrhythmias. Circ J *73*, 1561-1567.

El-Sherif, N. (2001). Mechanism of ventricular arrhythmias in the long QT syndrome: on hermeneutics. J Cardiovasc Electrophysiol *12*, 973-976.

Faber, G.M., and Rudy, Y. (2000). Action potential and contractility changes in [Na(+)](i) overloaded cardiac myocytes: a simulation study. Biophys J *78*, 2392-2404.

Faber, G.M., Silva, J., Livshitz, L., and Rudy, Y. (2007). Kinetic properties of the cardiac L-type Ca2+ channel and its role in myocyte electrophysiology: A theoretical investigation. Biophys J *92*, 1522-1543.

Fearon, I.M., Palmer, A.C., Balmforth, A.J., Ball, S.G., Mikala, G., Schwartz, A., and Peers, C. (1997). Hypoxia inhibits the recombinant alpha 1C subunit of the human cardiac L-type Ca2+ channel. Journal of Physiology *500*, 551-556.

Fearon, I.M., Palmer, A.C., Balmforth, A.J., Ball, S.G., Varadi, G., and Peers, C. (1999). Modulation of recombinant human cardiac L-type Ca2+ channel alpha1C subunits by redox agents and hypoxia. Journal of Physiology *514*, 629-637.

Fearon, I.M., Varadi, G., Koch, S.E., Isaacsohn, I., Ball, S.G., and Peers, C. (2000). Splice variants reveal the region involved in oxygen sensing by recombinant human L-type Ca2+ channels. Circulation Research *87*, 537-539.

Fernandez-Velasco, M., Rueda, A., Rizzi, N., Benitah, J.P., Colombi, B., Napolitano, C., Priori, S.G., Richard, S., and Gomez, A.M. (2009). Increased Ca2+ sensitivity of the ryanodine receptor mutant RyR2R4496C underlies catecholaminergic polymorphic ventricular tachycardia. Circ Res *104*, 201-209, 212p following 209.

Franzini-Armstrong, C., Protasi, F., and Ramesh, V. (1999). Shape, size, and distribution of Ca(2+) release units and couplons in skeletal and cardiac muscles. Biophys J *77*, 1528-1539.

Gallacher, D.J., Van de Water, A., van der Linde, H., Hermans, A.N., Lu, H.R., Towart, R., and Volders, P.G. (2007). In vivo mechanisms precipitating torsades de pointes in a canine model of drug-induced long-QT1 syndrome. Cardiovasc Res *76*, 247-256.

Gaur, N., and Rudy, Y. (2011). Multiscale modeling of calcium cycling in cardiac ventricular myocyte: macroscopic consequences of microscopic dyadic function. Biophysical Journal *100*, 2904-2912.

Gomez, A.M., Guatimosim, S., Dilly, K.W., Vassort, G., and Lederer, W.J. (2001). Heart failure after myocardial infarction: altered excitation-contraction coupling. Circulation *104*, 688-693.

Gomez, A.M., Valdivia, H.H., Cheng, H., Lederer, M.R., Santana, L.F., Cannell, M.B., McCune, S.A., Altschuld, R.A., and Lederer, W.J. (1997). Defective excitation-contraction coupling in experimental cardiac hypertrophy and heart failure. Science *276*, 800-806.

Greenstein, J.L., Hinch, R., and Winslow, R.L. (2006). Mechanisms of excitation-contraction coupling in an integrative model of the cardiac ventricular myocyte. Biophys J *90*, 77-91.

Greenstein, J.L., and Winslow, R.L. (2002). An integrative model of the cardiac ventricular myocyte incorporating local control of Ca2+ release. Biophys J *83*, 2918-2945.

Guo, T., Cornea, R.L., Huke, S., Camors, E., Yang, Y., Picht, E., Fruen, B.R., and Bers, D.M. (2010). Kinetics of FKBP12.6 binding to ryanodine receptors in permeabilized cardiac myocytes and effects on Ca sparks. Circ Res *106*, 1743-1752.

Gyorke, I., Hester, N., Jones, L.R., and Gyorke, S. (2004). The role of calsequestrin, triadin, and junctin in conferring cardiac ryanodine receptor responsiveness to luminal calcium. Biophys J *86*, 2121-2128.

Gyorke, S. (2009). Molecular basis of catecholaminergic polymorphic ventricular tachycardia. Heart Rhythm *6*, 123-129.

Gyorke, S., Gyorke, I., Lukyanenko, V., Terentyev, D., Viatchenko-Karpinski, S., and Wiesner, T.F. (2002). Regulation of sarcoplasmic reticulum calcium release by luminal calcium in cardiac muscle. Front Biosci *7*, d1454-1463.

Heijman, J., Volders, P.G., Westra, R.L., and Rudy, Y. (2011). Local control of beta-adrenergic stimulation: Effects on ventricular myocyte electrophysiology and Ca(2+)-transient. J Mol Cell Cardiol *50*, 863-871.

Hilliard, F.A., Steele, D.S., Laver, D., Yang, Z., Le Marchand, S.J., Chopra, N., Piston, D.W., Huke, S., and Knollmann, B.C. (2010). Flecainide inhibits arrhythmogenic Ca2+ waves by open state block of ryanodine receptor Ca2+ release channels and reduction of Ca2+ spark mass. J Mol Cell Cardiol *48*, 293-301.

Hinch, R. (2004). A mathematical analysis of the generation and termination of calcium sparks. Biophys J *86*, 1293-1307.

Hong, R.A., Rivera, K.K., Jittirat, A., and Choi, J.J. (2012). Flecainide Suppresses Defibrillator-Induced Storming in Catecholaminergic Polymorphic Ventricular Tachycardia. Pacing Clin Electrophysiol.

Hool, L.C. (2000). Hypoxia increases the sensitivity of the L-type Ca(2+) current to beta-adrenergic receptor stimulation via a C2 region-containing protein kinase C isoform. Circulation Research *87*, 1164-1171.

Hool, L.C. (2001). Hypoxia alters the sensitivity of the L-type Ca(2+) channel to alpha-adrenergic receptor stimulation in the presence of beta-adrenergic receptor stimulation. Circulation Research *88*, 1036-1043.

Hool, L.C. (2004). Differential regulation of the slow and rapid components of guinea-pig cardiac delayed rectifier K^+ channels by hypoxia. Journal of Physiology *554*, 743-754.

Hool, L.C. (2005). Acute hypoxia differentially regulates K(+) channels. Implications with respect to cardiac arrhythmia. Eur Biophys J *34*, 369-376.

Hool, L.C., and Arthur, P.G. (2002). Decreasing cellular hydrogen peroxide with catalase mimics the effects of hypoxia on the sensitivity of the L-type Ca2+ channel to beta-adrenergic receptor stimulation in cardiac myocytes. Circulation Research *91*, 601-609.

Hool, L.C., Di Maria, C.A., Viola, H.M., and Arthur, P.G. (2005). Role of NAD(P)H oxidase in the regulation of cardiac L-type Ca2+ channel function during acute hypoxia. Cardiovasc Res *67*, 624-635.

Hund, T.J., and Rudy, Y. (2004). Rate dependence and regulation of action potential and calcium transient in a canine cardiac ventricular cell model. Circulation *110*, 3168-3174.

Ikemoto, N., and Yamamoto, T. (2002). Regulation of calcium release by interdomain interaction within ryanodine receptors. Front Biosci *7*, d671-683.

Jafri, M.S., Rice, J.J., and Winslow, R.L. (1998). Cardiac Ca2+ dynamics: the roles of ryanodine receptor adaptation and sarcoplasmic reticulum load. Biophys J *74*, 1149-1168.

January, C.T., and Riddle, J.M. (1989). Early afterdepolarizations: mechanism of induction and block. A role for L-type Ca2+ current. Circulation Research *64*, 977-990.

Jiang, D., Wang, R., Xiao, B., Kong, H., Hunt, D.J., Choi, P., Zhang, L., and Chen, S.R. (2005). Enhanced store overload-induced Ca2+ release and channel sensitivity to luminal Ca2+ activation are common defects of RyR2 mutations linked to ventricular tachycardia and sudden death. Circ Res *97*, 1173-1181.

Jiang, D., Xiao, B., Yang, D., Wang, R., Choi, P., Zhang, L., Cheng, H., and Chen, S.R. (2004). RyR2 mutations linked to ventricular tachycardia and sudden death reduce the threshold for store-overload-induced Ca2+ release (SOICR). Proc Natl Acad Sci U S A *101*, 13062-13067.

Ju, Y.K., Saint, D.A., and Gage, P.W. (1994). Inactivation-resistant channels underlying the persistent sodium current in rat ventricular myocytes. Proceedings of the Royal Society of London - Series B: Biological Sciences *256*, 163-168.

Ju, Y.K., Saint, D.A., and Gage, P.W. (1996). Hypoxia increases persistent sodium current in rat ventricular myocytes. Journal of Physiology *497*, 337-347.

Kannankeril, P.J., Mitchell, B.M., Goonasekera, S.A., Chelu, M.G., Zhang, W., Sood, S., Kearney, D.L., Danila, C.I., De Biasi, M., Wehrens, X.H., Pautler, R.G., Roden, D.M., Taffet, G.E., Dirksen, R.T., Anderson, M.E., and Hamilton, S.L. (2006). Mice with the R176Q cardiac ryanodine receptor mutation exhibit catecholamine-induced ventricular tachycardia and cardiomyopathy. Proc Natl Acad Sci U S A *103*, 12179-12184.

Keating, M.T., and Sanguinetti, M.C. (2001). Molecular and cellular mechanisms of cardiac arrhythmias. Cell *104*, 569-580.

Knollmann, B.C., Chopra, N., Hlaing, T., Akin, B., Yang, T., Ettensohn, K., Knollmann, B.E., Horton, K.D., Weissman, N.J., Holinstat, I., Zhang, W., Roden, D.M., Jones, L.R., Franzini-Armstrong, C., and Pfeifer, K. (2006). Casq2 deletion causes sarcoplasmic reticulum volume increase, premature Ca2+ release, and catecholaminergic polymorphic ventricular tachycardia. J Clin Invest *116*, 2510-2520.

Kornyeyev, D., Petrosky, A.D., Zepeda, B., Ferreiro, M., Knollmann, B., and Escobar, A.L. (2012). Calsequestrin 2 deletion shortens the refractoriness of Ca(2)(+) release and reduces rate-dependent Ca(2)(+)-alternans in intact mouse hearts. J Mol Cell Cardiol *52*, 21-31.

Koumi, S., Wasserstrom, J.A., and Ten Eick, R.E. (1995). Beta-adrenergic and cholinergic modulation of inward rectifier K+ channel function and phosphorylation in guinea-pig ventricle. J Physiol *486 (Pt 3)*, 661-678.

Kubalova, Z., Terentyev, D., Viatchenko-Karpinski, S., Nishijima, Y., Gyorke, I., Terentyeva, R., da Cunha, D.N., Sridhar, A., Feldman, D.S., Hamlin, R.L., Carnes, C.A., and Gyorke, S. (2005). Abnormal intrastore calcium signaling in chronic heart failure. Proc Natl Acad Sci U S A *102*, 14104-14109.

Lahat, H., Pras, E., Olender, T., Avidan, N., Ben-Asher, E., Man, O., Levy-Nissenbaum, E., Khoury, A., Lorber, A., Goldman, B., Lancet, D., and Eldar, M. (2001). A missense mutation in a highly conserved region of CASQ2 is associated with autosomal recessive catecholamine-induced polymorphic ventricular tachycardia in Bedouin families from Israel. Am J Hum Genet *69*, 1378-1384.

Lakatta, E.G., Talo, A., Capogrossi, M.C., Spurgeon, H.A., and Stern, M.D. (1992). Spontaneous sarcoplasmic reticulum Ca2+ release leads to heterogeneity of contractile and electrical properties of the heart. Basic Res Cardiol *87 Suppl 2*, 93-104.

Laver, D.R. (2009). Luminal Ca(2+) activation of cardiac ryanodine receptors by luminal and cytoplasmic domains. Eur Biophys J *39*, 19-26.

Litwin, S.E., Zhang, D., and Bridge, J.H. (2000). Dyssynchronous Ca(2+) sparks in myocytes from infarcted hearts. Circ Res *87*, 1040-1047.

Liu, N., Colombi, B., Memmi, M., Zissimopoulos, S., Rizzi, N., Negri, S., Imbriani, M., Napolitano, C., Lai, F.A., and Priori, S.G. (2006). Arrhythmogenesis in catecholaminergic polymorphic ventricular tachycardia: insights from a RyR2 R4496C knock-in mouse model. Circ Res *99*, 292-298.

Liu, N., Denegri, M., Ruan, Y., Avelino-Cruz, J.E., Perissi, A., Negri, S., Napolitano, C., Coetzee, W.A., Boyden, P.A., and Priori, S.G. (2011). Short communication: flecainide exerts an antiarrhythmic effect in a mouse model of catecholaminergic polymorphic ventricular tachycardia by increasing the threshold for triggered activity. Circ Res *109*, 291-295.

Luo, C.H., and Rudy, Y. (1994). A dynamic model of the cardiac ventricular action potential. I. Simulations of ionic currents and concentration changes. Circ Res *74*, 1071-1096.

MacLennan, D.H., and Chen, S.R. (2009). Store overload-induced Ca2+ release as a triggering mechanism for CPVT and MH episodes caused by mutations in RYR and CASQ genes. J Physiol *587*, 3113-3115.

MacLennan, D.H., and Wong, P.T. (1971). Isolation of a calcium-sequestering protein from sarcoplasmic reticulum. Proc Natl Acad Sci U S A *68*, 1231-1235.

Marban, E., Robinson, S.W., and Wier, W.G. (1986). Mechanisms of arrhythmogenic delayed and early afterdepolarizations in ferret ventricular muscle. Journal of Clinical Investigation *78*, 1185-1192.

Marx, S.O., Gaburjakova, J., Gaburjakova, M., Henrikson, C., Ondrias, K., and Marks, A.R. (2001). Coupled gating between cardiac calcium release channels (ryanodine receptors). Circ Res *88*, 1151-1158.

Marx, S.O., Reiken, S., Hisamatsu, Y., Jayaraman, T., Burkhoff, D., Rosemblit, N., and Marks, A.R. (2000). PKA phosphorylation dissociates FKBP12.6 from the calcium

release channel (ryanodine receptor): defective regulation in failing hearts. Cell *101*, 365-376.

Mazur, A., Roden, D.M., and Anderson, M.E. (1999). Systemic administration of calmodulin antagonist W-7 or protein kinase A inhibitor H-8 prevents torsade de pointes in rabbits. Circulation *100*, 2437-2442.

McDonald, T.F., Pelzer, S., Trautwein, W., and Pelzer, D.J. (1994). Regulation and modulation of calcium channels in cardiac, skeletal, and smooth muscle cells. Physiological Reviews *74*, 365-507.

Michelakis, E.D., Rebeyka, I., Wu, X., Nsair, A., Thebaud, B., Hashimoto, K., Dyck, J.R., Haromy, A., Harry, G., Barr, A., and Archer, S.L. (2002). O2 sensing in the human ductus arteriosus: regulation of voltage-gated K+ channels in smooth muscle cells by a mitochondrial redox sensor. Circulation Research *91*, 478-486.

O'Hara, T., and Rudy, Y. (2012). Arrhythmia formation in subclinical ("silent") long QT syndrome requires multiple insults: quantitative mechanistic study using the KCNQ1 mutation Q357R as example. Heart Rhythm *9*, 275-282.

O'Hara, T., Virag, L., Varro, A., and Rudy, Y. (2011). Simulation of the undiseased human cardiac ventricular action potential: model formulation and experimental validation. PLoS Comput Biol *7*, e1002061.

Ogrodnik, J., and Niggli, E. (2010). Increased Ca(2+) leak and spatiotemporal coherence of Ca(2+) release in cardiomyocytes during beta-adrenergic stimulation. J Physiol *588*, 225-242.

Palygin, O.A., Pettus, J.M., and Shibata, E.F. (2008). Regulation of caveolar cardiac sodium current by a single Gsalpha histidine residue. Am J Physiol Heart Circ Physiol *294*, H1693-1699.

Penniman, J.R., Kim, D.C., Salata, J.J., and Imredy, J.P. (2010). Assessing use-dependent inhibition of the cardiac Na(+/-) current (I(Na)) in the PatchXpress automated patch clamp. J Pharmacol Toxicol Methods *62*, 107-118.

Picht, E., Zima, A.V., Shannon, T.R., Duncan, A.M., Blatter, L.A., and Bers, D.M. (2011). Dynamic calcium movement inside cardiac sarcoplasmic reticulum during release. Circ Res *108*, 847-856.

Priori, S.G., and Chen, S.R. (2011). Inherited dysfunction of sarcoplasmic reticulum Ca2+ handling and arrhythmogenesis. Circ Res *108*, 871-883.

Prosser, B.L., Ward, C.W., and Lederer, W.J. (2010). Subcellular Ca2+ signaling in the heart: the role of ryanodine receptor sensitivity. J Gen Physiol *136*, 135-142.

Qin, J., Valle, G., Nani, A., Chen, H., Ramos-Franco, J., Nori, A., Volpe, P., and Fill, M. (2009). Ryanodine receptor luminal Ca2+ regulation: swapping calsequestrin and channel isoforms. Biophys J *97*, 1961-1970.

Restrepo, J.G., and Karma, A. (2009). Spatiotemporal intracellular calcium dynamics during cardiac alternans. Chaos *19*, 037115.

Restrepo, J.G., Weiss, J.N., and Karma, A. (2008). Calsequestrin-mediated mechanism for cellular calcium transient alternans. Biophys J *95*, 3767-3789.

Rizzi, N., Liu, N., Napolitano, C., Nori, A., Turcato, F., Colombi, B., Bicciato, S., Arcelli, D., Spedito, A., Scelsi, M., Villani, L., Esposito, G., Boncompagni, S., Protasi, F., Volpe, P., and Priori, S.G. (2008). Unexpected structural and functional consequences of the R33Q homozygous mutation in cardiac calsequestrin: a complex arrhythmogenic cascade in a knock in mouse model. Circulation Research *103*, 298-306.

Rosso, R., Kalman, J.M., Rogowski, O., Diamant, S., Birger, A., Biner, S., Belhassen, B., and Viskin, S. (2007). Calcium channel blockers and beta-blockers versus beta-blockers alone for preventing exercise-induced arrhythmias in catecholaminergic polymorphic ventricular tachycardia. Heart Rhythm *4*, 1149-1154.

Royer, L., and Rios, E. (2009). Deconstructing calsequestrin. Complex buffering in the calcium store of skeletal muscle. J Physiol *587*, 3101-3111.

Sah, R., Ramirez, R.J., and Backx, P.H. (2002). Modulation of Ca(2+) release in cardiac myocytes by changes in repolarization rate: role of phase-1 action potential repolarization in excitation-contraction coupling. Circ Res *90*, 165-173.

Saint, D.A. (2008). The cardiac persistent sodium current: an appealing therapeutic target? Br J Pharmacol *153*, 1133-1142.

Shannon, T.R., Guo, T., and Bers, D.M. (2003). Ca2+ scraps: local depletions of free [Ca2+] in cardiac sarcoplasmic reticulum during contractions leave substantial Ca2+ reserve. Circ Res *93*, 40-45.

Shannon, T.R., Wang, F., Puglisi, J., Weber, C., and Bers, D.M. (2004). A mathematical treatment of integrated Ca dynamics within the ventricular myocyte. Biophys J *87*, 3351-3371.

Shaw, R.M., and Rudy, Y. (1997). Electrophysiologic effects of acute myocardial ischemia: a theoretical study of altered cell excitability and action potential duration. Cardiovasc Res *35*, 256-272.

Sims, C., Reisenweber, S., Viswanathan, P.C., Choi, B.R., Walker, W.H., and Salama, G. (2008). Sex, age, and regional differences in L-type calcium current are important determinants of arrhythmia phenotype in rabbit hearts with drug-induced long QT type 2. Circ Res *102*, e86-100.

Sipido, K.R. (2006). Calcium overload, spontaneous calcium release, and ventricular arrhythmias. Heart Rhythm *3*, 977-979.

Smani, T., Hernandez, A., Urena, J., Castellano, A.G., Franco-Obregon, A., Ordonez, A., and Lopez-Barneo, J. (2002). Reduction of Ca(2+) channel activity by hypoxia in human and porcine coronary myocytes. Cardiovascular Research *53*, 97-104.

Smith, G.D., Keizer, J.E., Stern, M.D., Lederer, W.J., and Cheng, H. (1998). A simple numerical model of calcium spark formation and detection in cardiac myocytes. Biophys J *75*, 15-32.

Sobie, E.A., Dilly, K.W., Cruz, J.D., Lederer, W.J., and Jafri, M.S. (2002a). Termination of cardiac Ca2+ sparks: An investigative mathematical model of calcium-induced calcium release. Biophys J *83*, 59-78.

Sobie, E.A., Dilly, K.W., dos Santos Cruz, J., Lederer, W.J., and Jafri, M.S. (2002b). Termination of cardiac Ca(2+) sparks: an investigative mathematical model of calcium-induced calcium release. Biophysical Journal *83*, 59-78.

Sobie, E.A., and Lederer, W.J. (2012). Dynamic local changes in sarcoplasmic reticulum calcium: physiological and pathophysiological roles. J Mol Cell Cardiol *52*, 304-311.

Sobie, E.A., Song, L.S., and Lederer, W.J. (2005). Local recovery of Ca2+ release in rat ventricular myocytes. J Physiol *565*, 441-447.

Sobie, E.A., Song, L.S., and Lederer, W.J. (2006). Restitution of Ca(2+) release and vulnerability to arrhythmias. J Cardiovasc Electrophysiol *17 Suppl 1*, S64-S70.

Soeller, C., and Cannell, M.B. (1999). Examination of the transverse tubular system in living cardiac rat myocytes by 2-photon microscopy and digital image-processing techniques. Circ Res *84*, 266-275.

Song, L., Alcalai, R., Arad, M., Wolf, C.M., Toka, O., Conner, D.A., Berul, C.I., Eldar, M., Seidman, C.E., and Seidman, J.G. (2007). Calsequestrin 2 (CASQ2) mutations increase expression of calreticulin and ryanodine receptors, causing catecholaminergic polymorphic ventricular tachycardia. J Clin Invest *117*, 1814-1823.

Song, L.S., Sobie, E.A., McCulle, S., Lederer, W.J., Balke, C.W., and Cheng, H. (2006a). Orphaned ryanodine receptors in the failing heart. Proc Natl Acad Sci U S A *103*, 4305-4310.

Song, L.S., Sobie, E.A., McCulle, S., Lederer, W.J., Balke, C.W., and Cheng, H.P. (2006b). Orphaned ryanodine receptors in the failing heart. P Natl Acad Sci USA *103*, 4305-4310.

Takeshima, H., Komazaki, S., Nishi, M., Iino, M., and Kangawa, K. (2000). Junctophilins: a novel family of junctional membrane complex proteins. Mol Cell *6*, 11-22.

Tanskanen, A.J., Greenstein, J.L., O'Rourke, B., and Winslow, R.L. (2005). The role of stochastic and modal gating of cardiac L-type Ca2+ channels on early after-depolarizations. Biophys J *88*, 85-95.

Tanskanen, A.J., and Winslow, R.L. (2006). Integrative structurally detailed model of calcium dynamics in the cardiac diad. Multiscale Model Sim *5*, 1280-1296.

Terentyev, D., Kubalova, Z., Valle, G., Nori, A., Vedamoorthyrao, S., Terentyeva, R., Viatchenko-Karpinski, S., Bers, D.M., Williams, S.C., Volpe, P., and Gyorke, S. (2008). Modulation of SR Ca release by luminal Ca and calsequestrin in cardiac myocytes: effects of CASQ2 mutations linked to sudden cardiac death. Biophys J *95*, 2037-2048.

Terentyev, D., Nori, A., Santoro, M., Viatchenko-Karpinski, S., Kubalova, Z., Gyorke, I., Terentyeva, R., Vedamoorthyrao, S., Blom, N.A., Valle, G., Napolitano, C., Williams, S.C., Volpe, P., Priori, S.G., and Gyorke, S. (2006). Abnormal interactions of calsequestrin with the ryanodine receptor calcium release channel complex linked to exercise-induced sudden cardiac death. Circ Res *98*, 1151-1158.

Thomas, G., Chung, M., and Cohen, C.J. (1985). A dihydropyridine (Bay k 8644) that enhances calcium currents in guinea pig and calf myocardial cells. A new type of positive inotropic agent. Circ Res *56*, 87-96.

Thomas, G., Killeen, M.J., Grace, A.A., and Huang, C.L. (2008). Pharmacological separation of early afterdepolarizations from arrhythmogenic substrate in DeltaKPQ Scn5a murine hearts modelling human long QT 3 syndrome. Acta Physiol (Oxf) *192*, 505-517.

Uchinoumi, H., Yano, M., Suetomi, T., Ono, M., Xu, X., Tateishi, H., Oda, T., Okuda, S., Doi, M., Kobayashi, S., Yamamoto, T., Ikeda, Y., Ohkusa, T., Ikemoto, N., and Matsuzaki, M. (2010). Catecholaminergic polymorphic ventricular tachycardia is caused by mutation-linked defective conformational regulation of the ryanodine receptor. Circ Res *106*, 1413-1424.

Valle, G., Galla, D., Nori, A., Priori, S.G., Gyorke, S., de Filippis, V., and Volpe, P. (2008). Catecholaminergic polymorphic ventricular tachycardia-related mutations R33Q and L167H alter calcium sensitivity of human cardiac calsequestrin. Biochem J *413*, 291-303.

van der Werf, C., Kannankeril, P.J., Sacher, F., Krahn, A.D., Viskin, S., Leenhardt, A., Shimizu, W., Sumitomo, N., Fish, F.A., Bhuiyan, Z.A., Willems, A.R., van der Veen, M.J., Watanabe, H., Laborderie, J., Haissaguerre, M., Knollmann, B.C., and Wilde, A.A. (2011). Flecainide therapy reduces exercise-induced ventricular arrhythmias in patients with catecholaminergic polymorphic ventricular tachycardia. J Am Coll Cardiol *57*, 2244-2254.

van Oort, R.J., Garbino, A., Wang, W., Dixit, S.S., Landstrom, A.P., Gaur, N., De Almeida, A.C., Skapura, D.G., Rudy, Y., Burns, A.R., Ackerman, M.J., and Wehrens,

X.H. (2011). Disrupted junctional membrane complexes and hyperactive ryanodine receptors after acute junctophilin knockdown in mice. Circulation *123*, 979-988.

Viatchenko-Karpinski, S., Terentyev, D., Gyorke, I., Terentyeva, R., Volpe, P., Priori, S.G., Napolitano, C., Nori, A., Williams, S.C., and Gyorke, S. (2004). Abnormal calcium signaling and sudden cardiac death associated with mutation of calsequestrin. Circ Res *94*, 471-477.

Viskin, S., Fish, R., Zeltser, D., Belhassen, B., Heller, K., Brosh, D., Laniado, S., and Barron, H.V. (2000). Arrhythmias in the congenital long QT syndrome: how often is torsade de pointes pause dependent? Heart *83*, 661-666.

Walsh, K.B., and Kass, R.S. (1991). Distinct voltage-dependent regulation of a heart-delayed IK by protein kinases A and C. American Journal of Physiology *261*, C1081-C1090.

Wang, S.Q., Song, L.S., Lakatta, E.G., and Cheng, H.P. (2001). Ca2+ signalling between single L-type Ca2+ channels and ryanodine receptors in heart cells. Nature *410*, 592-596.

Wang, W., Ma, J., Zhang, P., and Luo, A. (2007). Redox reaction modulates transient and persistent sodium current during hypoxia in guinea pig ventricular myocytes. Pflugers Arch *454*, 461-475.

Watanabe, H., Chopra, N., Laver, D., Hwang, H.S., Davies, S.S., Roach, D.E., Duff, H.J., Roden, D.M., Wilde, A.A., and Knollmann, B.C. (2009). Flecainide prevents catecholaminergic polymorphic ventricular tachycardia in mice and humans. Nat Med *15*, 380-383.

Wehrens, X.H., Lehnart, S.E., Huang, F., Vest, J.A., Reiken, S.R., Mohler, P.J., Sun, J., Guatimosim, S., Song, L.S., Rosemblit, N., D'Armiento, J.M., Napolitano, C., Memmi, M., Priori, S.G., Lederer, W.J., and Marks, A.R. (2003). FKBP12.6 deficiency and defective calcium release channel (ryanodine receptor) function linked to exercise-induced sudden cardiac death. Cell *113*, 829-840.

Weir, E.K., and Archer, S.L. (1995). The mechanism of acute hypoxic pulmonary vasoconstriction: the tale of two channels. FASEB Journal *9*, 183-189.

Weir, E.K., Hong, Z., Porter, V.A., and Reeve, H.L. (2002). Redox signaling in oxygen sensing by vessels. Respiratory Physiology & Neurobiology *132*, 121-130.

Wier, W.G., and Balke, C.W. (1999). Ca(2+) release mechanisms, Ca(2+) sparks, and local control of excitation-contraction coupling in normal heart muscle. Circ Res *85*, 770-776.

Wier, W.G., Egan, T.M., Lopezlopez, J.R., and Balke, C.W. (1994). Local-Control of Excitation-Contraction Coupling in Rat-Heart Cells. J Physiol-London *474*, 463-471.

Wu, X., and Bers, D.M. (2006). Sarcoplasmic reticulum and nuclear envelope are one highly interconnected Ca2+ store throughout cardiac myocyte. Circ Res *99*, 283-291.

Wu, Y., Temple, J., Zhang, R., Dzhura, I., Zhang, W., Trimble, R., Roden, D.M., Passier, R., Olson, E.N., Colbran, R.J., and Anderson, M.E. (2002). Calmodulin kinase II and arrhythmias in a mouse model of cardiac hypertrophy. Circulation *106*, 1288-1293.

Xie, L.H., and Weiss, J.N. (2009). Arrhythmogenic consequences of intracellular calcium waves. Am J Physiol Heart Circ Physiol *297*, H997-H1002.

Ylanen, K., Poutanen, T., Hiippala, A., Swan, H., and Korppi, M. (2010). Catecholaminergic polymorphic ventricular tachycardia. Eur J Pediatr *169*, 535-542.

Zeng, J., and Rudy, Y. (1995). Early afterdepolarizations in cardiac myocytes: mechanism and rate dependence. Biophys J *68*, 949-964.

Zima, A.V., Bovo, E., Bers, D.M., and Blatter, L.A. (2010). Ca(2)+ spark-dependent and -independent sarcoplasmic reticulum Ca(2)+ leak in normal and failing rabbit ventricular myocytes. J Physiol *588*, 4743-4757.

Zima, A.V., Picht, E., Bers, D.M., and Blatter, L.A. (2008). Termination of cardiac Ca2+ sparks: role of intra-SR [Ca2+], release flux, and intra-SR Ca2+ diffusion. Circ Res *103*, e105-115.

Zipes, D.P., and Wellens, H.J. (1998). Sudden cardiac death. Circulation *98*, 2334-2351.